Effect of extra-cellular nutrient environment and intra-cellular biochemical conditions on the chemotactic performance of E. coli

by

Subrata Dev

A thesis submitted for the degree of Doctor of Philosophy in

Physics (Theoretical)

Department of Physics

University of Calcutta

2018

"People believe the only alternative to randomness is intelligent design"

Richard Dawkins

Acknowledgements

First of all I would like to give my sincere gratitude to my supervisor Dr. Sakuntala Chatterjee. Without her continuous support and guidance it would not be possible to finish my thesis. She always encouraged me to think independently and gave always freedom to work on my own. I would also like to thank Anandamohan Ghosh sir for being very good to me. I would like to thank Dr. Punyabrata Pradhan for his questions and encouragement during our stat physics group meetings, seminars and conferences.

I would also like to acknowledge some of my teachers whom I met in my life. I'm very lucky to have teachers like Mr. Ashim Dutta Chowdhury(School Math Teacher), Dr. Bidhan Chandra Roy (B.Sc. Physics), Smt. Basabdatta Bose (B.Sc. Physics), Dr. Amitabha Mukhopadhyay (M.Sc. Physics) and Prabhas Mali (M.Sc. Physics) for their wisdom and teaching.

My grateful thanks to my seniors, friends and juniors who are very close to my heart. Among the seniors Sayani Di, Subhasish Da, Tushar Da, Surajit Da, Arka Da, Biplab Da, Arghya Da, Jena Bhaiya, Debmalya Da, Dibakar Da, Pratik Da, Arnab Pal Da, Chaoba Di, Sreeraj Da, Siddhi Di, Sukla Di, Tilak Da and Chaitrali Di with whom I have shared many good times and shared their experience. Without friends life would have been so dull and meaningless. I would like to first name my school friends Aman, Surojit, Felu, Matu, Somraj, Bittu, atanu, Suvo, Raju, Geeta, Manti, Mitali and Rini. Then I would like to say my college friends Dipanjan, Manajit, Siddhartha, Dipak, Dipankar, Raja, Biswajit, Papiya, and Parthabi. I'm very grateful to my M.Sc. friends Manoj, Tapas, Amit, Bhaskar, Nihar, Uma, Ishita and Sreemoyee. I'm also very grateful to my SNB friends Sova, Lalu, Aslam, Kartik, Deba, Goba, Dada, Somnath, Krishnendu, Suman Aich, Arpita, Anindita, Karan, Shirsendu, Poulami, Supriyo, Sagar, Soumya, Suman Dutta, Ganesh, Vinode and Subhasree. I'm also thankful to Sabana, Moutushi, Sushmita and Heena for their support and friendship. I would like to mention my SNB juniors Ananda, Rakesh, Sudipta, Sumanta, Rajkumar, Shauri, Keshab, Dhrimadri, Ransell, Tukun, anita, Priyanka, Imadul, Sandip, Samrat, Ritam, Sourav, Juriti, Dipanjan, Subrata, Mahbub, Indranil, Arunava, Kajol(Mess) and Ramu(mess).

Special thanks to the SNB football group without which my life in S N Bose would be so frustrated. I thank SNB Khaja Band for providing regular entertainment to our life and also giving me chance to sing some songs.

I would like to acknowledge my parents and my brother for their love and support throughout my life. I like to mention my Boromama who would have been very proud. I give my gratitude to all other family members whose love was important to me.

Finally I would like to give my gratitude to the S N Bose staffs, all the cleaners, Cooking team and other administrative staffs for whom the SNB environment was so comfortable during last six years.

Lastly I would like to acknowledge all those good peoples in my life who has somehow made my life happier.

Publication lists:

1. **Optimal search in E. coli chemotaxis**, by Subrata Dev and Sakuntala Chatterjee Phys. Rev. E 91, 042714, 2015.

2. **Optimal methylation noise for best chemotactic performance of E. coli**, by Subrata Dev and Sakuntala Chatterjee, Phys. Rev. E 97, 032420.

3. **Run-and-tumble motion with step-like response to a stochastic input** by Subrata Dev and Sakuntala Chatterjee. (Submitted).

Contents

Acknowledgements ii

List of Figures vii

1 Introduction 1
- 1.1 A brief review on E. coli chemotaxis . . . 2
  - 1.1.1 Phenotypic response of E.coli bacteria: bilobe nature and adaptation . . . 2
  - 1.1.2 Signaling pathway of the E. coli bacterium . . . 3
  - 1.1.3 The collective behavior of E. coli chemotaxis . . . 5
  - 1.1.4 Single cell behavior of *E.coli* chemotaxis . . . 6
- 1.2 Motivation and the plan of the thesis . . . 9

2 Effects of extracellular environment on search process of E. coli 18
- 2.1 Introduction . . . 18
- 2.2 Model for the simulation and measurement of the first passage time . 20
- 2.3 Analytical calculation in a coarse-grained Markovian description . . . 22
- 2.4 Analytical calculation of first passage time . . . 23
- 2.5 Simulation results on first passage time in presence of static Gaussian nutrient concentration . . . 27
- 2.6 First passage time for time-varying Gaussian concentration field . . . 29
- 2.7 Conclusion . . . 31

3 Signaling noise in a homogeneous environment 35
- 3.1 Introduction . . . 35
- 3.2 Model description . . . 36
- 3.3 Simulation results of the run-length and CheY-P level distribution in a homogeneous nutrient environment . . . 39
- 3.4 Analytical calculation of the CheY-P level distribution and average run duration of the bacterium in a homogeneous concentration . . . 41
- 3.5 Conclusion . . . 44

4 Effects of intracellular environment on the chemotactic performance of E. coli in a spatially varying nutrient profile 48

4.1 Introduction 48
4.2 Steady state distribution of cell position 50
4.3 Chemotactic drift velocity in steady state 51
4.3.1 Explanation of optimal noise strength 53
4.4 Search time for favorable region 58
4.5 Conclusion 60

5 Effects of intracellular environment on the chemotactic performance of E. coli in a time varying nutrient profile 63
5.1 Decaying nutrient profile 64
5.2 Nutrient profile with decay and diffusion 66
5.3 Conclusion 68

6 Effects of signaling noise and the motor adaptation on the behavior of E. coli in a spatially varying nutrient profile 71
6.1 Peak of localization and drift velocity at optimum noise 73
6.2 Conclusion 74

7 Run-and-tumble motion with step-like response to a stochastic input 76
7.1 Introduction 76
7.2 Run-and-tumble motion in a homogeneous environment 79
7.2.1 Steady state probability distribution of y in run and tumble modes 81
7.2.2 Average run and tumble duration decreases with signaling noise 82
7.2.3 Distribution of the run duration of the random walker 85
7.3 Run and Tumble motion in an environment with spatial variation . . 86
7.4 Conclusion 88

A Drift velocity of a random walker in presence of a linear nutrient concentration field for response function $R(t) = \delta(t)$ 92

List of Figures

1.1 **Impulse response function of wild-type E. coli cell:** $R(t)$ is the ratio between the average change in run duration of a wild type E. coli bacterium at time t due to an impulse to the run duration of the cell in a constant background concentration. We have used a discrete sampling of data instead of working with the complete data set presented in Ref. [7]. This response function has been used for the simulation in Chapter 2. 3

1.2 **Simplified chemotaxis pathway inside an E.coli cell** 4

2.1 Results for the mean first passage time with a fixed initial position. The main plot shows $T_1(x)$ (in seconds) as a function of standard deviation σ (in μm) of the Gaussian nutrient concentration field with $R(t) = \alpha\delta(t - \Delta)$ and $\Delta = 0.5s$, $x = 300\mu m$. The top-right and bottom-left insets show the variation of the optimum width σ^* (in μm) as a function of Δ (in seconds) and the initial position x (in μm), respectively. The top-left inset shows $T_1(x)$ (in seconds) vs σ (in μm) variation for the bilobe response kernel, shown in Fig. 1.1. The discrete symbols correspond to simulations and the continuous lines correspond to analytical calculations. Here $L = 1000\mu m$, $x_0 = 490\mu m$, $\bar{x} = 500\mu m$, $q = 0.5$, $\tau = 1s$. 28

2.2 Mean first passage time with stochastic initial positions. Top panel shows data for impulse response $R(t) = \alpha\delta(t - \Delta)$ and bottom pannel for the bilobe response. (A) and (B) show data for uniform initial condition, when x can take any value in the range $[0, x_0]$ with uniform probability P_0. (C) and (D) show data for steady state initial condition, when the value of x in the range $[0, x_0]$ is drawn from the steady state distribution $P(x)$ in Eq. 2.8. Here the first passage time is measured in the units of seconds and σ in μm. The other simulation parameters are same as in Fig. 2.1. The discrete symbols are for numerical data and the continuous lines are for analytical calculations. 29

2.3 First passage time for time-dependent concentration of the nutrient. (A) shows the variation of $T_1(x)$ (in seconds) as a function of σ_0 (in μm) with $\mathcal{D}$ held fixed at $0.01\mu m^2/s$ (red squares), $10\mu m^2/s$ (green circles) and $37\mu m^2/s$ (black diamonds). (B) shows $T_1(x)$ (in seconds) vs $\mathcal{D}$ (in $\mu m^2/s$) plot for $\sigma_0 = 30\mu m$ (red squares), $50\mu m$ (green circles) and $120\mu m$ (black diamonds). The other simulation parameters are same as in Fig. 2.1 main plot. 30

3.1 **Distribution of the run duration for different signaling noise.** The probability $P(\tau_0)$ to observe a run duration τ_0 for different noise strengths λ, in presence of a homogeneous nutrient concentration. For small λ, we find $P(\tau_0)$ has an exponential form, but for large λ it is a power law with exponent 2.1 ± 0.1, close to experimental observation [11]. The thin line shows a power law function with power 2.1. All other simulation parameters are as specified in Sec.3.2. 40

3.2 **CheY-P level statistics of the bacterial biochemical pathway**. The probability distribution $P_{tum}(y_P)$ for the fraction y_P of phosphorylated CheY molecules for a homogeneous nutrient concentration $c(x) = c_0$ for different noise strengths. With increasing noise strength, $P_{tum}(y_P)$ peak shifts rightward and width of the distribution increases. The dashed lines show (binned) simulation data and the continuous lines correspond to analytical calculation, which shows good agreement with simulation. Inset shows the left tail region of the distribution on a zoomed scale. We find that as noise increases, the tail becomes longer. The simulation parameters are as in Fig. 3.1. 41

3.3 **Average run duration for different signaling noise.** The average run duration τ decreases with λ. The discrete points are for simulation and the continuous line shows analytical result from Eq. 3.13. We find good agreement. Here, we have used one dimensional system and a homogeneous nutrient concentration with a constant background concentration $c(x) = c_0 = 200\mu M$. All other simulation parameters are as in Fig. 3.1. 44

4.1 **Localization shows a peak as a function of noise strength. (A)**: $\langle C \rangle - c_0$ vs the noise strength λ with $c(x) = c_0(1 + x/x_0)$ with $x_0 = 20000\mu m$. The optimum noise strength $\lambda^* \simeq 0.005$ in this case. Inset shows the plot for λ^* vs x_0. We find no strong dependence of λ^* on x_0. **(B)**: The variation of $\langle C \rangle - c_0$ with λ for $c(x) = c_0(1 + \frac{1}{\sqrt{2\pi\sigma^2}} \exp[-\frac{(x-\bar{x})^2}{2\sigma^2}])$. This case also shows similar value for λ^*. The inset shows the plot of λ^* vs σ. **(C).** $\langle C \rangle - c_0$ vs the noise strength λ in two dimension with $c(x) = c_0(1 + x/x_0)$ with $x_0 = 20000\mu m$. The localization shows a peak at the same value as in **(A)** and **(B)**. The inset shows the variation of λ^* with the x_0. For two dimension case also we find no strong dependence of the optimum noise strength on the gradient present in the system. We have used $c_0 = 200\mu M$, $x_0 = 10^4\mu m$, $\sigma = 100\mu m$, $\bar{x} = 500\mu m$. 50

4.2 Slope of $\mathcal{P}_\lambda(x)$ shows a peak as a function of noise strength. The optimum noise strength λ^* is close to 0.005. Here, we have scaled the slope by a factor of 10^8. The simulation parameters are as in Fig. 4.1. 51

4.3 **Chemotactic drift velocity shows a peak as a function of the noise strength.** Left and right panels show the data for one dimensional and two dimensional systems, respectively. In both cases, the optimal noise strength λ_o is found to be higher than that for localization data in Fig. 4.1. We have used $c(x) = c_0(1 + x/x_0)$ here and all simulation parameters are as in Fig. 4.1. 53

4.4 **The net displacement Δ in a run and the average run-duration τ as a function of noise strength.** Δ shows a peak at an optimum noise value close to λ^*, and τ decreases monotonically with noise. The upper panel shows data for one dimension and the lower panel shows data for two dimensions. All the simulation parameters for one and two dimension are same as in Fig. 4.3. 54

4.5 **Average change in CheY-P level during a run, as a function of the initial CheY-P level, at the start of the run.** y_P denotes the fraction of phosphorylated CheY molecules and δ_{y_P} denotes its average change. The circles (squares) show the data for leftward (rightward) runs. **(A)**: In absence of methylation noise, average CheY-P level always goes down (up) during a rightward (leftward) run. **(B)**: For intermediate noise strength, change in CheY-P becomes positive (negative) during a rightward (leftward) run for small (large) values of CheY-P concentration. **(C)**: As noise increases, the difference between the two curves become smaller. These data are for the one dimensional system and the simulation parameters are same as in Fig. 4.3A. . . . 55

4.6 **Net displacement during a run for different noise strengths.** y_P denotes the fraction of phosphorylated CheY molecules, at the start of the run, and $\Delta(y_P)$ denotes the average displacement in that run. The left panel shows the complete range of y_P values, while the right panel zooms onto the large y_P values. **(A)**: $\Delta(y_P)$ vanishes for very small or very large y_P values and attains a large negative peak and small positive peak for intermediate y_P values. The position and height of the peaks depend strongly on noise. **(B)**: The positive peak of $\Delta(y_P)$ shown on a zoomed scale. While the position of the peak shifts towards left as noise increases, the height of the peak clearly shows non-monotonic behavior with noise, the highest peak being observed close to the optimal noise λ^*. These data are for one dimension and all simulation parameters are same as in Fig. 4.3A. 56

4.7 Variation of $N_R(y_P) - N_L(y_P)$ against y_P for different noise strengths. **(A):** As y_P increases, $N_R(y_P) - N_L(y_P)$ starts from zero, reaches a negative peak, followed by a positive peak, and again becomes zero for very large y_P values. The negative values observed at small y_P show that in this range, the cell motion is biased towards decreasing nutrient concentration. **(B):** Similar behavior is observed at large λ, but the point of zero-crossing shifts towards smaller y_P values. All simulation parameters are same as in Fig. 4.6 57

4.8 **Mean first passage time decreases as a function of noise strength.** **(A)** shows the data in one dimension and **(B)** shows the data in two dimensions. Square symbols correspond to a homogeneous concentration profile of the nutrient, $c(x) = c_0$, circles correspond to a linear concentration form $c(x) = c_0(1 + x/x_0)$ in both panels. The triangles in left panel correspond to a Gaussian $c(x) = c_0(1 + \frac{1}{\sqrt{2\pi\sigma^2}} \exp[-\frac{(x-\bar{x})^2}{2\sigma^2}])$. We have used $c_0 = 200\mu M$, $x_0 = 10^4\mu m$, $\sigma = 100\mu m$, $\bar{x} = 500\mu m$. The mean first passage time $T(x_i, x_f)$ has been measured from an initial position $x_i = 300\mu m$ to a final target position at $x_f = 490\mu m$. 59

5.1 **First passage time vs noise strength for degrading nutrient profile.** **(A)**: Mean first passage time $T(x_0, x_f)$ decreases with λ. The mean first passage time has higher values than that in Fig. 4.8 where no degradation is considered. **(B)**: The typical first passage time $\mathcal{T}(x_i, x_f)$ has much smaller value than the mean, but also decreases with λ. The circles show the data for $c(x,t) = c_0 e^{-t/\tau_d}$ and squares are for $c(x,t)$ given by Eq. 5.1 with $\mathcal{D} = 0$. These data are for the one dimensional case and we have used $\tau_d = 500sec$, $\sigma_0 = 100\mu m$. Other parameters are as in Fig. 4.8A. 66

5.2 **Change in uptake as a function of noise strength for decaying Gaussian concentration profile**: **(A-C):** For fast degradation of the nutrient, uptake increases with λ, since maximum contribution to $\mathcal{U}$ in this case comes from those trajectories with small first passage times. **(D-G):** For a slower degradation of the nutrient, uptake starts decreasing for very large noise, and a peak is observed. Reaching the peak in the shortest possible time is not the single most important criterion any more. When the nutrient lasts for some time, those trajectories where the cell takes longer to reach the peak and then spends longer time in the peak region, contribute more towards uptake. **(H-I):** For a very slow degradation, the peak of uptake moves closer to the optimal noise λ^*, observed in Fig. 4.1B. The values of $\mathcal{U}_0$ used in panels **(A-I)** are 406, 1628, 2449, 3064, 5956, 10023, 11782, 15068, 17551 mM, respectively. These data are for one dimensional system and we have used $t_{obs} = 1000sec$. Other simulation parameters are as in Fig. 5.1. 67

5.3 **Change in uptake as a function of noise strength for nutrient profile with diffusion and degradation.** **(A-D):** For slow diffusion of the nutrient, uptake increases with noise for our choice of τ_d. In this case, uptake is governed by those trajectories where cell executes long runs. **(E-F):** For a faster diffusion of nutrient, uptake shows a peak as a function of λ. But the variation is much weaker. **(G-I):** For very fast diffusion of nutrient, uptake decreases with noise. The values of $\mathcal{U}_0$ used are: 1730, 1736, 1738 mM in panels **A,B,I**, respectively, $1740mM$ in panels **C,H**, $1741mM$ in **G**, and $1742mM$ in **D,E,F**. We have used one dimensional system and the nutrient concentration in Eq. 5.1 with $\tau_d = 100sec$, $\sigma = 10\mu m$, $t_{obs} = 200sec$ here. Other simulation parameters are same as Fig. 5.2. 68

6.1 **Localization shows a peak as a function of noise strength.** $\langle C \rangle - c_0$ vs the noise strength λ with $c(x) = c_0(1 + x/x_0)$ with $x_0 = 20000\mu m$. The optimum noise strength $\lambda^* \simeq 0.002$ in this case. Inset shows the plot for λ^* vs x_0. We find no strong dependence of λ^* on x_0. All others parameters are same as in Chapter 4 73

6.2 **Chemotactic drift velocity shows a peak as a function of the noise strength.** The optimal noise strength λ_o is found to be higher than that for localization data in Fig. 6.1. We have used $c(x) = c_0(1 + x/x_0)$ here and all simulation parameters are as in Fig. 4.1. . . 74

7.1 A typical time series of the signal $y(t)$. The purple (continuous) segments correspond to tumbles and the green (dashed) segments correspond to runs. The threshold value $y_0 = 0.32$ and the boundaries of the Δ range at $y_0 \pm \Delta/2$ are marked by horizontal line. Every time $y(t)$ exits the range through a boundary different from the one it had used to enter the range, a switch happens. 77

7.2 **Steady state probability distribution of the signal variable. A:** For different noise strength λ, probability to observe a particular value y of the signal variable is plotted against y. Discrete points are from simulation and continuous lines are from analytical calculation using Eq. 7.5. **B:** Probability $P_R(y)$ and $P_T(y)$ to observe a runner and a tumbler, respectively, with a given y value in the range $[y_0 - \Delta/2, y_0 + \Delta/2]$. The decreasing curves correspond to $P_R(y)$ and increasing curves are for $P_T(y)$. The discrete points from simulations show excellent agreement with continuous lines from analytics. All simulation parameters are as specied in Sec. 7.2 and Sec. 3.2. 82

7.3 **Average run and tumble duration as a function of signaling noise strength λ. A.** The average run duration τ_1 decreases as a function of λ. The range of variation of τ_1 is quite significant. **B.** The average tumble duration τ_2 decreases with λ but the range of variation is much smaller than that for τ_1. Discrete points are from simulations and continuous lines are from analytics. The simulation parameters are same as in Fig. 7.2. 83

7.4 **Distribution of run duration for different value of noise strength. A:** Simulation results for the distribution of the run duration of the bacterium $P_{run}(t)$. The distribution has a peak whose position shifts leftward as noise increases. **B:** The Laplace transform of $P_{run}(t)$ analytically calculated and plotted in continuous lines. The discrete points show Laplace transform calculated from the data in panel A and we find good agreement. The simulation parameters are same as in Fig. 7.2 85

7.5 **The distribution $P_\lambda(x)$ of the random walker position x for different noise strengths.** We have used $c(x) = c_0(1 + x/x_0)$ here and for all λ values, $P_\lambda(x)$ shows a positive slope. For large λ, the slope is less. We have chosen $c_0 = 200\mu M$ and $x_0 = 200000\mu m$ here and all other parameters are as in Fig. 7.2. 87

Dedicated to my family

Chapter 1

Introduction

'Chemotaxis' is a phenomenon of movement of an organism along or against a chemical concentration gradient. When there is an inhomogeneous concentration of some chemo-attractant present in a system, certain organisms show a tendency to migrate towards regions of higher chemical concentration. In the case of a chemo-repellant, the organisms tend to move away from the regions of high chemical concentration. The term 'chemotaxis' was first introduced by the botanist Wilhelm Pfeffer while studying the responses of a number of different species of bacteria to a variety of chemicals. EsCheRichia coli (E. coli) is one of the simplest and best understood micro-organism which shows chemotaxis [1]. In a medium of inhomogeneous nutrients E. coli shows a chemotactic behavior by accumulating in the higher regions of nutrient concentrations [2].

The size of the E. coli bacterium is very small and the cells are rod-shaped, about 2.5 μm long and about 0.8 μm in diameter, with hemispherical end caps. The cell has a thin three-layered wall enclosing the cytoplasm which does not have any membrane enclosed organelles. It has external organelles, thin straight filaments, called 'pilli', which enable it to attach host cells, and thicker longer helical filaments, called flagella [3], those enable it to swim. This flagella are driven by a rotary motor at their base which can can turn clockwise(CW) or counterclockwise(CCW).

E.coli cell uses run-and-tumble motion to move around in a medium. During a run, all the flagellar motors of E. coli rotate counter-clockwise when one looks at the cell from the back [5]. In run mode the cell moves with an almost constant forward velocity of about 20 $\mu m/sec$, along a near-straight line about 1 sec. When some of the flagellar motor turns clockwise, the bacterium undergoes a tumble, during which they

do not undergo appreciable displacement but change their orientation randomly. The tumble duration have a mean value 0.1 sec. In presence of spatially varying nutrient concentration, E.coli bacteria accumulate in the region of higher concentrations and it is achieved by the modulation of run durations.

Over the last two-three decades, there has been a rapidly growing understanding of the mechanisms through which Escherichia coli moves in response to external stimuli. There are many experiments and models which study different aspects of chemotactic behavior of E. coli. In this chapter we shall first discuss a set of pioneering experiments in this field and then we will also discuss some theoretical models explaining collective behavior and single cell behavior exhibited by E. coli bacteria. In the last section of this chapter, we motivate the problem considered in this thesis and briefly outline the content of each chapter.

1.1 A brief review on E. coli chemotaxis

1.1.1 Phenotypic response of E.coli bacteria: bilobe nature and adaptation

To characterize the behavior of E. coli bacterium Block and his colleagues performed an experiment [6] where cells were tethered [5] by a single flagellum to a glass plate and exposed to pulses of chemicals. When cells were exposed to a very brief diffusive wave of attractant, the probability of CCW spin of the motors peaked quickly, then fell below the pre-stimulus value, returning to baseline within a few seconds. The repellent responses were similar but inverted. In Fig. 1.1 the impulse response of a single bacterium in response to a pulse of an attractant is shown. $R(t)$ is the ratio between the average change in run duration at time t to the run duration of the cell in a constant background concentration. In another experiment by Segall et al. [7] the responses of E. coli bacteria to impulse, step and exponential-ramp were studied. The attractant or repellent concentration were in physiological range, i.e. the stimuli does not saturate the response of the organisms. The response function indicates that the cell integrates sensory inputs over a period of seconds, while the bilobe character implies that they also take time derivatives of these inputs, i.e., the cell compare between two different concentration experienced in the past and then decide whether to go upside or downside the concentration gradient. The wild type cells exposed

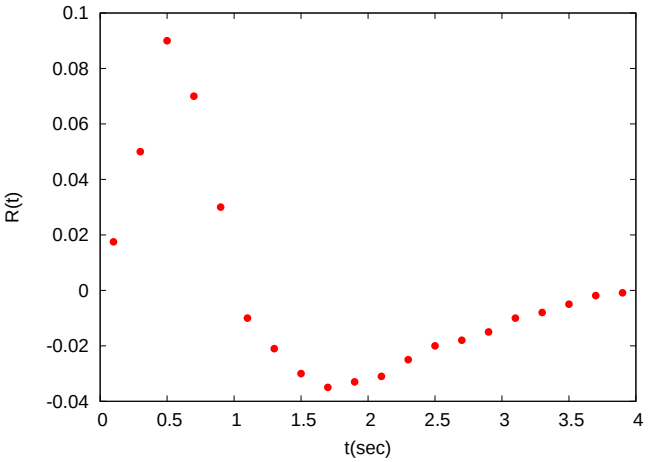

FIGURE 1.1: **Impulse response function of wild-type E. coli cell:** $R(t)$ is the ratio between the average change in run duration of a wild type E. coli bacterium at time t due to an impulse to the run duration of the cell in a constant background concentration. We have used a discrete sampling of data instead of working with the complete data set presented in Ref. [7]. This response function has been used for the simulation in Chapter 2.

to stimuli make short-term temporal comparisons extending 4 seconds into the past. Stimuli received during the past second are given a positive weighting, and stimuli received during the 3 seconds before that are given a negative weighting, and the cells respond to the difference. Impulse responses of mutant cells (cells which has a some defect in bio-chemical circuits present in it) were similar to those of wild-type cells, but did not fall as far below the baseline, indicating a partial defect in adaptation. When exposed to small steps, they fail to adapt over periods of up to 12 sec, when exposed to longer steps in a flow cell, they partially adapt.

1.1.2 Signaling pathway of the E. coli bacterium

The experiments done by Eisenbach [8], Sourjik et.al [9] , Falke et al [10] and others gives the comprehensive picture of how bacteria modulate their flagellar motion during chemotaxis. The changes in attractant concentrations are sensed by a protein assembly consisting of transmembrane receptors, a coupling protein (CheW) and a histidine kinase (CheA) (Fig. 1.2). These components are organized at the cell poles in tight clusters that contain several thousand copies of each proteins. The results in [9] indicate that assemblies of bacterial chemoreceptors work in a highly cooperative manner, i.e. the affinity for attractant molecules by the receptors are influenced by the occupancy of the binding sites of the receptors. The attractant molecules

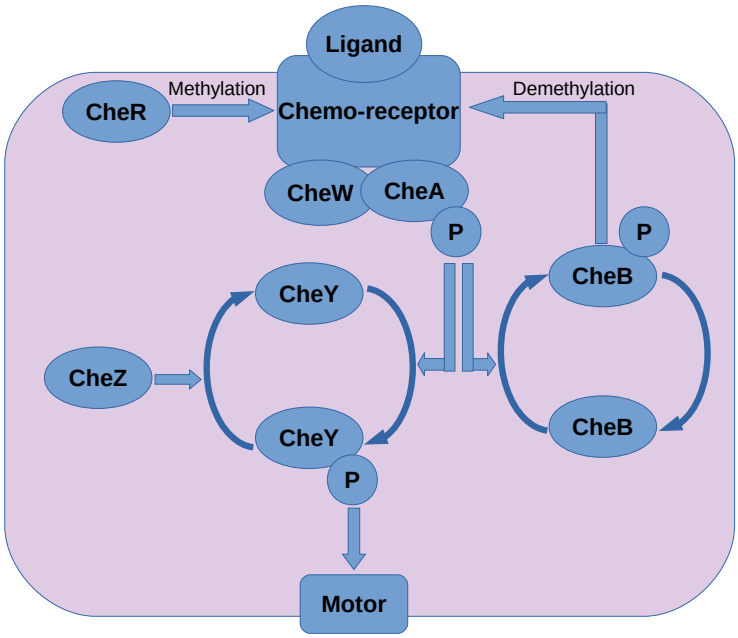

FIGURE 1.2: **Simplified chemotaxis pathway inside an E.coli cell**

bind to the chemoreceptor [8] called methyl accepting chemotactic protein (MCP) [10] spanned over the cell membrane of the bacteria. The cytoplasmic side of the MCP interacts with two proteins called CheW and CheA. When MCP is not bound to the attractant it stimulates CheA autophospholyration by using ATP molecules. This autophospholyration is inhibited when the MCP is bound to the attractant. The phosphrylated CheA donates the phosphate group to the motor protein CheY. CheW acts as a mediator between the receptor and CheA protein. The phosphate of CheY are continually removed by the protein CheZ. When there is no attractant present the bacterium maintains an intermediate levels of CheA phosphate and CheY phosphate. The rotational bias of the flagellar motors of E. coli is controlled by phosphorylated CheY-P inside the cell, which binds to the motors and increases their CW bias. Importantly, the dependence of CW bias on CheY-P concentration[11] is very sensitive and experiments measure an almost sigmoidal dependence[12], where CW bias changes sharply from 0 to 1 as CheY-P concentration varies within a small range. Since CW bias is the direct measure of tumbling rate, this means the probability for a cell to tumble is vanishingly small when CheY-P level falls below a certain value, and when CheY-P level goes slightly higher, the tumbling probability becomes very close to 1 and the cell almost always tumbles.

When attractant molecules bind to MCP proteins the levels of CheY phosphate drops and the lack of phosphorylated CheY protein(CheY-P) results in CCW rotation of

the flagellum, so that smooth run occurs. E. coli must be able to compare between the most recent attractant concentration to the immediately previous one. This is accomplished by methylation of MCP. CheR continuously methylates MCP whereas phosphorylated CheB protein removes the methyl group. When attractant binds to MCP the CheA-CheW-receptor complex becomes a good substrate for CheR and poor substrate for CheB-P. The levels of CheB-P drops because of phosphorylation of CheA is inhibited. Similarly removal of attractant causes the stimulation of autophosphorylation of CheA, which increases the levels of CheY-P and CheB-P. This simultaneously induces tumbles and demethylation and the system returns to the lower level of autophosphorylation.

For the system to operate in an inhomogeneous concentration field the adaptation mechanism must be precise, i.e. the E. coli bacteria must have a well defined internal signaling mechanism so that the rotational bias of the flagellar motors returns to their prestimulus value. Though adaptation need not be exact, but it has to be sufficiently precise to keep cells somewhere near the middle of the motor response curve. In the model of Barkai and Leibler [13], receptors are in either of two states: active or inactive. Perfect adaptation is achieved by allowing only methylated receptors to be active, specifying that CheR works at saturation, and letting CheB-P act only on receptors that are active. In this scheme, adaptation is robust, in the sense that return to the initial steady state occurs even when the concentrations of system components vary widely. This proposition has been confirmed experimentally [14].

1.1.3 The collective behavior of E. coli chemotaxis

Most of the studies in the literature are related to the collective motion of the bacteria and pattern formation. In 1976 Adler showed the formation of chemotactic rings in swarm assay which was useful for finding the mutant cells. The formation of chemotactic rings involves interactions between cells that influence one another to remove the chemoattractants from the growth medium. Rings also form when chemoattractants are absent in the growth medium [15], provided that cells excrete a chemoattractant and this phenomenon was also explained by a mathematical model [16]. When cells of E. coli under conditions of certain cellular stresses excrete attractants, they form different types of stable multicellular structures. Fluorescence microscopy was used to characterize the macroscopic properties of the clusters and to track individual E. coli cells in the clusters in real time. In a quantitative analysis [17] this equilibrium

cluster size, tumble frequency of an individual cell and the morphology of the cluster were determined. By considering the E. coli as self-propelled particles undergoing run-and-tumble dynamics and adding both interactions and noise to the particle density one can explain the domain formation by 'self-trapping' and other collective phenomena [18]. In recent studies one found the emergence of spontaneously forming migrating bands of E.coli bacteria inside a microchannel containing microstructured ratchets [19]. A decrease of bacterial motility with density can also produce a phase separation of two coexisting densities and which is an arrested nonequilibrium phase separation in which dense droplets or rings become separated by less dense regions, with a characteristic length scale [20]. The bacteria, in their natural environment, need to extract useful information from complex temporal signals that vary over a wide range of intensities and time scales. Tu et al. [21] studied how this signal is processed by E. coli during chemotaxis, by developing a theoretical model based on receptor−receptor cooperativity and receptor adaption. Measured responses to various monotonic, oscillatory, and impulsive stimuli are all explained consistently by the underlying adaptation kinetics within this model. This model provides a quantitative system-level description of the chemotaxis signaling pathway and can be used to predict E. coli chemotaxis responses to arbitrary temporal signals.

1.1.4 Single cell behavior of *E.coli* chemotaxis

For a given response function the E. coli bacterium can be thought of as a biased random walker. Schnitzer [22] formulated a general theory of random walks in continuum, considering the collision rate is a direction dependent quantity. This consideration leads to an effective Smoluchowski equation which enables a description of biased random walk of E. coli during chemotaxis. According to this model if the bacteria accumulate in higher concentration region during steady state then the response function of cells which perform temporal comparison between the attractant concentration must be positive and cells which measures averages of the attractant concentration must be negative. This former prediction explains the observed behavior of wild-type cells but the later behavior has not bee observed. De Gennes [23] calculated the drift velocity of a chemotactic bacteria moving up to the gradient during the life time of CCW rotation of the flagella. The drift velocity was found to be proportional to the concentration gradient in this calculation. In the short run, a favorable response function should move bacteria up chemoattractant gradients and in the long run, bacteria should aggregate at peaks of chemoattractant concentration,

Clark et. al [24] shows that these two criteria conflict, so that when one performance criterion is most favorable, the other is unfavorable. If both performance criteria are used to calculate the response function, the theoretical function closely matches the empirical biphasic bias curve measured by Segall et al. [7]. In another studies Celani and Vergassola [25] shows that the experimental bacterial response corresponds to the maximin strategy that determines the highest minimum uptake of chemoattractants for any profile of concentration. They have also shown that the maximin response is the unique one that always outcompetes motile but nonchemotactic bacteria. The maximin strategy is adapted to the variable environments experienced by bacteria.

A study by Chatterjee et. al [26] shows that actually there is no conflict between the different performance criterion observed in different time regime. They have modeled the E coli bacteria as non-markovian random walker with drift velocity V and diffusion coefficient D. In linear concentration profile for non-adaptive response function the competition between the constant drift velocity and position dependent diffusion coefficient will determine whether they will accumulate in the higher concentration region or not. For adaptive response function the bacteria will behave like a biased random walker and accumulate in higher food concentration region. This model also can explain the results obtained in ref [22].

Although there are many theoretical and simulation results for single cell, many early experiments for *E. coli* chemotaxis were done with population average to reduce the noise. Inside a single cell, the number of protein molecules which take part in the reactions, is often small depending on the type of the signaling protein. This small number of proteins gives rise to the fluctuation inside a single cell and in recent experiment it is shown that this fluctuation has significant role in the tumble bias of an unstimulated cell over long time scale. In absence of any noise in the signaling pathway, the switching of rotational bias of the flagellar motors is expected to be a Poisson process and consequently, the duration of a particular run or tumble should follow an exponential distribution. However, in [27] the switching events of a single cell in an isotropic medium were monitored in experiment and the residence time of the motors in the CCW bias was found to follow a power law distribution. It was argued that the stochastic fluctuation present in the methylation/demethylation process mediated by CheR and CheB makes it possible to have large fluctuations in the CCW lifetimes and consequently, the cell can execute really long runs with significant probability. Since the number of CheR and CheB proteins are of the order of $200 - 400$ in comparison to the total methylation site of the order of $60,000$,

the CheR and CheB proteins work at saturation so that adaption of the cell can withstand a large variation of behavior of the adapted cell.

In [28] a theoretical model was considered where the CCW and CW bias states of the motors were modelled as a two-level system whose energy levels depend on the concentration of the motor protein CheY-P, and as the noise present in the network causes this protein number to fluctuate, the energy levels also fluctuate with time. It was explicitly shown that such fluctuations give rise to power law distribution for the lifetime of the CCW state. Similar power laws have been obtained by considering the fluctuations in CheR protein level in the pathway of non-stimulated cells [29, 30]. For a single bacterial motor, the time-series of switching events were experimentally measured and for large CW bias, which corresponds to higher CheY-P level, and hence smaller fluctuations, the CCW intervals show exponential distribution, while for small CW bias, when fluctuations in CheY-P level are more significant, CCW intervals show power law distribution [31, 32].

Interestingly, the large fluctuations present at the single cell level do not impair the chemotactic response or robust adaptation [13, 14] observed at the population level [33]. The ultra-sensitivity of the signaling network, caused by break down of first order reaction kinetics, is responsible for amplification of molecular noise and generating large variability on one had, and giving rise to accurate chemotactic response to small stimuli, on the other [34]. The behavioral variability and chemotactic response are infact found to be related to each other via fluctuation-response theorem which enables one to predict the response from pre-stimulus variability [35]. In [36] it has been shown that the overall chemotactic performance improves as a result of interplay between the signaling noise and multiple flagellar motors. While presence of multiple motors brings down the motor response time, the lack of coordination in their switching may interrupt the long runs. In presence of a steep gradient of chemo-attractant concentration, a shorter response time is beneficial, but when the gradient is shallow, longer runs are typically needed to perform chemotaxis. Presence of noise in the signaling pathway generates longer runs and improves the chemotactic performance in shallow gradients [36]. In [37] a direct coupling between the flagellar motors was suggested as a possible mechanism of their coordinated switch. The benefit of network noise for special choices of the nutrient concentration profile was highlighted in [38] where by studying the motor response to the noisy output of signaling network it was shown that in presence of a sinusoidal concentration profile of the nutrient, the long term chemotactic performance of the cells does not improve as the noise falls below

a threshold level. Moreover, the chemotactic drift velocity for an exponential gradient of nutrient concentration is enhanced with noise and reaches a maximum value at a noise level which is comparable to the above threshold value [38]. Noise may prove beneficial even in a more generic nutrient environment, where large variability in a cellular population ensures that different cells behave in different ways and each type of behavior may be suitable for one particular type of environment [39, 40]. In [41] the motor response was studied for wild-type and mutant bacterial cells and by comparing the response obtained in models with and without noise, it was shown that noise enhances the chemotactic sensitivity of the signaling network. In [33] the connection between cellular noise and robust adaptation was directly probed in experiment. The correlations between the motile behavior of the cell and the number of CheR and CheB protein molecules in the signaling network were measured and it was shown that while the mean behavior of the cell depends on the ratio of CheR and CheB, the variance can be changed by tuning the global concentration levels of these two proteins. This shows that it is possible to control variability of a cell population without affecting the robustness, which is related to the mean behavior. In more recent experiments [42, 43] it is shown that the fluctuation present in the single cell not only comes from the proteins involved in the adaptation mechanism but also from the allosteric interactions within receptor clusters.

1.2 Motivation and the plan of the thesis

In this thesis, we are interested in two broad questions. The first one is related to chemotactic performance of an E. coli cell and the second one is related to its run-and-tumble motion. We briefly describe these questions below.

We ask how the chemotactic performance depends on the extra-cellular nutrient environment and the intra-cellular biochemical conditions. Particularly, are there any optimum conditions that make this performance most efficient? For an efficient chamotactic performance, the cell should be able to find the nutrient-rich regions quickly and localize there. We identify a set of well-defined response functions which characterize different aspects of chemotactic performance and study their dependence on the extra-cellular environments as well as the intracellular signaling pathway [44] of the bacteria. For quick search process we measure the average first passage time, which is defined as the time taken to reach the target for the first time (or complete the search process). An efficient search process corresponds to a short first passage

time [45–47]. The chemotactic drift velocity is defined as the steady state average velocity with which the cell climbs up the chemical concentration gradient, and larger values of drift velocity clearly indicates a better performance. The nutrient concentration, averaged over the steady state distribution of the cell position, measures how effectively the cells are localized in the nutrient-rich regions. For many time dependent nutrient concentrations, the study of the amount of nutrient encountered by the cell along its trajectory, which is called uptake [25], becomes useful to study. We investigate how these different response functions depend on the external environment and the internal biochemical pathway of the E. coli cell and at what conditions the chemotactic performance becomes most efficient.

The second question of this thesis deals with the run-and-tumble motion of the cell. Experiments[12] show that the CW bias of the flagellar motors has a sensitive dependence on the intra-cellular concentration of CheY-P motor protein which fluctuates with time. As the CheY-P level varies within a small range, the CW bias changes from 0 to 1. Since CW bias is interpreted as the tumbling probability of the cell, this means the tumbling probability is zero (one) as the CheY-P concentration falls below (above) a certain small range. These observations give rise to a more general and interesting theoretical question: what is the effect of a sharp or sigmoidal switching response on a simple run-and-tumble motion? To address this general question, we consider a run-and-tumble random walker whose switching probabilities between run and tumble modes depend on a certain (stochastic) input signal. We characterize the motion of this random walker in the long time limit, and investigate how the fluctuations present in the input signal affect the motion.

In Chapter 2 we study chemotaxis motion of a single bacterium in presence of a diffusing nutrient profile. We take a Gaussian concentration field of the nutrient and measure the average first passage time of the bacterium at the neighborhood of the Gaussian peak using Monte Carlo simulation. When the nutrient diffuses very slowly, the average first passage time shows a minimum as a function of σ, where σ is the width of the nutrient at the time of starting the chemotaxis. In other words, there is an optimum value of σ for which the search process is most efficient. This finding is interesting, since σ is a parameter that can be easily tuned in an experiment and our study shows that when σ is set at a special value, the bacterium becomes the most efficient searcher and is able to find its favorable region in the shortest possible time. We also perform analytical calculations of mean first passage time within a coarse-grained model which allows an approximate Markovian

description of the bacterial motion [26]. We find reasonably good agreement between our analytics and numerics. We consider deterministic initial condition as well as stochastic initial condition, drawn from uniform and steady state distribution. In all the cases our numerical simulation and analytical calculations show existence of an optimum width of the nutrient concentration profile when the search process is most efficient. For time-varying nutrient concentration profile, our simulations show that if the chemotaxis starts at an early stage of nutrient diffusion, when the width of the Gaussian is still small, then the mean first passage time shows a minimum as a function of the nutrient diffusivity. But if the chemotaxis starts at a late stage, when the nutrient has already spread considerably in the medium and the width of the Gaussian profile is large, the mean first passage time increases monotonically with nutrient diffusivity.

In Chapter 3 we see the effects of the fluctuation present in the chemotactic pathway on the behavior of a single cell E. coli bacterium in presence of a homogeneous nutrient environment. We argue that the most important source of signaling noise is the methylation-demethylation reaction. Our simulation results show that while for small noise, the run-length distribution is exponential, as noise increases, the distribution becomes a power law. We also calculate the CheY-P level distribution, which is important for the bacterial run-tumble motion, analytically for various strength of methylation noise. From this we calculate the average run-length of the bacterium, when there is a constant background concentration. We found a good agreement between the analytics and the simulation results. The CheY-P level distribution becomes narrow if the noise is small but for very large noise distribution becomes wide and develops a long tail.

In Chapter 4 we study the effects of noise in the signaling pathway on the efficiency of chemotactic performance of a single cell in presence of a nutrient concentration profile that varies in space but does not change with time. For this we study the variation of localization and drift velocity. Our simulation shows that, the localization and drift velocity show non-monotonic variation with noise strength. There is an optimal noise strength at which each of these quantities becomes maximum. As explained in second paragraph of this section, these quantities characterize different aspects of the chemotactic performance and our result shows that a particular noise level in the intracellular reactions brings out the best possible performance from the bacterial cells. This finding is rather interesting and counter-intuitive. We explain this striking effect by performing detailed measurement of CheY-P level statistics. We argue that

the chemotactic response is the result of differential behavior of the cell up and down the nutrient concentration gradient. At very large noise level, this difference becomes small since the tumbling frequency is almost totally controlled by the stochastic fluctuations of the methylation level, and not by the local nutrient concentration. The chemotactic performance is therefore poor when noise level is high. To understand why the performance gets worse again when the noise level is very low, we resort to a detailed analysis of CheY-P level fluctuation. We show that when CheY-P level falls below a certain threshold value, the cell shows a tendency to migrate towards regions of low nutrient concentration, which affects its overall chemotactic performance adversely. This threshold value decreases with noise strength, and hence the performance improves with noise.

In Chapter 5 we consider the case where the chemoattractant concentration has an explicit time-dependence, *e.g.* the chemoattractant molecules can have a finite lifetime, beyond which it degrades, or the molecules can perform diffusive motion in the medium. In such situations, the long term chemotactic performance, based on the steady state location of the cells, may not be a suitable criteria to consider. Rather an efficient chemotaxis in this case will involve climbing up the concentration gradient while it lasts, and spotting the nutrient-rich regions as quickly as possible. For this case we measure the first passage time and the uptake of the bacterium and see the effects of the noise on this quantities. We find that the first passage time of the cell decays monotonically with noise. Since long runs are more probable at large noise, the cell explores the system faster and the first passage time goes down. For time-dependent environment, when the nutrient is degrading, or diffusing in the medium, our measurement of uptake again shows a peak at a particular noise strength. However, in this case, there are more parameters in the system, *e.g.* lifetime or diffusivity of the nutrient, and one has to tune these parameters also to find the best chemotactic performance.

The simple biochemical pathway model that we have used in Chapters 3,4 and 5 does not include the adaptation mechanism of the flagellar motors. To verify how sensitive our results are on motor adaptation properties, we have studied in Chapter 6 a model that explicitly considers motor adaptation. We find that all our qualitative conclusions remain valid in this case.

In Chapter 7, we address the second broad question of the thesis, that is related to run-and-tumble motility in general. We define a simple run-and-tumble random walker whose switching probability from run mode to tumble mode and the reverse

depend on a stochastic signal. We consider a particularly sharp, step-like dependence. We are interested in characterizing the effect of signaling noise on the long time behavior of the random walker. We consider two different time-evolutions of the stochastic signal. In one case, the signal dynamics is an independent stochastic process and does not depend on the run-and-tumble motion. In this case we can analytically calculate the mean value and the complete distribution function of the run duration and tumble duration. In the second case, we assume that the signal dynamics is influenced by the spatial location of the random walker. For this system, we numerically measure the steady state position distribution of the random walker. We discuss some similarities and differences between this simple random walk model and the system of E. coli chemotaxis.

Bibliography

[1] Berg HC (2003) E. coli in Motion (Springer-Verlag, NewYork).

[2] Adler, J. 1976. The Sensing of Chemicals by Bacteria, Sci. Am. 234 (4): 40-47.

[3] Linda Turner, William S. Ryu and H. C. Berg, Real-Time Imaging of Fluorescent Flagellar Filaments, Journal of Bacteriology, May 2000, p. 27932801 Vol. 182, No. 10.

[4] Berg, H. C. , and D. A. Brown. 1972. Nature 239:500-504.

[5] Larsen, S.H., R.W. Reader, E. N. Kort, W. Tso, and J. Adler. 1974 Nature 249:74-77.

[6] Steven M. Block, Jeffrey E. Segall Howard C. Berg Cell, Vol. 31, 215-226, November 1982.

[7] J, E. Segall, S. M. Block, and H. C. Berg Proc. Nati. Acad. Sci. USA Vol. 83, pp. 8987-8991, December 1986 Biophysics.

[8] M Eisenbach Molecular Microbiology (1996) 20(5), 903-910.

[9] Victor Sourjik and Howard C. Berg NATURE VOL 428 25 MARCH 2004.

[10] Joseph J. Falke, Randal B. Bass, Scott L. Butler, Stephen A. CheRvitz, and Mark A. Danielson. Annu Rev Cell Dev Biol. 1997 ; 13: 457512.

[11] Bren A, Eisenbach M (2000) How signals are heard during bacterial chemotaxis: protein-protein interactions in sensory propagation. J Bacteriol 182: 6865-6873.

[12] Cluzel P, Surette M, Leibler S (2000) An ultrasensitive bacterial motor revealed by monitoring signaling proteins in single cells. Science (New York, NY) 287:1652-1655.

[13] N. Barkai and S. Leibler, Robustness in simple biochemical networks, Nature 387, 913 (1997).

[14] U. Alon, M. G. Surette, N. Barkai and S. Leibler, Robustness in bacterial chemotaxis, Nature 397, 168 (1999).

[15] Budrene, Elena O.; Berg, Howard C Volume 376(6535), 6 July 1995, pp 49-53.

[16] Michael P. Brenner, Leonid S. Levitov, and Elena . Budrene Biophysical Journal, Volume 74, April 1998, 16771693.

[17] Nikhil Mittal, Elena O. Budrene, Michael P. Brenner, and Alexander van Oudenaarden PNAS, November 11, 2003, vol. 100,no. 23, 13259-13263.

[18] J. Tailleur and M. E. Cates PRL 100, 218103 (2008).

[19] Guillaume Lambert, David Liao, and Robert H. Austin PRL 104, 168102 (2010).

[20] M. E. Cates, D. Marenduzzoa, I. Pagonabarragab, and J. Tailleur PNAS June 29, 2010 vol. 107 no. 26 1171511720.

[21] Yuhai Tu, Thomas S, Shimizu, and Howard C. Berg PNAS September 30, 2008 vol. 105 no. 39 1485514860

[22] M J Schnitzer vol 48, no 4, Physical Review E.

[23] P.-G. de Gennes Eur Biophys J (2004) 33:691-693.

[24] Damon A. Clark and Lars C. Grant 9150 9155, PNAS, June 28, 2005, vol. 102, no. 26.

[25] Celani A, Vergassola M (2010) Bacterial strategies for chemotaxis response. Proc Natl Acad Sci USA 107: 13911396.

[26] S. Chatterjee, R.A Seilveria, Y Kafri(2011) Chemotaxis When Bacteria Remembers:Drift vs Diffusion. PLoS Comp. Biol. volume:7 Issue:12.

[27] Korobkova E, Emonet T, Vilar JM, Shimizu TS, Cluzel P (2004) From molecular noise to behavioural variability in a single bacterium. Nature 428:574-578.

[28] Tu Y, Grinstein G (2005) How White Noise Generates Power-Law Switching in Bacterial Flagellar Motors, PRL 94, 208101.

[29] F. Matthaus, M. Jagodic and J. Dobnikar, E. coli Superdiffusion and Chemotaxis-Search Strategy, Precision, and Motility, Biophys. J. 97, 946 (2009).

[30] F. Matthaus, M. S. Mommer, T. Curk and J. Dobnikar, On the Origin and Characteristics of Noise-Induced Lévy Walks of E. Coli, PLoS ONE 6, e18623 (2011).

[31] E. A. Korobkova, T. Emonet, H. Park and P. Cluzel, Hidden stochastic nature of a single bacterial motor, Phys. Rev. Lett. 96, 058105 (2006).

[32] H. Park, P. Oikonomou, C. C. Guet and P. Cluzel, Noise Underlies Switching Behavior of the Bacterial Flagellum, Biophys. J. 101, 2336 (2011).

[33] Dufour YS, Gillet S, Frankel NW, Weibel DB, Emonet T. Direct correlation between motile behaviors and protein abundance in single cells. PLoS Comput Biol. 2016 Sep;12(9):e1005041.

[34] Emonet T, Cluzel P (2008) Relationship between cellular response and behavioral variability in bacterial chemotaxis. Proc Natl Acad Sci U S A 105:33043309.

[35] Park H, Pontius W, Guet CC, Marko JF, Emonet T, et al. (2010) Interdependence of behavioural variability and response to small stimuli in bacteria. Nature 468: 819823.

[36] Sneddon MW, Pontius W, Emonet T (2012) Stochastic coordination of multiple actuators reduces latency and improves chemotactic response in bacteria. Proc Natl Acad Sci U S A 109: 805810.

[37] Hu B, Tu Y (2013) Coordinated Switching of Bacterial Flagellar Motors: Evidence for Direct Motor-Motor Coupling?. PRL 110, 158703.

[38] Flores M, Shimizu TS, ten Wolde PR, Tostevin F (2012) Signaling noise enhances chemotactic drift of E. coli. PRL 109, 148101.

[39] Frankel NW, Pontius W, Dufour YS, Long J, Hernandez-Nunez L, Emonet T (2014) Adaptability of non-genetic diversity in bacterial chemotaxis, eLife Sciences Publications Limited; 2014; 3: 130.

[40] Taute KM, Gude S, Tans SJ, Shimizu TS (2015) High-throughput 3D tracking of bacteria on a standard phase contrast microscope, Nat Commun. Nature Publishing Group; 6: 8776.

[41] He R, Zhang R, Yuan J (2016) Noise-Induced Increase of Sensitivity in Bacterial Chemotaxis. Biophys J 111:430437.

[42] R. Colin, C. Rosazza, A. Vaknin and V. Sourjik, Multiple sources of slow activity fluctuations in a bacterial chemosensory network, eLife 6, e26796 (2017).

[43] N W Frankel, W Pontius, Y S Dufour, J Long, L Hernandez-Nunez, T Emonet, Adaptability of non-genetic diversity in bacterial chemotaxis, eLife 2014;3:e03526 (2018).

[44] Sourjik V (2004) Receptor clustering and signal processing in E.coli chemotaxis. Trends Microbiol 12: 569-576.

[45] Redner S (2007) A guide to first-passage processes. New York: Cambridge University Press, first edition.

[46] M. R. Evans and S. N. Majumdar, Phys. Rev. Lett. 106, 160601 (2011); ,J. Phys. A 44, 435001 (2011); M. R. Evans, S. N. Majumdar, and K. Mallick, *ibid.* 46, 185001 (2013).

[47] L. Kusmierz, S. N. Majumdar, S. Sabhapandit, and G. Schehr, Phys. Rev. Lett. 113, 220602 (2014).

Chapter 2

Effects of extracellular environment on search process of E. coli

2.1 Introduction

In a wide variety of physical systems, search process plays an important role [1]. Examples can be found in systems like animals searching for food [2], proteins searching for the binding site on DNA [3], or in general diffusion-limited reactions [4]. A search process is often characterized by the first passage time, which is defined as the time taken to reach the target for the first time (or complete the search process). An efficient search process corresponds to a short first passage time. Therefore it is crucial to determine how the first passage time depends on the system parameters. The most efficient search strategy is often determined by looking into the minimum of the first passage time in this parameter space [5, 6]. Here we consider the search process in one of the most well-studied biological systems, *viz.* E.coli chemotaxis, which describes the motion of E. coli bacteria in response to a chemical concentration gradient. When such bacteria are placed in an inhomogeneous concentration of a nutrient, they show a tendency to migrate towards the nutrient-rich region. We ask the question: how long does it take for the bacteria to find the most favorable region and under what conditions this search process is most efficient.

Now imagine a situation where a puff of nutrient is injected into the medium such that immediately after injection, all the chemical is concentrated in a narrow region. As time goes on, this chemical spreads over the medium via diffusion and at any given time its concentration profile has the form of a Gaussian. At a certain stage of this nutrient diffusion, when the nutrient has already spread through some distance in the medium, a bacterium is released somewhere in the medium which then performs chemotaxis. If the time-scale of nutrient diffusion is much longer than that of bacterial motion, the bacterium would effectively experience a Gaussian concentration profile of fixed width. When the nutrient diffusion and bacterial motion occur over comparable time-scales, then the concentration sensed by the bacterium will be time-dependent and can be described as a Gaussian whose width keeps increasing (and peak height keeps decreasing) with time, as follows from the diffusion equation. The region around the peak of the Gaussian profile is the most favorable region for the bacteria, where the nutrient concentration is highest.

In this chapter, we study chemotaxis motion of a single bacterium in presence of a Gaussian concentration field of the nutrient. We measure the average and the typical first passage time of the bacterium at the neighborhood of the Gaussian peak using Monte Carlo simulation. For slow nutrient diffusion we found that the average first passage time shows a minimum as a function of σ, where σ is the width of the nutrient at the time of starting the chemotaxis. In other words, there is an optimum value of σ for which the search process is most efficient. This finding is interesting, since σ is a parameter that can be easily tuned in an experiment and our study shows that when σ is set at a special value, the bacterium becomes the most efficient searcher and is able to find its favorable region in the shortest possible time. We also perform analytical calculations of mean first passage time within a coarse-grained model which allows an approximate Markovian description of the bacterial motion [7]. We find reasonably good agreement between our analytics and numerics. We consider deterministic initial condition as well as stochastic initial condition, drawn from uniform and steady state distribution. In all the cases our numerical simulation and analytical calculations show existence of an optimum width of the nutrient concentration profile when the search process is most efficient.

In the case when the time-scale of nutrient diffusion is comparable to that of bacterial motion, the bacterium experiences a time-varying concentration profile—a Gaussian whose width increases with time. The search process now crucially depends on the nurtrient diffusivity, as well as the extent of spread of the nutrient in the medium at

the onset of chemotaxis. Our simulations show that if the chemotaxis starts at an early stage of nutrient diffusion, when the width of the Gaussian is still small, then the mean first passage time shows a minimum as a function of the nutrient diffusivity. But if the chemotaxis starts at a late stage, when the nutrient has already spread considerably in the medium and the width of the Gaussian profile is large, the mean first passage time increases monotonically with nutrient diffusivity.

In the next section 2.2, we present our model for simulation and the coarse-grained model for analytical calculation of the first passage time in presence of time-independent Gaussian concentration profile. Sections 2.4 and 2.5 contain our analytical and numerical results, respectively, for a time independent Gaussian nutrient concentration. In section 2.6 we present our results for time-varying Gaussian concentration field. The conclusion is presented in section 2.7.

2.2 Model for the simulation and measurement of the first passage time

Following [7–9] we model the motion of a single bacterium in one dimension as a non-Markovian random walker whose dynamics is governed by runs and tumbles. During a run the bacterium moves along one particular direction with a fixed velocity. The duration of a run is a stochastic variable and follows a Poissonian distribution with a mean of one second in a homogeneous medium [10–12]. At the end of a run, the bacterium goes into a tumbling mode, when it rotates about itself in a random fashion, without much net displacement, before it starts running again in a new direction. An average tumble duration ($0.1s$) being much smaller than runs , tumbles are modeled as instantaneous events which allow the bacterium to change its direction between two successive runs. The probability that the run direction is changed (reversed) is denoted as q. In presence of a nutrient concentration gradient in the medium, the tumbling rate depends on the recent history. The probability that a running bacterium tumbles during a time-interval $[t, t + dt]$ is then given by

$$\frac{dt}{\tau}\left(1 - \int_{-\infty}^{t} dt' R(t - t')c[x(t')]\right) \tag{2.1}$$

where τ is the mean run duration in a homogeneous environment, $c[x(t')]$ is the concentration experienced at a past instant $t' < t$ and $R(t)$ is the response kernel.

$R(t)$ contains information about the signaling pathway present inside the bacterial cell and it was measured experimentally for wild type bacteria in [12, 13]. $R(t)$ was shown to have a bilobe shape, with a relatively sharp positive lobe at smaller t and a shallow negative lobe at larger t that vanishes for $t \gtrsim 4s$ (see Fig. 1.1).

We are interested in the linear response regime, where the integral in Eq. 2.1 is much less than unity. Within this linear regime, one can decompose the above bilobe response kernel into a sum of delta-functions of suitably chosen amplitude and can be written as $R(t) = \sum_{i=1}^{n} \alpha_i \delta(t - \Delta_i)$, so that the Eq. 2.1 becomes

$$\frac{dt}{\tau}\left(1 - \sum_{i=1}^{n} \alpha_i c[x(t - \Delta_i)]\right) \tag{2.2}$$

where, α_i's are the amplitudes of single delta function response functions and Δ_i's are the memory parameters. For $\Delta_i = 0$, the tumbling probability at time t in Eq. 2.2 depends on the nutrient concentration experienced by the bacterium at time t, hence the process becomes Markovian. But for non-zero Δ_i's the tumbling probability will depend on the concentration experienced at time $t-\Delta_i$, which makes the process Non-Markovian. We have chosen $\alpha_i << 1$ for all delta functions so that the summation in Eq. 2.2 becomes much less than the unity. We first consider a single delta function $R(t) = \alpha\delta(t-\Delta)$ and analyze this case in detail, where we keep terms only upto first order in α. Later we generalize our results for the full response kernel by superposing the solutions for this single delta-function kernels to obtain the solution for the full bilobe response.

We perform our simulation on a one dimensional box of size L, with reflecting boundary walls at the two ends. In a time-interval dt the bacterium moves by a distance vdt. At the end of each time-step, we compute the tumbling probability, as in Eq. 2.2. For an impulse response function $R(t) = \alpha\delta(t - \Delta)$, the tumbling probability at time t is given by $dt/\tau\,(1 - \alpha c[x(t - \Delta)])$, where $x(t - \Delta)$ is the position of the bacterium at a time Δ back in the past, $c[x(t - \Delta)]$ is the concentration experienced by the bacterium at that past instant of time. At the end of one time-step the bacterium attempts to tumble with this probability. If the tumbling attempt is unsuccessful, it continues to move in the same direction with same velocity v and if the tumbling attempt is successful, the bacterium changes its direction (in this one-dimensional case, it reverses the sign of v) with probability q. Starting from a given initial position x at $t = 0$, we measure the first passage time at a position x_0, and average

over different trajectories. In order to avoid the region with rapid spatial variation of the concentration field, we consider a target which is one mean free path away from the Gaussian peak in the same direction as the starting position of the bacterium: $x_0 = \overline{x} - v\tau$.

2.3 Analytical calculation in a coarse-grained Markovian description

In an earlier study [7] a coarse-grained model was proposed for describing a single bacterium in a nutrient concentration gradient in one dimension. The bacterium was assumed to be confined in a one-dimensional box of length L with reflecting boundary walls. Although the underlying run-tumble motion is non-Markovian, one can still expect that at a coarse-grained level, a Markovian description might be possible. For this purpose, we coarse-grain over a time-scale which is much larger than the typical run-duration τ and assume that the average bacterial density within the spatial resolution of coarse-graining, which is much greater than $v\tau$, has a Markovian dynamics. For the time-evolution of this coarse-grained density $P(x,t)$ at point x, at time t, the following Fokker-Planck equation was formulated in [7].

$$\partial_t P(x,t) = -\partial_x \left[V(x)P(x,t) - \partial_x(D(x)P(x,t))\right] \tag{2.3}$$

which is the equation for a random walker with position dependent drift and diffusion. The chemotactic drift velocity $V(x)$ and the diffusivity $D(x)$ will depend on the nutrient concentration profile $c(x)$ and the dependence can be derived from the microscopic dynamics. In an earlier calculation by de Gennes[14] an approximate expression for the average displacement in a run was obtained within the simplifying assumption that whenever a running bacterium tumbles, its past memory is lost. The resulting expression for average displacement in a single run for $R(t) = \alpha\delta(t-\Delta)$

$$\Delta x = \alpha v^2 \tau^2 e^{-\frac{\Delta}{\tau}} \partial_x c(x) \tag{2.4}$$

was found to show good agreement with the simulation results in [7] for $q = 0.5$.

The drift velocity for $q \neq 1/2$ is given by [Appendix A],

$$V(x) = \alpha c \frac{v^2\tau}{2q}. \tag{2.5}$$

The above expression for drift velocity was calculated for the choice of response function $R(t) = \delta(t)$, where, $\Delta = 0$. For non-Markovian case where $\Delta \neq 0$, the Eq. 2.5 will have an extra factor $e^{-\frac{2q\Delta}{\tau}}$ as in Eq. 2.4. For a non-Markovian random walker in presence of any concentration profile $c(x)$ Eq. 2.5 becomes

$$V(x) = \alpha \frac{v^2\tau}{2q} e^{-\frac{2q\Delta}{\tau}} \partial_x c(x) \tag{2.6}$$

provided that the gradient remains small or in another words this expression is valid in weak gradient limit.

To calculate the diffusivity $D(x)$, the effective tumbling frequency was calculated within the coarse-grained model, by averaging over a population of non-interacting bacteria within the coarse-graining length-scale. Although the tumbling frequency of a single bacterium depends on the details of its past trajectory, this dependence is lost when averaged over a large number of bacteria with two possible run-directions in one dimension. The average tumbling frequency at a position x can be shown to be $[1 - \alpha c(x)]/\tau$ from which the diffusivity turns out to be [7]

$$D(x) = \frac{v^2\tau}{2q}[1 + \alpha c(x)]. \tag{2.7}$$

Using Eqs. 2.6 and 2.7 it can be easily shown from Eq. 2.3 that in the steady state the bacterial density $P(x)$ has the form

$$P(x) = P_0 + \alpha P_0 (e^{-\frac{2q\Delta}{\tau}} - 1) \left(c(x) - P_0 \int_0^L c(x)dx \right). \tag{2.8}$$

In the next section, we use the above coarse-grained model to calculate the mean first passage time of the bacteria at the nutrient-rich region. Note that unlike the steady state behavior, studied in [7], we study first-passage properties, away from steady state.

2.4 Analytical calculation of first passage time

Let $P(y, t|x, 0)$ be the conditional probability to find the bacterium at position y at time t, given that it started at x at $t = 0$. This conditional probability follows the

backward Fokker-Planck equation [15]

$$\partial_t P(y,t|x,0) = V(x)\partial_x P(y,t|x,0) + D(x)\partial_x^2 P(y,t|x,0). \tag{2.9}$$

One should note that this Eq. 2.9 is different from the forward Fokker Plank equation, where the space derivative in the right hand is with respect to the current position at time t. But in this Eq. 2.9 the space derivative in r.h.s. is with respect to the initial position x at time $t = 0$. To find out the first passage time at a certain point x_0 (which we call the target), we consider an absorbing boundary at x_0, in addition to the reflecting boundary at $x = 0$ and $x = L$. Without any loss of generality, we perform all our measurements for $x < x_0$. The survival probability $G(x,t)$ that starting from an initial position x, the bacteria has not reached the target till time t can be written as $G(x,t) = \int_0^{x_0} dy P(y,t|x,0)$. From Eq. 2.9 it follows that $G(x,t)$ satisfies the following equation

$$\partial_t G(x,t) = V(x)\partial_x G(x,t) + D(x)\partial_x^2 G(x,t) \tag{2.10}$$

with the initial condition $G(x,0) = 1$. The reflecting and absorbing boundary conditions are implemented as $\partial_x G(0,t) = 0$ and $G(x_0,t) = 0$, respectively.

By definition, $G(x,t)$ is the probability that the first passage time of the walker starting from x to reach at $x = x_0$, is larger than t and hence the first passage time distribution is given by $-\partial_t G(x,t)$. Mean first passage time $T(x) = -\int_0^\infty dt\, t\, \partial_t G(x,t) = \int_0^\infty dt\, G(x,t)$ which follows the equation

$$V(x)\partial_x T(x) + D(x)\partial_x^2 T(x) = -1. \tag{2.11}$$

The solution of this equation has the form

$$T(x) = \int_x^{x_0} \frac{dy}{\psi(y)} \int_0^y \frac{\psi(z)}{D(z)} \tag{2.12}$$

where $\psi(x) = \exp\left[\int_0^x dx' V(x')/D(x')\right]$. Now, using Eqs. 2.6 and 2.7 and keeping terms only upto first order in α, one can write $\psi(x) = \exp\left[\alpha e^{-2q\Delta/\tau}\{c(x) - c(0)\}\right] = 1 + \alpha e^{-2q\Delta/\tau}[c(x) - c(0)]$. After few steps of simple algebra we finally have

$$\begin{aligned} T(x) = \; & \tfrac{2q}{v^2\tau}\big[\tfrac{x_0^2 - x^2}{2} - \alpha(1 - e^{-2q\Delta/\tau}) \textstyle\int_x^{x_0} dy \int_0^y dz\, c(z) \\ & - \alpha e^{-2q\Delta/\tau} \textstyle\int_x^{x_0} dy\, y\, c(y)\big] \end{aligned} \tag{2.13}$$

which can be written in the form $T(x) = T_0(x) + \alpha T_1(x)$, where $T_0(x)$ stands for the mean first passage time for the case when $V(x) = 0$ and $D(x) = \frac{v^2\tau}{2q}$, and $T_1(x)$ gives the first order correction term when position-dependent drift and diffusion are present, due to a spatially varying concentration field $c(x)$. In the rest of this chapter we focus on $T_1(x)$.

For a Gaussian concentration profile $c(x) = \dfrac{\exp[-(x-\overline{x})^2/2\sigma^2]}{\sqrt{2\pi\sigma^2}}$ the drift velocity $V(x)$ and diffusivity $D(x)$ show rapid variation close to the peak at $\overline{x}$. In our coarse-grained description, that allows for analytical treatment, we deal with length scales much larger than the mean free path of the bacteria and any spatial variation that occurs over a smaller length scale must be neglected in our coarse-grained model. When σ is not too large, the variation of $V(x)$ and $D(x)$ around the peak are too fast to be considered in our coarse-grained formalism. Because of this we avoid the peak position in our calculation of first passage time, by choosing the target position x_0 such that both the initial position x and the target lies on the same side of the peak. For our choice of $x < x_0 < \overline{x}$ we use the Gaussian $c(x)$ in Eq. 2.13 and get

$$\begin{aligned} T_1(x) \;=\; & \frac{2q}{v^2\tau}\Bigg[\frac{1}{2}Erf\left(\frac{\overline{x}-x_0}{\sqrt{2}\sigma}\right)\left(e^{-\frac{2q\Delta}{\tau}}(2\overline{x}-x_0)-(\overline{x}-x_0)\right) \\ & +\frac{1}{2}Erf\left(\frac{\overline{x}-x}{\sqrt{2}\sigma}\right)\left(e^{-\frac{2q\Delta}{\tau}}(x-2\overline{x})-(x-\overline{x})\right) \\ & +\frac{1}{2}Erf\left(\frac{\overline{x}}{\sqrt{2}\sigma}\right)\left(\left(e^{-\frac{2q\Delta}{\tau}}-1\right)(x_0-x)\right) \\ & +\left(e^{-\frac{(\overline{x}-x_0)^2}{2\sigma^2}}-e^{-\frac{(\overline{x}-x)^2}{2\sigma^2}}\right)\left(2e^{-\frac{2q\Delta}{\tau}}-1\right)\frac{\sigma}{\sqrt{2\pi}}\Bigg], \end{aligned} \tag{2.14}$$

where $Erf(x)$ is the Error function and defined as $Erf(x) = \frac{2}{\sqrt{\pi}}\int_0^x e^{-t^2}dt$.

So far we have considered the first passage time with a fixed initial condition, where the bacterium always starts from a fixed initial position x. But this initial condition easily can be generalized to the cases where, the initial position x is stochastic and can take any value within the interval $0 < x < x_0$, i.e. the initial position can lie anywhere between the left boundary and the target, with a certain distribution function. We consider two specific cases: (i) when x follows a uniform distribution P_0 and (ii) when x is drawn from the steady state distribution $P(x)$ in Eq. 2.8. In the first case, the α-order correction in the first passage time can be obtained by simply

integrating Eq. 7.10 over x:

$$\begin{aligned} T_1^{(u)} &= P_0 \int_0^{x_0} dx T_1(x) \\ &= \frac{2qP_0}{v^2\tau}\left[\frac{1}{4}\left\{Erf(\frac{\bar{x}}{\sqrt{2}\sigma}) - Erf(\frac{\bar{x}-x_0}{\sqrt{2}\sigma})\right\}\right. \\ &\quad \left\{e^{-\frac{2q\Delta}{\tau}}(x_0^2 - 3\bar{x}^2 - 3\sigma^2) - (x_0^2 - \bar{x}^2 - \sigma^2)\right\} \\ &\quad \left. + \frac{1}{2\sqrt{2\pi}}\sigma(3e^{-\frac{2q\Delta}{\tau}} - 1)\left((x_0+\bar{x})e^{-\frac{(x_0-\bar{x})^2}{2\sigma^2}} - \bar{x}e^{-\frac{\bar{x}^2}{2\sigma^2}}\right)\right] \end{aligned} \tag{2.15}$$

For the case (ii) the initial position x follows the steady state distribution in Eq. 2.8. The mean first passage time is then written as

$$\begin{aligned} \int_0^{x_0} dx P(x) T(x) &= \int_0^{x_0} dx \left[P_0 + \alpha P_0(e^{-\frac{2q\Delta}{\tau}} - 1)\right. \\ &\quad \left.\left(c(x) - P_0\int_0^L c(x)dx\right)\right](T_0(x) + \alpha T_1(x)) \,. \end{aligned} \tag{2.16}$$

For a Gaussian form of $c(x)$ the α-order term becomes

$$\begin{aligned} T_1^{(s)} &= P_0\int_0^{x_0} dx T_1(x) + P_0\frac{(e^{-\frac{2q\Delta}{\tau}} - 1)}{\sqrt{2\pi\sigma^2}}\int_0^{x_0} dx e^{-\frac{(x-\bar{x})^2}{2\sigma^2}} T_0(x) \\ &\quad -P_0^2(e^{-\frac{2q\Delta}{\tau}} - 1) Erf\left(\frac{x_0}{\sqrt{2}\sigma}\right)\int_0^{x_0} dx T_0(x) \end{aligned} \tag{2.17}$$

where $T_0(x)$ and $T_1(x)$ are defined in Eqs. 2.13 and 7.10. After straight-forward algebra the α-order term in first passage time with steady state initial condition becomes

$$\begin{aligned} T_1^{(s)} &= \frac{2qP_0}{v^2\tau}\left[\frac{1}{2}\left\{Erf\left(\frac{\bar{x}}{\sqrt{2}\sigma}\right) - Erf\left(\frac{\bar{x}-x_0}{\sqrt{2}\sigma}\right)\right\}\right. \\ &\quad \left(e^{-\frac{2q\Delta}{\tau_R}}(x_0^2 - 2\bar{x}^2 - 2\sigma^2) - (x_0^2 - \bar{x}^2 - \sigma^2)\right) \\ &\quad + \frac{\sigma}{\sqrt{2\pi}}\left(2e^{-\frac{2q\Delta}{\tau_R}} - 1\right)\left\{(x_0+\bar{x})e^{-\frac{(\bar{x}-x_0)^2}{2\sigma^2}} - \bar{x}e^{-\frac{\bar{x}^2}{2\sigma^2}}\right\} \\ &\quad \left. - \frac{P_0 x_0^3}{3}\left(2e^{-\frac{2q\Delta}{\tau_R}} - 1\right) Erf\left(\frac{\bar{x}}{\sqrt{2}\sigma}\right)\right] \end{aligned} \tag{2.18}$$

The results in Eqs 7.10, 2.16 and 2.18 are for an impulse response kernel $R(t) = \alpha\delta(t-\Delta)$ and these can be easily generalized for any arbitrary response function. In

the next section, we measure the first passage time in simulation and compare with above analytical calculation.

2.5 Simulation results on first passage time in presence of static Gaussian nutrient concentration

In Fig. 2.1 we show the variation of $T_1(x)$ with σ (discrete symbols) and compare with our analytical result in Eq. 7.10 (continuous lines). We find reasonably good agreement between our simulation and analytical calculation. For very small σ the concentration variation can be perceived only within a very narrow region around the peak $\overline{x}$. Hence the bacterial trajectory starting from x and ending at x_0, which does not cross the peak at $\overline{x}$, consists of isotropic diffusion for most part. As a result, in the limit of small σ the mean first passage time is given by that for an ordinary Brownian motion and is equal to $T_0(x)$ in Eq. 2.13 and the first order term $T_1(x)$ goes to zero. Similarly, in the limit of very large σ the profile is almost flat and even in this case the motion is close to isotropic diffusion and $T_1(x)$ vanishes. Our simulation and analytical calculation are consistent with this simple argument.

For intermediate σ values, $T_1(x)$ must show a non-monotonic variation, since it vanishes for small and large σ. We find a minimum for $T_1(x)$ at a particular width σ^*. In other words, there exists an optimal width σ^*, when the first passage time at the nutrient-rich region becomes shortest and the bacterium becomes the most efficient searcher. The bottom-right and the top-right insets of Fig. 2.1 show the variation of the optimal width σ^* as a function of the initial position x and the memory Δ of the bacterium, respectively. Note that even in the Markovian limit, when the bacterium does not have any memory, and in the long time limit does not accumulate in the nutrient-rich region [7], its first passage properties still show existence of an optimal width when the search is most efficient.

For wild-type bacteria, the response kernel has a bilobe shape and we can reconstruct the kernel as a linear superposition of impulse response functions with suitable amplitudes, as shown in Fig. 1.1. We use this response kernel to calculate the mean first passage time for various σ. Even for this adaptive bilobe kernel we find there exists an optimal width when the mean first passage time hits a minimum. Our analytical calculations show similar results. Interestingly, the value of the optimum width σ^* does not change even when the initial position and the target position are

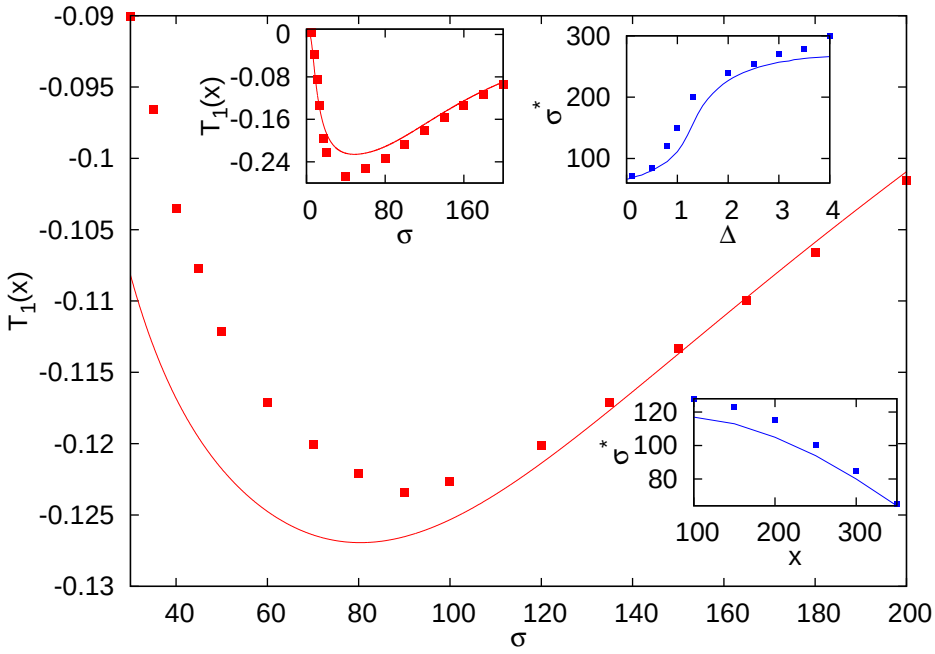

FIGURE 2.1: Results for the mean first passage time with a fixed initial position. The main plot shows $T_1(x)$ (in seconds) as a function of standard deviation σ (in μm) of the Gaussian nutrient concentration field with $R(t) = \alpha\delta(t - \Delta)$ and $\Delta = 0.5s$, $x = 300\mu m$. The top-right and bottom-left insets show the variation of the optimum width σ^* (in μm) as a function of Δ (in seconds) and the initial position x (in μm), respectively. The top-left inset shows $T_1(x)$ (in seconds) vs σ (in μm) variation for the bilobe response kernel, shown in Fig. 1.1. The discrete symbols correspond to simulations and the continuous lines correspond to analytical calculations. Here $L = 1000\mu m$, $x_0 = 490\mu m$, $\bar{x} = 500\mu m$, $q = 0.5$, $\tau = 1s$.

varied (data not shown here). In other words, an wild-type E.coli bacterium becomes the most efficient searcher when placed in an environment of Gaussian concentration profile of nutrient with a width of $\sim 50\mu m$.

Instead of starting from a fixed position, even when the initial position is a random variable which can choose any value between the left boundary wall at $x = 0$ and the target at $x = x_0$ with a certain distribution, our results show existence of an optimum σ that minimizes the first passage time. We have considered initial positions chosen from uniform distribution as well as from steady state distribution in Eq. 2.8 and present our data in Fig 2.2. Note that for the choice of a steady state initial condition, $T_1^{(s)}$ does not vanish in the limit of small σ but approaches a constant value. In other words, even when the width of the nutrient concentration profile is vanishingly small, the first passage time of the bacterium is not same as in a homogeneous medium. In fact when the system is in steady state, the bacterium has explored the full system and has already experienced the narrow concentration profile present in the middle

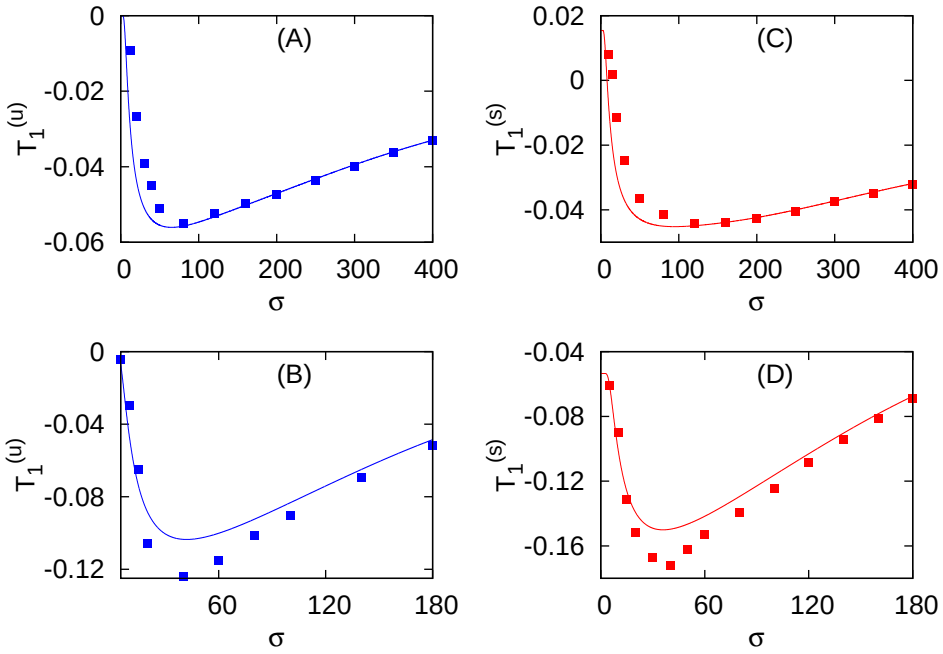

FIGURE 2.2: Mean first passage time with stochastic initial positions. Top panel shows data for impulse response $R(t) = \alpha\delta(t-\Delta)$ and bottom pannel for the bilobe response. (A) and (B) show data for uniform initial condition, when x can take any value in the range $[0, x_0]$ with uniform probability P_0. (C) and (D) show data for steady state initial condition, when the value of x in the range $[0, x_0]$ is drawn from the steady state distribution $P(x)$ in Eq. 2.8. Here the first passage time is measured in the units of seconds and σ in μm. The other simulation parameters are same as in Fig. 2.1. The discrete symbols are for numerical data and the continuous lines are for analytical calculations.

of the box. The steady state measure $P(x)$ is therefore not same as P_0, but contains information about the narrow concentration field. This gives rise to a non-vanishing α-order correction term in the limit $\sigma \to 0$.

2.6 First passage time for time-varying Gaussian concentration field

In this section, we consider the case when the nutrient diffusion in the medium occurs over a time-scale comparable to that of bacterial motion. The bacterium will then experience a time-varying concentration field. Our analytical formalism in section 2.4 does not work in this case and we study the system using numerical simulations. The simplest description of the nutrient concentration profile can be given by a Gaussian whose width is increasing with time: $c(x,t) = \exp\left(-\frac{(x-\overline{x})^2}{\sigma_0^2 + 4\mathcal{D}t}\right) / \sqrt{2\pi(\sigma_0^2 + 4\mathcal{D}t)}$,

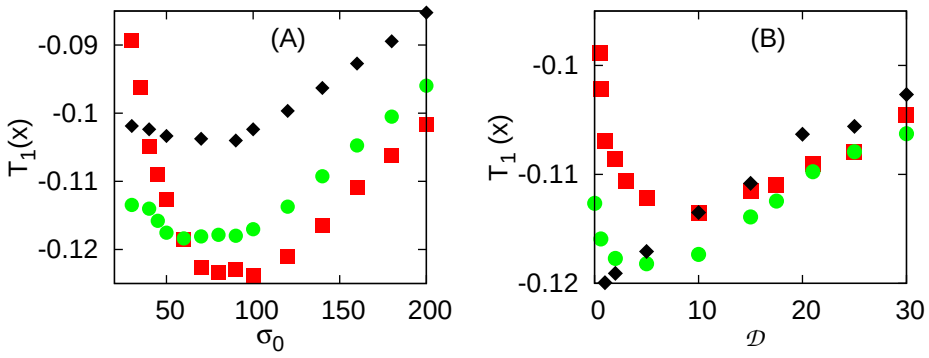

FIGURE 2.3: First passage time for time-dependent concentration of the nutrient. (A) shows the variation of $T_1(x)$ (in seconds) as a function of σ_0 (in μm) with $\mathcal{D}$ held fixed at $0.01\mu m^2/s$ (red squares), $10\mu m^2/s$ (green circles) and $37\mu m^2/s$ (black diamonds). (B) shows $T_1(x)$ (in seconds) vs $\mathcal{D}$ (in $\mu m^2/s$) plot for $\sigma_0 = 30\mu m$ (red squares), $50\mu m$ (green circles) and $120\mu m$ (black diamonds). The other simulation parameters are same as in Fig. 2.1 main plot.

where σ_0 is the width at the time when the chemotaxis motion starts, and $\mathcal{D}$ is the nutrient diffusivity.

The bacterial motion will depend on σ_0 and $\mathcal{D}$ depending on the time-scale $t_c \sim \sigma_0^2/\mathcal{D}$. For $t \ll t_c$ the motion depends on σ_0 and for $t \gg t_c$ the motion is mainly controlled by $\mathcal{D}$. In the limit of very small $\mathcal{D}$, therefore, one would expect the first passage time to be a function of σ_0 alone. In fact this is the limit when the nutrient diffusion is very slow, and during the time-interval of the first passage at the target, the width of $c(x,t)$ changes very little. In this limit, therefore, one expects similar results as in a static concentration profile. Our simulation data in In Fig. 2.3A indeed shows that for small $\mathcal{D}$ there is an optimum width σ_0 where $T_1(x)$ becomes minimum. As $\mathcal{D}$ increases, t_c becomes smaller when $T_1(x)$ does not show much variation with σ_0 and the minimum becomes less and less pronounced. In Fig. 2.3A we verify this.

In Fig. 2.3B we show the variation of $T_1(x)$ against $\mathcal{D}$ for fixed σ_0 values. For very large $\mathcal{D}$ the Gaussian profile quickly flattens out and the bacterial motion becomes an isotropic diffusion. In this limit $T_1(x)$ becomes zero. For very small $\mathcal{D}$ values, the limit for a static Gaussian profile is recovered and (as shown in our data in Fig. 2.1 main plot) $T_1(x)$ has a negative value that depends on σ_0. Therefore, for a given σ_0, as $\mathcal{D}$ is varied, $T_1(x)$ starts from a negative value at small $\mathcal{D}$ and becomes 0 at large $\mathcal{D}$. Whether this variation is monotonic or not depends on the choice of σ_0. Our data in Fig. 2.3B show that for large σ_0 the variation is monotonic but for small σ_0 a minimum is reached at a particular $\mathcal{D}$, *i.e.* there is an optimum diffusivity of

the nutrient when the search is most efficient. For our various choice of σ_0 values over a wide range (full dataset not presented here), we also notice that an optimum diffusivity is observed whenever σ_0 is fixed at a value smaller than σ^*, the optimum width for the static concentration profile (see Fig. 2.1 main plot). For $\sigma_0 > \sigma^*$, on the other hand, $T_1(x)$ increases monotonically with $\mathcal{D}$.

Above observation tentatively indicates that it may be possible to describe the results for the time-dependent nutrient concentration in terms of a static concentration profile with an 'effective width' σ_e. For a given value of σ_0 and $\mathcal{D}$ the width of $c(x,t)$ keeps increasing during bacterial motion—at the start of the motion the width is σ_0 and at the end of the first passage the average width is $\sqrt{\sigma_0^2 + 4\mathcal{D}T(x)}$. Let us assume that σ_e is some measure of the average or effective width experienced by the bacterium during this process. Obviously, σ_e is a function of both σ_0 and $\mathcal{D}$—for a fixed σ_0 as $\mathcal{D}$ is varied, $\sigma_e \approx \sigma_0$ for very small $\mathcal{D}$ and as $\mathcal{D}$ becomes very large, so does σ_e. In course of this variation, if σ_e crosses σ^*, then $T_1(x)$ shows a minimum and if $\sigma_0 > \sigma^*$ such that σ_e never reaches σ^* (because σ_e can never fall below σ_0), then $T_1(x)$ shows a monotonic increase with $\mathcal{D}$. Although for this case we do not have any mathematical expression for σ_e in terms of σ_0 and $\mathcal{D}$, but the above picture explains our numerical data well.

2.7 Conclusion

In this chapter, we have considered the chemotaxis motion of a bacterium in a medium where the nutrient is also undergoing diffusion and its concentration profile is given by a Gaussian whose width increases with time. To characterize the efficiency of the chemotactic performance of *E. coli* bacterium, we have measured the mean first passage time of the bacterium at the neighborhood of the Gaussian peak. In the limit when the nutrient diffusion is slow compared to the bacterial motion, the bacterium experiences an effectively static concentration profile, a Gaussian with a fixed width, and in this regime we calculate the mean first passage time analytically, within a coarse-grained formalism. We find that the mean first passage time shows a minimum as a function of the width of the Gaussian, which means that the search process becomes most efficient at a certain optimum width. Our numerical simulation matches well with the analytical result.

For a time-dependent concentration profile, *i.e.* in the regime when the nutrient diffusion occurs over a time-scale comparable to bacterial motion, we find that the first passage time is a function of nutrient diffusivity $\mathcal{D}$ and the width σ_0 of the Gaussian at the onset of chemotaxis motion. When $\mathcal{D}$ is held fixed at a small value, the mean first passage time shows a minimum against variation of σ_0, as in the static case. But for large $\mathcal{D}$ the minimum becomes less pronounced. As a function of $\mathcal{D}$, the mean first passage time shows a minimum if σ_0 is held fixed at a small value. But no such minimum is observed when σ_0 is set at a large value.

We end this chapter with a short discussion on possible experimental verifications of some of our results. Recently, *E. coli* chemotaxis has been studied in a microfluidic channel whose width is comparable to the bacterial mean free path [16–18]. In such a setup, the motion of the bacterium can be considered to be effectively one-dimensional. It is possible to generate a Gaussian chemical concentration profile using techniques of diffusive microfluidics [19]. The motion of the bacterium can be tracked to measure its first passage properties. Our model predicts that for a static Gaussian profile of width $\sigma \sim 50\mu m$, wild-type *E. coli* have the shortest first passage time. However, it can be experimentally challenging to verify our results for a time-dependent nutrient concentration profile. Most common chemoattractants such as aspartate and serine have diffusivity $\mathcal{D} \sim 1000\mu m^2/s$, which is much larger than bacterial diffusivity. As a result, the chemical diffuses very quickly in the medium, and initially localized concentration quickly flattens out. Thus the bacterium experiences a very weak concentration gradient. and the chemotactic correction T_1 to its first passage time may become too small for experimental detection.

Bibliography

[1] S. Redner, *A Guide to First Passage Processes* Cambridge University Press (2001)

[2] J. W. Bell, *Searching Behaviour, the Behavioural Ecology of Finding Resources, Animal Behaviour Series*, Chapman and Hall, London (1991)

[3] M. Sheinman, O. Bénichou, Y. Kafri and R. Voituriez, *Rep. Prog. Phys.* **75** 026601 (2012)

[4] O. Bénichou, C. Loverdo, M. Moreau and R. Voituriez, *Rev. Mod. Phys.* **83** 81 (2011)

[5] M.R. Evans and S.N. Majumdar, *Phys. Rev. Lett.* **106** 160601 (2011), *J. Phys. A: Math. Theor.* **44** 435001 (2011); M.R. Evans, S.N. Majumdar and K. Mallick, *J. Phys. A: Math. Theor.* **46** 185001 (2013)

[6] L. Kusmierz, S.N. Majumdar, S. Sabhapandit and G. Schehr, *arxiv 1409.1733*

[7] S. Chatterjee, R.A. de Silveira and Y. Kafri *PLoS Comp. Biol.* **7** e1002283 (2011)

[8] A. Celani and M. Vergassola, *Proc. Natl. Acad. Sc. USA* **107** 1391 (2010)

[9] Y. Kafri and R.A. da Silveira, *Phys. Rev. Lett.* **100** 238101 (2008)

[10] H.C. Berg, *E.coli in Motion* Springer-Verlag, New York (2003)

[11] J. Adler, *J. Gen. Microbiol.* **74** 77 (1973)

[12] S.M. Block, J.E. Segall and H.C. Berg, *Cell* **31** 215 (1982)

[13] J.E. Segall, S.M. Block and H.C. Berg, *Proc. Natl. Acad. Sc. USA* **83** 8957 (1986)

[14] P.G. de Gennes, *Eur. Biophys. J.* **33** 691 (2004)

[15] Gardiner CW (2004) Handbook of stochastic methods for Physics, Chemistry and the Natural Sciences. Berlin: Springer-Verlag.

[16] H. C. Berg and L. Turner, Biophy. J. 58, 919 (1990).

[17] M. Binz, A. P. Lee, C. Edwards, and D. V. Nicolau, Microelectron. Eng. 87, 810 (2010).

[18] J. Mannik, R. Driessen, P. Galajda, J. E. Keymer, and C. Dekker, Proc. Natl. Acad. Sci. USA 106, 14861 (2009).

[19] M. Kim, M. Jia, Y. Kim, and T. Kim, Microfluid Nanofluid 16, 645 (2014).

Chapter 3

Signaling noise in a homogeneous environment

3.1 Introduction

Behavior of a cell is controlled by the intracellular biochemical reactions in its signaling pathway. These reactions crucially depend on the expression levels of each protein involved and any fluctuations in the numbers of protein molecules have important consequences on the cell performance [1, 2]. These fluctuations are also expected, since inside a single cell, the number of protein molecules which take part in the reactions, is often small [3] and can range between 10 molecules per cell to 1000 molecules per cell, depending on the type of the signaling protein [4]. How the variability in protein numbers affects the cell behavior is an important question to understand [5–8].

A model system for studying these effects of noisy environement inside of a cell on the cellular behavior, is the chemotaxis pathway of E. coli bacteria. In absence of any noise in the signaling pathway (Fig. 1.2) of the cell, the switching of rotational bias of the flagellar motors is expected to be a Poisson process and consequently, the duration of a particular run or tumble should follow an exponential distribution. Many early experiments and theoretical models which involve measurement over a bacterial population, indeed found exponential distribution [9, 10]. However, in [11] the switching events of a single cell in an isotropic medium were monitored in experiment and the residence time of the motors in the CCW bias was found to follow a

power law distribution. It was argued that the noise present in the signalling network of a single cell makes it possible to have large fluctuations in the CCW lifetimes and consequently, the cell can execute really long runs with significant probability. In [12] a theoretical model was considered where the CCW and CW bias states of the motors were modelled as a two-level system whose energy levels depend on the concentration of the motor protein CheY-P, and as the noise present in the network causes this protein number to fluctuate, the energy levels also fluctuate with time. It was explicitly shown that such fluctuations give rise to power law distribution for the lifetime of the CCW state. Similar power laws have been obtained by considering the fluctuations in CheR protein level in the pathway of non-stimulated cells [13, 14]. For a single bacterial motor, the time-series of switching events were experimentally measured and for large CW bias, which corresponds to higher CheY-P level, and hence smaller fluctuations, the CCW intervals show exponential distribution, while for small CW bias, when fluctuations in CheY-P level are more significant, CCW intervals show power law distribution [15, 16].

In this chapter, we will see the effect of this fluctuation present in the chemotactic pathway on the behavior of a single cell E. coli bacterium in presence of a homogeneous nutrient environment. Our simulation results shows that as the noise increases the runlength distribution of the bacterium will become power law. We shall also calculate the CheY-P level distribution, which is important for the bacterial run-tumble motion, analytically as a function of the methylation noise. From which we shall calculate the average run-length of the bacterium , when there is a constant background concentration. We found a good agreement with the analytics with the simulation results. The CheY-P level distribution becomes very narrow if the noise is very small but for very large noise distribution becomes wide.

In the next section, we introduce the model in details. In Sec 3.3 we show our simulation results on the effect of methylation noise in a homogeneous nutrient concentration. In Sec 3.4 we discusses the analytical results in homogeneous medium. Our conclusions for this chapter are presented in Sec 3.5.

3.2 Model description

In [17, 18] the chemotactic pathway was modelled in terms of three dynamical variables, the activity $a(t)$ of the receptor complex, the methylation level $m(t)$ and the

CheY-P level $y_P(t)$. In [19] this description was modified by incorporating methylation noise. In this chapter, we use the same model as in [19].

The activity of a receptor complex is defined as the probability to find it in the active state. The free energy difference between the active and inactive state is denoted as $\epsilon(m, c_0)$, which is a function of the methylation level m and the constant background nutrient concentration c_0. Then within quasi-equilibrium approximation, activity can be written as

$$a = \frac{1}{1 + \exp[N\epsilon(m, c_0)]}, \tag{3.1}$$

where $N = 6$ is the number of chemo-receptors participating in the signaling pathway. The free energy $\epsilon(m, c_0)$ can be written as a sum of contributions coming from m and c_0 as follows [20, 21]:

$$\epsilon(m, c_0) = \alpha(m_0 - m) + f(c_0) \tag{3.2}$$

where, $f(c_0) = -\log\left(\frac{1 + c_0/K_A}{1 + c_0/K_I}\right)$. In Eq. 3.2 $K_A = 3mM$ and $K_I = 18.2\mu M$ [18, 19] set the range of concentration that the cell is able to sense. The cell is insensitive to chemical concentration outside this range. The other parameter values are $\alpha = 1.7$, $m_0 = 1$ [18, 19].

The methylation level of the receptor goes up under the action of the enzyme CheR (and goes down due to CheB-P). The concentration of CheR that is bound to the receptor fluctuates with time due to low abundance of the enzyme [22] and also due to binding-unbinding dynamics between free and bound state enzyme molecules [13, 14, 23, 24]. This gives rise to fluctuations in the methylation level of the receptor. The resulting dynamics governing receptor methylation and demethylation is given by the stochastic equation [19]

$$\frac{dm}{dt} = k_R(1 - a) - k_B a + \eta(t). \tag{3.3}$$

Here, k_R and k_B denote the methylation and demethylation rate constants, respectively [18] and $\eta(t)$ is the stochastic noise with properties $< \eta >= 0$ and $< \eta(t)\eta(t') >= \lambda(k_R(1 - \bar{a}) + k_B\bar{a})\delta(t - t')$, where $\bar{a} = 1/2$ is the average activity level in absence of any noise. The strength of the noise which determines the variance of methylation, depends on various biochemical rate constants and total concentration level of proteins like CheA, CheY and CheZ [25]. While the rate parameters are generally expected to be constant for a given biochemical pathway, the total concentration level of different proteins can vary from cell to cell due to noisy

gene expressions. Within our simple model, we vary the noise strength by varying the dimensionless parameter λ. We consider only small values of λ and within our range of variation, the fluctuation (measured as the standard deviation) in $m(t)$ remains significantly smaller than the average methylation value. The rate parameters k_R and k_B are significantly smaller than all other rates which characterize different reactions in the biochemical pathway. This makes the methylation fluctuation a slow process and hence the noise $\eta(t)$ cannot be integrated out. In our simulation, we have used $k_R = k_B = 0.015s^{-1}$ [19, 26], which gives $< \eta(t)\eta(t') >= \lambda k_R \delta(t - t')$. Our main results remain unaffected even when k_R and k_B have small but different values.

Fluctuations in methylation level will also cause fluctuations in activity which in turn affects the phosphorylation of CheY proteins. In the phosphorylated state, CheY-P proteins bind to the flagellar motors and cause the cell to tumble. Denoting the fraction of phosphorylated CheY proteins as y_P, we can write [19]

$$\frac{dy_P}{dt} = k_Y a(1 - y_P) - k_Z y_P, \tag{3.4}$$

where the phosphorylation and dephosphorylation rates of CheY molecules have the values $k_Y = 1.7s^{-1}$ and $k_Z = 2s^{-1}$ which are much higher than the rates for methylation and demethylation [17, 19]. This is why no additive white noise in Eq. 3.4 has been included in the model, since it is expected that such noise would give rise to fluctuations much faster than that induced by methylation noise. The tumbling rate $\omega(y_P)$ is a sigmoidal function of y_P

$$\omega(y_P) = \Omega y_P^H \tag{3.5}$$

with $H = 10$ and $\Omega = 282250s^{-1}$ [19, 27]. The value of Ω was estimated in [19] using the criterion that in an adapted state, the flagellar motors have a CW bias of 25%. Although we use the same Ω value, in our simulation in one dimension, we consider instantaneous tumbling, *i.e.* the cell does not spend a finite time in the tumbling state, but immediately after tumbling it starts running in a new direction. This is justified since the fraction of time spent in a CW bias state is negligible compared to that in CCW state. However, we have also checked that including a finite tumbling duration does not affect our conclusions.

In this chapter, we consider motion of the bacterial cell in one dimension. While one dimensional case is simpler to study and also relevant in view of recent experiments [28, 29] where bacterial chemotaxis has been studied in narrow microfluidic channel

inside which motion of the cell can be effectively considered to be one dimensional. In higher dimensions the rotational diffusion will play a crucial role to affect the run duration of the bacterium. But for homogeneous nutrient environment, since c_0 does not depend on the the position of the bacterium so apart from the magnitude of the run duration all our results will not depend on the dimension and hence we do not show these result in two or higher dimension.

To perform simulations in one dimension, we consider a one dimensional box of length L, at the two ends of which there are reflecting boundary walls. In a time-step dt, the cell moves a distance vdt where v is the run speed. At the end of each step, the tumbling probability $\omega(y_P)dt$ is calculated and if a tumble does take place, the sign of v is reversed with probability q. In each time-step the activity, methylation and CheY-P levels are updated according to Eqs. 3.1, 3.3 and 3.4. Throughout we have used $L = 1000\mu m$, $v = 10\mu m/s$, $dt = 0.01s$. To check for finite size effects we have also considered larger L and smaller dt values and found that our conclusions remain unaffected.

3.3 Simulation results of the run-length and CheY-P level distribution in a homogeneous nutrient environment

We study the motion of a single cell in presence of a homogeneous nutrient concentration in the medium. Even in the absence of any concentration gradient of the nutrient, the effect of signaling noise is strongly felt. A qualitative change in the run-length distribution is observed as the noise strength is varied. When noise strength is zero, in a background of constant nutrient concentration, the activity level, methylation level and CheY-P level do not fluctuate and stay constant at their respective adapted values. The tumbling rate in Eq. 3.5 then also takes a constant value and the bacterial motion consists of run and tumble modes with constant switching rates. The run-length distribution in that case is expected to be exponential. Over a length scale much larger than the average run-length, the motion of the cell can be described by a diffusion process.

On the other hand, when the noise strength is high, then methylation level in Eq. 3.3 shows large fluctuations, which in turn induces fluctuations in the activity and

in CheY-P level. The tumbling rate, which is a function of CheY-P concentration also fluctuates with time. For large noise, the run-length distribution is known to decay like a power law with an exponent $\simeq 2.2$ [11] and the motion of the cell can be described by a Lévy walk [14]. A power law decay indicates the possibility of observing long runs in the system [11] and an exponent 2.2 implies that although average run-length remains finite, the variance of the distribution diverges. The mean-squared displacement of the cell shows super-diffusive behavior in this limit. Within our model also, we verify the crossover of run-length distribution from an exponential to a power law with increasing noise strength in Fig. 3.1. Note that in our simulations we consider a finite system. This brings about an exponential cut-off in the tail of the run-length distribution which in turn restores diffusive behavior in the long time limit.

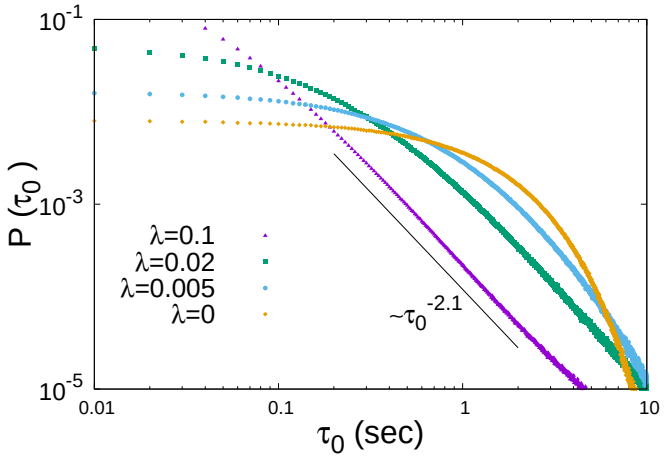

FIGURE 3.1: **Distribution of the run duration for different signaling noise.** The probability $P(\tau_0)$ to observe a run duration τ_0 for different noise strengths λ, in presence of a homogeneous nutrient concentration. For small λ, we find $P(\tau_0)$ has an exponential form, but for large λ it is a power law with exponent 2.1 ± 0.1, close to experimental observation [11]. The thin line shows a power law function with power 2.1. All other simulation parameters are as specified in Sec.3.2.

The crossover from exponential to power law shown in Fig. 3.1 happens due to fluctuations present in the CheY-P level, which directly controls the motor bias [12]. To gain a deeper insight into this noise induced fluctuations, we measure the distribution of CheY-P concentration at the time of tumbling. Our simulation data in Fig. 3.2 shows that the CheY-P concentration follows a unimodal distribution. As noise increases, the distribution gets wider, as expected. Interestingly, the peak of the distribution shifts towards right with increasing noise, and the distribution develops a

long tail for small values of CheY-P concentration. In the next section, we calculate calculate the distribution analytically to explain these features.

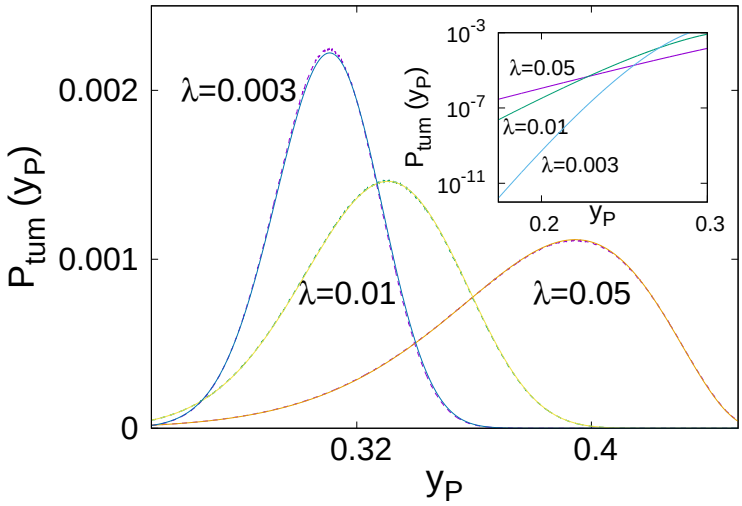

FIGURE 3.2: **CheY-P level statistics of the bacterial biochemical pathway**. The probability distribution $P_{tum}(y_P)$ for the fraction y_P of phosphorylated CheY molecules for a homogeneous nutrient concentration $c(x) = c_0$ for different noise strengths. With increasing noise strength, $P_{tum}(y_P)$ peak shifts rightward and width of the distribution increases. The dashed lines show (binned) simulation data and the continuous lines correspond to analytical calculation, which shows good agreement with simulation. Inset shows the left tail region of the distribution on a zoomed scale. We find that as noise increases, the tail becomes longer. The simulation parameters are as in Fig. 3.1.

3.4 Analytical calculation of the CheY-P level distribution and average run duration of the bacterium in a homogeneous concentration

The fluctuation in the methylation level can be expressed in terms of the following stochastic differential equation by inserting Eq. 3.1 in Eq. 3.3[7]

$$dm = k_R \frac{c_0 e^{N\alpha(m_0-m)} - 1}{c_0 e^{N\alpha(m_0-m)} + 1} dt + \sqrt{k_R \lambda} dW(t), \tag{3.6}$$

where c_0 is the uniform nutrient concentration in the medium and $dW(t)$ is a stochastic variable with uni-variate normal distribution. Using the expression of activity in

Eq. 3.1 and applying the Ito calculus we can have

$$\begin{aligned} da &= [k_R \frac{c_0 e^{N\alpha(m_0-m)} - 1}{c_0 e^{N\alpha(m_0-m)} + 1} \frac{\partial a}{\partial m} + \frac{\lambda k_R}{2} \frac{\partial^2 a}{\partial m^2}]dt + \sqrt{\lambda k_r} \frac{\partial a}{\partial m} dW(t) \\ &= k_R N\alpha a(1-a)(1-2a)(1+\frac{N\alpha\lambda}{2})dt + \sqrt{k_R\lambda} N\alpha a(1-a)dW(t) \end{aligned} \quad (3.7)$$

Let $F(a,t)$ denote the probability to find the cell with activity a at time t. From Eq. 7.1 we can construct the Fokker Planck equation for $F(a,t)$ which has the form

$$\frac{\partial F(a,t)}{\partial t} = -\frac{\partial}{\partial a}[k_R N\alpha a(1-a)(1-2a)(1+\frac{N\alpha\lambda}{2})F(a,t)] + \frac{k_R\lambda}{2}\frac{\partial^2}{\partial a^2}[N^2\alpha^2 a^2(1-a)^2 F(a,t)]. \quad (3.8)$$

In the steady state, the time-derivative on the left hand side vanishes and by making the transformation $a = (1+u)/2$ and $F(a) = [(1-u^2)/4]^{\kappa/2-1}G(a)$, with $\kappa = 2/(N\alpha\lambda)$, the above equation gets reduced to associated Legendre equation

$$(1-u^2)\frac{d^2G}{du^2} - 2u\frac{dG}{du} + [\kappa(\kappa+1) - \frac{\kappa^2}{1-u^2}]G = 0. \quad (3.9)$$

The general solution of this equation can be written as

$$F(a) = \left[\frac{1-(2a-1)^2}{4}\right]^{\kappa/2-1} [A_1 P_\kappa^\kappa(2a-1) + A_2 Q_\kappa^\kappa(2a-1)] \quad (3.10)$$

where P_κ^κ and Q_κ^κ are associated Legendre polynomial of first and second kind, respectively. The constants A_1 and A_2 can be determined from fitting with the numerical data.

If we use the reflecting boundary conditions of the activity a at $a = 0$ and $a = 1$, so that the activity always lies within 0 and 1, one can calculate easily calculate the distribution function from Eq. 3.8. The corresponding reflecting boundary conditions for the $F(a)$ are $(i)\frac{\partial F(a)}{\partial a}|_{a=0} = 0$ and $(ii)\frac{\partial F(a)}{\partial a}|_{a=1} = 0$. By applying these conditions in Eq. 3.8 one can get a first order differential equation at steady state for $F(a)$. From which one can get finally the normalized distribution

$$F(a) = \frac{[a(1-a)]^{\kappa-1}}{B(\kappa,\kappa)}, \quad (3.11)$$

where $B(\kappa,\kappa) = \int_0^\infty (x(1-x))^{\kappa-1}dx = \frac{\Gamma[\kappa]^2}{\Gamma[2\kappa]}$. The distribution function for CheY-P follows from here, by noting that in steady state CheY-P concentration can be

assumed to be equal to $\frac{a}{a+k_Z/k_Y}$. Here, we have used an assumption that the fluctuations present in activity a are slow enough, such that for each level of activity, CheY-P level reaches a steady state. Then the probability that the fraction of phosphorylated CheY proteins has a given value y_P is

$$F_1(y_P) = F(a)\frac{da}{dy} = \frac{k_Y}{k_Z}(a+\frac{k_Z}{k_Y})^2 F(a) \tag{3.12}$$

The probability distribution for CheY-P concentration at tumble can simply be calculated as $P_{tum}(y_P) = \omega(y_P)F_1(y_P)$. In Fig. 3.2 we compare our analytical results with simulations and find good agreement. As noise strength increases, the peak of the distribution shifts towards higher CheY-P level and the distribution also develops a long tail, as shown in the inset. We discuss in Chapter 4 that these facts play important role in understanding the chemotactic efficiency of the cell in presence of nutrient concentration gradient.

Although large noise increases the probability of very long runs, the average run-duration still decreases with noise, as shown in our data in Fig. 3.3. We will in the next chapter that this has important consequence for the chemotactic response of the cell. The first moment of the distribution $P_{tum}(y_P)$ gives the average CheY-P level at tumble from which average tumbling rate can be calculated using Eq. 3.5, and the average run-duration can be estimated as the inverse of average tumbling rate,

$$\begin{aligned}\tau &= \frac{1}{\int_0^1 P_{tum}(y_P)dy_P} \\ &= \left[\left(\frac{k_z}{k_Y}\right)^{-H}\frac{\Gamma[2\kappa]\Gamma[\kappa+H]}{\Gamma[\kappa]}2F1[H,H+\kappa;H+2\kappa;-\frac{k_Y}{k_Z}]\right]^{-1},\end{aligned} \tag{3.13}$$

where, ${}^2F_1[H,H+\kappa;H+2\kappa;-\frac{k_Y}{k_Z}]$ is the Gauss Hyper-geometric function. Note that in presence of a large signaling noise, the tumbling events are not Poissonian and replacing average run duration by inverse of average tumbling rate is an approximation. However this gives good agreement with simulation results as shown in Fig. 3.3.

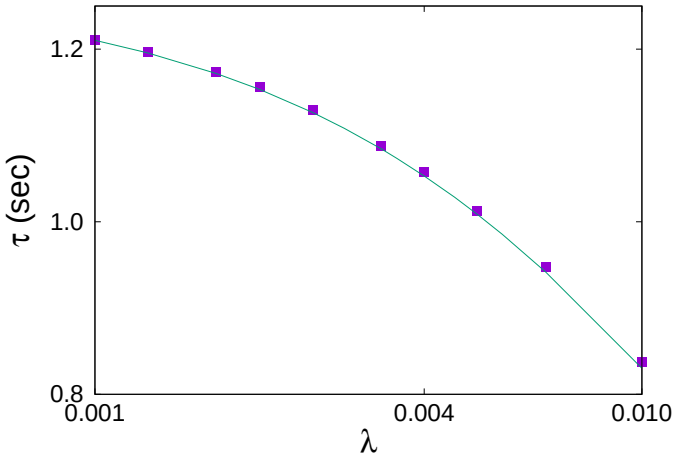

FIGURE 3.3: **Average run duration for different signaling noise.** The average run duration τ decreases with λ. The discrete points are for simulation and the continuous line shows analytical result from Eq. 3.13. We find good agreement. Here, we have used one dimensional system and a homogeneous nutrient concentration with a constant background concentration $c(x) = c_0 = 200\mu M$. All other simulation parameters are as in Fig. 3.1.

3.5 Conclusion

In this chapter we have measured the run-length distribution in a homogeneous medium for different noise strength. We found that as the noise increases the distribution becomes power law instead of exponential distribution. These results suggest that as the internal noise increases bacteria can have long runs. These long runs will be beneficial for the bacteria when there will be nutrient concentration gradient present in the system. In chapter 4 we will see that this noise would actually increase the chemotactic performance of the bacteria in presence of spatially varying nutrient profile. In harsh environment where the nutrient is diffusing and decaying with time this long runs would be important for the bacteria to reach to the nutrient rich region quickly(see chapter 5). We have also measured the CheY-P protein level distribution both numerically and analytically. We found a good agreement. Finally we have measured the average run-duration, which decreases as the noise strength increases. This result will be important when we will study the effect of the noise on the chemotactic performance of the bacteria in presence of spatially varying nutrient profile in chapters 4 and 5.

Bibliography

[1] M. Jeschke, S. Baumgartner and S. Legewie, Determinants of Cell-to-Cell Variability in Protein Kinase Signaling, PLoS Comput. Biol. 9, e1003357 (2013).

[2] M. B. Elowitz, A. J. Levine, E. D. Siggia and P. S. Swain, Stochastic Gene Expression in a Single Cell, Science 297, 1183 (2002).

[3] A. Eldar and M. B. Elowitz, Functional roles for noise in genetic circuits, Nature 467, 167 (2010).

[4] R. Milo, P. Jorgensen, U. Moran, G. Weber, and M. Springer, BioNumbers–the database of key numbers in molecular and cell biology, Nucl. Acid. Res. 38, D750 (2010).

[5] C. V. Rao, D. M. Wolf and A. P. Arkin, Control, exploitation and tolerance of intracellular noise, Nature 420, 231 (2002).

[6] L. S. Tsimring, BioNumbers–the database of key numbers in molecular and cell biology, Rep. Prog. Phys. 77, 026601 (2014).

[7] G. Lan and Y. Tu, Information processing in bacteria: memory, computation, and statistical physics: a key issues review, Rep. Prog. Phys. 79, 052601 (2016).

[8] P. C. Bressloff, Stochastic processes in cell biology (Springer, Heidelberg, 2014).

[9] S. M. Block, J. E. Segall and H. C. Berg, Impulse responses in bacterial chemotaxis, Cell 31, 215 (1982).

[10] S. M. Block, J. E. Segall and H. C. Berg, Adaptation kinetics in bacterial chemotaxis, J. Bacteriol. 154, 312 (1983).

[11] E. Korobkova, T. Emonet, J. M. Vilar, T. S. Shimizu and P. Cluzel, From molecular noise to behavioral variability in a single bacterium, Nature 428, 574 (2004).

[12] Y. Tu and G. Grinstein, How White Noise Generates Power-Law Switching in Bacterial Flagellar Motors, Phys. Rev. Lett. 94, 208101 (2005).

[13] F. Matthaus, M. Jagodic and J. Dobnikar, E. coli Superdiffusion and Chemotaxis-Search Strategy, Precision, and Motility, Biophys. J. 97, 946 (2009).

[14] F. Matthaus, M. S. Mommer, T. Curk and J. Dobnikar, On the Origin and Characteristics of Noise-Induced Lévy Walks of E. Coli, PLoS ONE 6, e18623 (2011).

[15] E. A. Korobkova, T. Emonet, H. Park and P. Cluzel, Hidden stochastic nature of a single bacterial motor, Phys. Rev. Lett. 96, 058105 (2006).

[16] H. Park, P. Oikonomou, C. C. Guet and P. Cluzel, Noise Underlies Switching Behavior of the Bacterial Flagellum, Biophys. J. 101, 2336 (2011).

[17] Y. Tu, T. S. Shimizu and H. C. Berg, Modeling the chemotactic response of Escherichia coli to time-varying stimuli, Proc. Natl. Acad. Sci. U.S.A. 105, 14855 (2008).

[18] L. Jiang, Q. Ouyang and Y. Tu, Quantitative modelling of Escherichia coli chemotactic motion in environments varying in space and time, PLoS Comp. Biol. 6, e1000735 (2010).

[19] M. Flores, T. S. Shimizu, P. R. ten Wolde and F. Tostevin, Signaling noise enhances chemotactic drift of E. coli, Phys. Rev. Lett. 109, 148101 (2012).

[20] B. A. Mello and Y. Tu, An allosteric model for heterogeneous receptor complexes: Understanding bacterial chemotaxis responses to multiple stimuli, Proc. Natl. Acad. Sci. U.S.A. 105, 6403 (2008).

[21] J. E. Keymer, R. G. Endres, M. Skoge, Y. Meir and N. S. Wingreen, Chemosening in Escherichia coli: two regimes of two-state receptors, Proc. Natl. Acad. Sci. U.S.A. 103, 1786 (2006).

[22] M. S. Li and G. L. Hazelbauer, Cellular stoichiometry of the components of the chemotaxis signaling complex, J. Bacteriol. 186, 3687 (2004).

[23] M. S. Li and G. L. Hazelbauer, Adaptational assistance in clusters of bacterial chemoreceptors, Mol. Mibrobiol. 56, 1617 (2005).

[24] S. Schulmeister, M. Ruttorf, S. Thiem, D. Kentner, D. Lebiedz and V. Sourjik, Protein exchange dynamics at chemoreceptor clusters in Escherichia coli, Proc. Natl. Acad. Sci. U.S.A. (2008).

[25] N. W. Frankel, W. Pontius, Y. S. Dufour, J. Long, L. Hernandez-Nunez and T. Emonet, Adaptability of non-genetic diversity in bacterial chemotaxis, eLife 3, e03526(2014).

[26] T. S. Shimizu, Y. Tu and H. C. Berg, A modular gradient-sensing network for chemotaxis in Escherichia coli revealed by responses to time-varying stimuli, Mol. Syst. Biol. 6, 382 (2010).

[27] P. Cluzel, M. Surette and S. Leibler, An ultrasensitive bacterial motor revealed by monitoring signaling proteins in single cells, Science 287, 1652 (2000).

[28] M. Binz, A. P. Lee, C. Edwards and D. V. Nicolau, Motility of bacteria in microfluidic structures, Microelectron. Eng. 87, 810 (2010).

[29] Li *et al.*, Barrier Crossing in Escherichia coli Chemotaxis, Phys. Rev. Lett. 118, 098101 (2017).

Chapter 4

Effects of intracellular environment on the chemotactic performance of E. coli in a spatially varying nutrient profile

4.1 Introduction

In the previous chapter, we have discussed the behavior of a single cell bacterium in presence of a homogeneous nutrient concentration, where we have seen that the tumbling rate and run duration get strongly affected due to noise. It is expected therefore, that in presence of a concentration gradient of the chemo-attractant, the chemotactic motion of the cell will also be seriously altered due to noise. In this chapter, we focus on what are the consequences of this on the chemotactic performance of the cell. We measure various different quantities which characterize different aspects of the chemotactic efficiency in presence of a static nutrient profile and study their properties for different strengths of the signaling noise in both one and two dimensions. The first quantity that we are interested is the chemotactic drift velocity which is defined as the steady state average velocity with which the cell climbs up the chemical concentration gradient, and larger values of drift velocity clearly indicates a better performance. The nutrient concentration, averaged over the steady state distribution of the cell position, measures how effectively the cells are localized in the nutrient-rich regions. This quantity is defined as localization and it takes a high

value for a given concentration profile of the nutrient when in the long time limit most of the cells are present in the regions which contains maximum nutrient. High values of localization and drift velocity ensures a good chemotactic performance in the long time limit. We present our results on steady state chemotactic response characterized by localization and chemotactic drift velocity in sections 4.1 and 4.3 respectively. In section 4.4 we present our results on the first passage time of the cell that measures how quickly the cell manages to find the nutrient-rich region in the medium for the first time.

To measure the different response functions in presence of static nutrient concentration we use the same chemotactic model discussed in section 3.2. But here we consider the nutrient profile is a function of the position. The equation Eq. 3.1 in Sec. 3.2 now will be of the form

$$a = \frac{1}{1 + \exp(N\epsilon(m, c(x)))}, \tag{4.1}$$

where $c(x)$ is the spatially varying nutrient profile instead of homogeneous nutrient profile c_0. We have used linear and Gaussian concentration profile to see the chemotactic behavior of the single cell bacterium. As the cell position x changes with time, the nutrient concentration $c(x)$ experienced by the cell also changes. The other equation remains same as in Sec. 3.2.

We consider motion of the bacterial cell in one and two dimensions. While one dimensional case is simpler to study and also relevant in view of recent experiments [1, 2] where bacterial chemotaxis has been studied in narrow microfluidic channel inside which motion of the cell can be effectively considered to be one dimensional, we also verify that all our main results remain valid in two dimensions as well. To perform simulations in one dimension we use same method as in Sec. 3.2. For simulations in two dimensions, we consider an $L \times L$ box with reflecting boundaries in the x and y directions. The nutrient concentration gradient is assumed to be present only along the x direction, but the cell moves on the xy plane with velocity $\mathbf{v}$, whose magnitude remains fixed but direction changes abruptly after each tumble. In this case we include finite tumble duration and rotational diffusion to make our model more realistic. The average tumble duration is taken to be $\tau_T = 0.1s$ and rotational diffusivity $D_\theta = 0.062\mu m^2/s$ [3–5] allows gradual bending of the cell trajectory during a run. All other parameters remain same as in one dimensional case.

4.2 Steady state distribution of cell position

Let $\mathcal{P}_\lambda(x)$ be the steady state probability to find the cell in one dimension at position x, for a given noise strength λ. A good chemotactic performance implies strong localization of the cell in the nutrient-rich neighborhood. This means that $\mathcal{P}_\lambda(x)$ should be large whenever nutrient concentration $c(x)$ is large and $\mathcal{P}_\lambda(x)$ should take small value for those x where nutrient is sparse, $c(x)$ is close to zero. A quantitative way to characterize this is to measure the average nutrient concentration experienced by the cell population in steady state, *i.e.* $\langle C\rangle = \int_0^L dx c(x)\mathcal{P}_\lambda(x)$. Note that the integrand has a large value only when both $c(x)$ and $\mathcal{P}_\lambda(x)$ are large, indicating strong localization in favorable region. $\langle C\rangle - c_0$ indicates the difference between the average nutrient concentration captured by the cell and the background nutrient concentration.

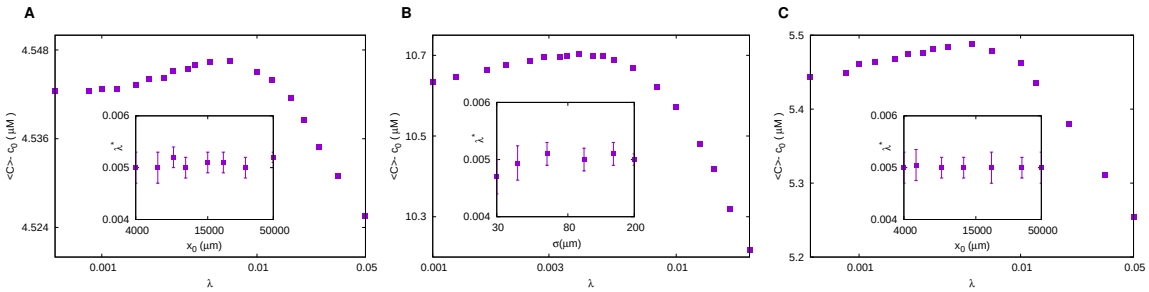

FIGURE 4.1: **Localization shows a peak as a function of noise strength. (A)**: $\langle C\rangle - c_0$ vs the noise strength λ with $c(x) = c_0(1+x/x_0)$ with $x_0 = 20000\mu m$. The optimum noise strength $\lambda^* \simeq 0.005$ in this case. Inset shows the plot for λ^* vs x_0. We find no strong dependence of λ^* on x_0. **(B)**: The variation of $\langle C\rangle - c_0$ with λ for $c(x) = c_0(1 + \frac{1}{\sqrt{2\pi\sigma^2}}\exp[-\frac{(x-\bar{x})^2}{2\sigma^2}])$. This case also shows similar value for λ^*. The inset shows the plot of λ^* vs σ. **(C).** $\langle C\rangle - c_0$ vs the noise strength λ in two dimension with $c(x) = c_0(1 + x/x_0)$ with $x_0 = 20000\mu m$. The localization shows a peak at the same value as in **(A)** and **(B)**. The inset shows the variation of λ^* with the x_0. For two dimension case also we find no strong dependence of the optimum noise strength on the gradient present in the system. We have used $c_0 = 200\mu M$, $x_0 = 10^4\mu m$, $\sigma = 100\mu m$, $\bar{x} = 500\mu m$.

We find that $\langle C\rangle - c_0$ shows a non-monotonic variation with noise strength λ: while for very small and very large λ values $\langle C\rangle$ is low, for intermediate noise level, $\langle C\rangle$ reaches a peak. This means that there is an optimum level of the signaling noise when the chemotactic performance, as measured by $\langle C\rangle$, is at its best. In Fig. 4.1A, we present the data for the linear concentration profile and find that best chemotaxis is observed for $\lambda = \lambda^* \simeq 0.005$. The value of λ^* does not seem to depend strongly on the concentration gradient (see inset of Fig. 4.1A). In Fig. 4.1B we show the data for

a Gaussian form of $c(x) = c_0(1 + \frac{1}{\sqrt{2\pi\sigma^2}} \exp[-\frac{(x-\bar{x})^2}{2\sigma^2}])$ which also shows a comparable value of λ^*. In Fig. 4.1C we present our results for the two dimensional case with a linear concentration profile $c(x)$ and find similar behavior.

Although localization does reach a peak at λ^*, the peak is not so pronounced. For a linear $c(x)$, our choice of large x_0 ensures a weak gradient and this yields a linear $\mathcal{P}_\lambda(x)$. The slope of this distribution can be used as another characteristic to measure the chemotactic performance. As expected, this slope in one dimension also shows a peak at the same λ^* value in Fig. 4.2. It is clear that a peak in slope implies a peak in localization, we find that the peak in slope is much more pronounced than the localization peak.

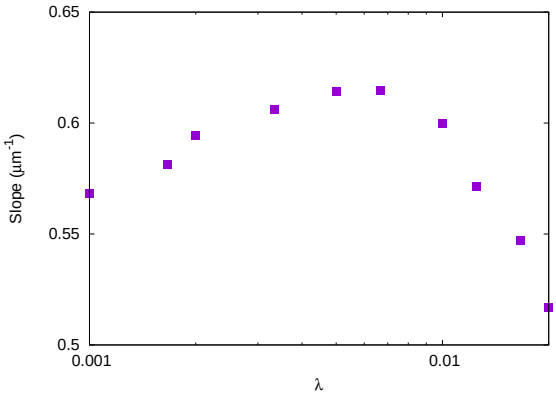

FIGURE 4.2: Slope of $\mathcal{P}_\lambda(x)$ shows a peak as a function of noise strength. The optimum noise strength λ^* is close to 0.005. Here, we have scaled the slope by a factor of 10^8. The simulation parameters are as in Fig. 4.1.

4.3 Chemotactic drift velocity in steady state

The signaling network inside the cell is such that the runs in the direction of increasing concentration gradient of the chemo-attractant are extended and those in the opposite direction are shortened. This gives rise to an overall drift motion up the concentration gradient [6]. Even in the absence of any methylation noise, the inherent stochasticity in the run-tumble motion of the cell gives rise to an effective diffusion in the long time limit which tends to homogenize the cell population. It is the drift motion which helps the system sustain the spatial variation in the steady state population density [7, 8]. In the presence of methylation noise, the cell trajectories may show super-diffusive behavior, which would again flatten out $\mathcal{P}_\lambda(x)$, had there been no drift motion. Therefore, chemotactic drift is crucial for chemotactic response. A

large value of the chemotactic drift velocity means that the cell can quickly climb up the concentration gradient. It is certainly an important criterion for chemotactic performance.

We measure the chemotactic drift velocity of the cell in one dimension in presence of a linear concentration profile of the nutrient. Before presenting our simulation data, we include a brief discussion on how we measure the drift velocity from the run-and-tumble trajectory of the cell. Note first that the existence of a non-zero drift velocity means that the average run duration in the rightward direction (up the gradient) is different from that in the leftward direction (down the gradient). We measure this difference at an arbitrary position x where the cell tumbles and a new run begins, and finally average over all x values. Let $N_R(x)$ and $N_L(x)$ be the total number of rightward and leftward runs starting at x, within an observation time window t_{obs}. Let $d_R(x)$ and $d_L(x)$ be the total durations of these rightward and leftward runs. The average run duration (in either direction) starting at x is then given by $\tau(x) = \dfrac{d_R(x) + d_L(x)}{N_R(x) + N_L(x)}$. Note that $\tau(x)$ is in general different from $[\tau_R(x) + \tau_L(x)]/2$, where $\tau_R(x)$ is the average duration of a rightward run starting at x and is equal to $d_R(x)/N_R(x)$. Similarly, $\tau_L(x) = d_L(x)/N_L(x)$. The difference stems from the fact that $N_R(x)$ and $N_L(x)$ are not equal in general.

The probability that a run starts from the position x is $Q_{tum}(x) = \mathcal{N}^{-1}[N_R(x) + N_L(x)]$ with the normalization constant $\mathcal{N} = \int dx'[N_R(x') + N_L(x')]$. The average displacement in a run can then be calculated as $\Delta = \int dx Q_{tum}(x) v \dfrac{d_R(x) - d_L(x)}{N_R(x) + N_L(x)}$. The chemotactic drift velocity is obtained on dividing the average displacement in a run by the average run duration $\tau = \int dx \tau(x) Q_{tum}(x)$. Thus the final expression for chemotactic drift velocity [4] is

$$V = \frac{\Delta}{\tau} = \frac{v \int dx[d_R(x) - d_L(x)]}{\int dx'[d_R(x') + d_L(x')]} \tag{4.2}$$

In Fig. 4.3 we plot V for different noise strengths λ and find that V shows a peak as a function of λ. The position of the peak does not match exactly with what we observed for localization $\langle C \rangle$. The chemotactic drift velocity reaches a peak value for an optimum noise strength $\lambda_o \simeq 0.01$, somewhat higher than the optimum noise strength λ^* for $\langle C \rangle$. To explain this difference, we separately plot τ and Δ as a function of noise in Fig. 4.4. We find that τ decreases monotonically with noise, as in a homogeneous nutrient environment (also see Fig. 3.1B). However, Δ shows a peak at a noise value, which again matches with λ^*. Although the non-monotonic

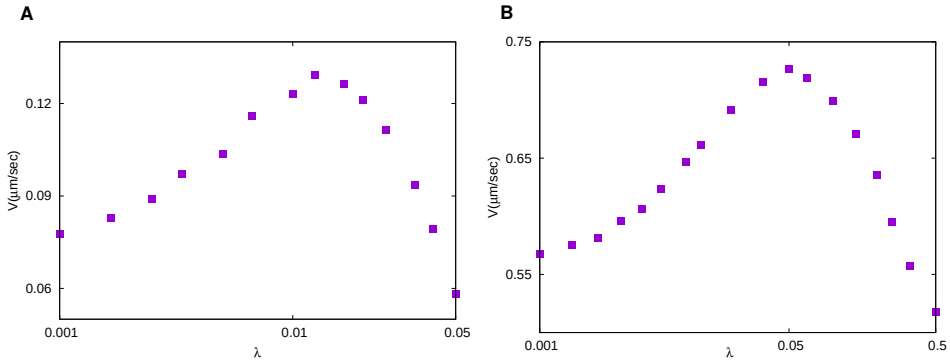

FIGURE 4.3: **Chemotactic drift velocity shows a peak as a function of the noise strength.** Left and right panels show the data for one dimensional and two dimensional systems, respectively. In both cases, the optimal noise strength λ_o is found to be higher than that for localization data in Fig. 4.1. We have used $c(x) = c_0(1 + x/x_0)$ here and all simulation parameters are as in Fig. 4.1.

variation of V with noise arises due to that of Δ, we can also see why the peak of V occurs at a higher noise value. Using $V = \dfrac{\Delta}{\tau}$, at the peak position λ_o one must satisfy the condition that $\tau\Delta' - \Delta\tau' = 0$, where the primes denote derivative with respect to λ. Since $\tau' < 0$ for all λ, it immediately follows that $\Delta' < 0$ at $\lambda = \lambda_o$. In other words, Δ decreases with noise at $\lambda = \lambda_o$, which means it has reached its peak at a smaller λ value. We verify all these results in two dimensions as well. Here, the nutrient concentration gradient is applied along x-direction and hence the chemotactic drift is also present only in x-direction. The motion of the cell along y-direction is expected to be purely diffusive in this case. We present our results for V, Δ and τ as a function of λ in Figs. 4.3B, 4.4C and 4.4D, respectively, for the two dimensional case.

The fact that the peak position of Δ matches with that of $\langle C \rangle$ indicates that there is indeed a unique noise strength at which the chemotactic performance of the cell is at its best. Moreover, this also shows that the chemotactic response is drift mediated and to understand the origin of optimality, we need to examine the noise dependence of Δ in detail. We discuss this in the following subsection. For the sake of simplicity, we limit our discussion to the one dimensional case here, but our arguments can be generalized to the two dimensional case as well.

4.3.1 Explanation of optimal noise strength

First let us consider the case of very low methylation noise. In this limit, the only source of fluctuations in activity, methylation or CheY-P level is the change in the

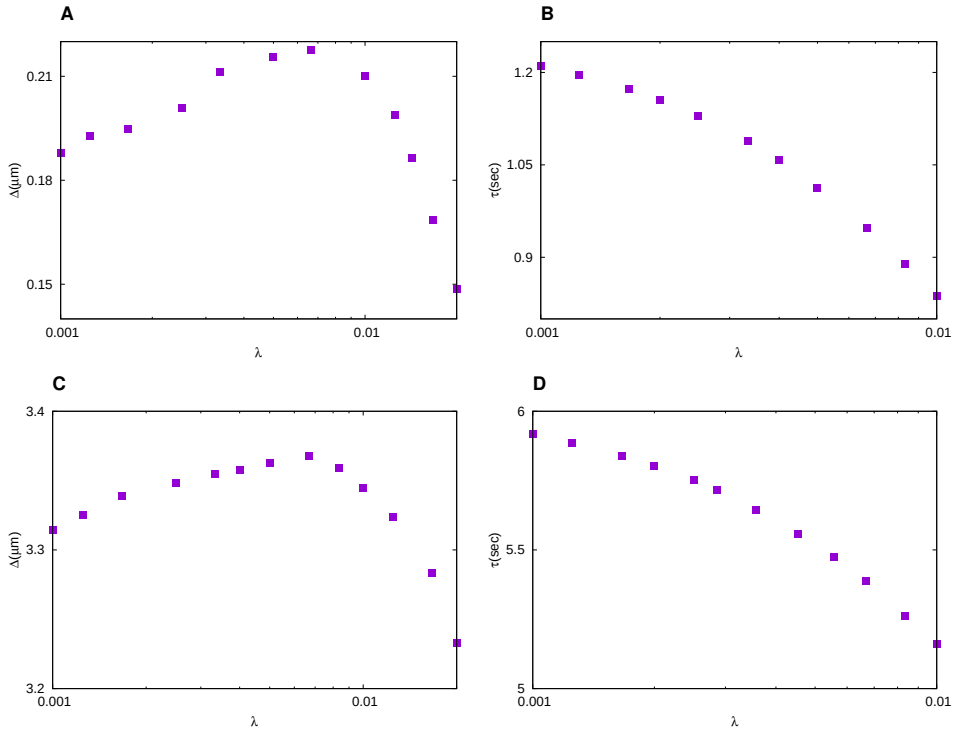

FIGURE 4.4: **The net displacement Δ in a run and the average run-duration τ as a function of noise strength.** Δ shows a peak at an optimum noise value close to λ^*, and τ decreases monotonically with noise. The upper panel shows data for one dimension and the lower panel shows data for two dimensions. All the simulation parameters for one and two dimension are same as in Fig. 4.3.

position of the cell. As the cell moves rightward, the concentration $c(x)$ of the chemo-attractant increases, and the free energy due to ligand concentration increases, causing the activity to decrease. Similarly, in a leftward run activity increases when the methylation noise is low. This in turn, causes CheY-P level to go down (up) in a rightward (leftward) run. In our simulation, we measure the average change in CheY-P level in between two tumbles, when the intervening run is directed rightward (leftward). We plot this quantity as a function of y_P, which is the value of the CheY-P concentration at the time of the first tumble, *i.e.* at the beginning of the run. Our data in Fig. 4.5A indeed show that for small noise strength λ, rightward runs bring down the CheY-P level and leftward runs push the level up [4].

However, as λ increases, the change in activity is not solely controlled by the positional change of the cell, but also by the methylation level fluctuations and the feedback it produces on the reaction network. Moreover, our analytical calculation for the homogeneous environment shows that with increasing λ, the range of variation of activity increases and its mean value (measured at a tumble) also increases. When activity becomes too low (high), the methylation level increases, which in turn

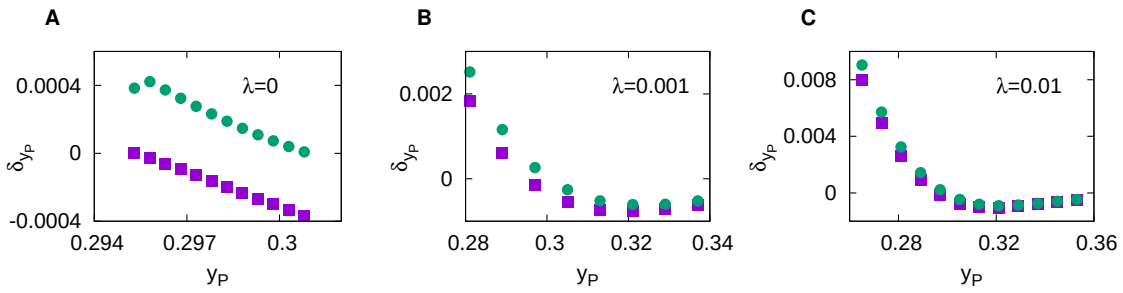

FIGURE 4.5: **Average change in CheY-P level during a run, as a function of the initial CheY-P level, at the start of the run.** y_P denotes the fraction of phosphorylated CheY molecules and δ_{y_P} denotes its average change. The circles (squares) show the data for leftward (rightward) runs. **(A)**: In absence of methylation noise, average CheY-P level always goes down (up) during a rightward (leftward) run. **(B)**: For intermediate noise strength, change in CheY-P becomes positive (negative) during a rightward (leftward) run for small (large) values of CheY-P concentration. **(C)**: As noise increases, the difference between the two curves become smaller. These data are for the one dimensional system and the simulation parameters are same as in Fig. 4.3A.

causes the activity to increase (decrease). The feedback effect becomes stronger, as the activity falls further away from its average value. For large λ, when the activity varies over an wider range, the feedback effect is thus more prominent and can easily override the change in activity due to change in cell position. This means that although in a rightward run, the activity is expected to decrease for low λ, when λ becomes high, activity can also increase during a rightward run, especially when its value at the start of the run is sufficiently small. Similarly, in a leftward run activity may decrease when its value is high enough. In terms of CheY-P level, this means that during a rightward (leftward) run the CheY-P level y_P can increase (decrease) when y_P has small (large) values. We verify this from our simulation data presented in Fig. 4.5B.

With the above observations on the effect of noise strength on the variation of activity or CheY-P level during a run, let us now turn our attention to the quantity Δ, the net displacement of the cell in a run. In the previous subsection, we had measured Δ in terms of position dependent quantities like $d_R(x)$, $N_R(x)$, etc. and then averaged over all positions. Alternatively, one can measure these quantities as a function of CheY-P concentration y_P and do a weighted average with $P_{tum}(y_P)$ over different CheY-P levels. This approach may be particularly instructive since CheY-P directly controls the tumbling rate of the cell. For this purpose, we define $\Delta(y_P) = \dfrac{d_R(y_P) - d_L(y_P)}{N_R(y_P) + N_L(y_P)}$, where $N_R(y_P)$ ($N_L(y_P)$) denotes number of rightward (leftward) runs starting with

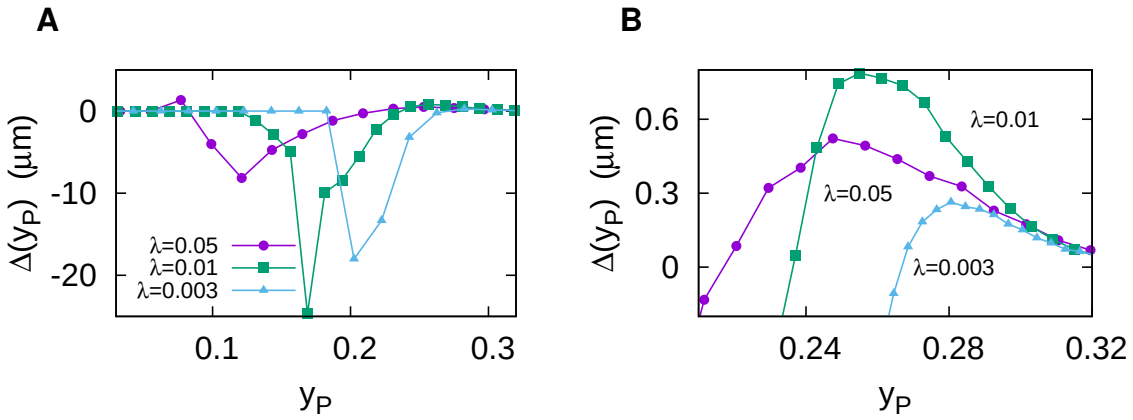

FIGURE 4.6: **Net displacement during a run for different noise strengths.** y_P denotes the fraction of phosphorylated CheY molecules, at the start of the run, and $\Delta(y_P)$ denotes the average displacement in that run. The left panel shows the complete range of y_P values, while the right panel zooms onto the large y_P values. **(A)**: $\Delta(y_P)$ vanishes for very small or very large y_P values and attains a large negative peak and small positive peak for intermediate y_P values. The position and height of the peaks depend strongly on noise. **(B)**: The positive peak of $\Delta(y_P)$ shown on a zoomed scale. While the position of the peak shifts towards left as noise increases, the height of the peak clearly shows non-monotonic behavior with noise, the highest peak being observed close to the optimal noise λ^*. These data are for one dimension and all simulation parameters are same as in Fig. 4.3A.

CheY-P concentration value y_P and $d_R(y_P)$ ($d_L(y_P)$) denotes the total rightward (leftward) displacement of the cell position in these runs. Clearly, weighted average of $\Delta(y_P)$ with the distribution $P_{tum}(y_P)$ over different y_P values gives back the same Δ as shown in Fig. 4.4A. We plot $\Delta(y_P)$ as a function of y_P for different noise strengths in Fig. 4.6.

For low noise, our data in Fig. 4.6 show that $\Delta(y_P)$ is negative for small y_P, increases to a positive value as y_P increases, then reaches a peak with y_P and then decays to zero for large y_P. Note that a rightward run starting with a given y_P must be preceded by a leftward run which terminates at the same y_P. This leftward run must have originated from a lower y_P value since for low noise, y_P value can only increase during a leftward run. This event becomes particularly unlikely when y_P values are already small, near the left-tail of the distribution $P_{tum}(y_P)$. Therefore, for small y_P values, $N_R(y_P) < N_L(y_P)$ and as a result, $d_R(y_p) < d_L(y_p)$, which makes $\Delta(y_P)$ negative. As y_P increases and comes out of the tail region, $N_R(y_P)$ gradually increases and overtakes $N_L(y_P)$, and $\Delta(y_P)$ becomes positive, as expected for a system with positive drift velocity. However, as y_P becomes very large, run durations become rather small and while $N_R(y)$ remains above $N_L(y)$, their individual values start

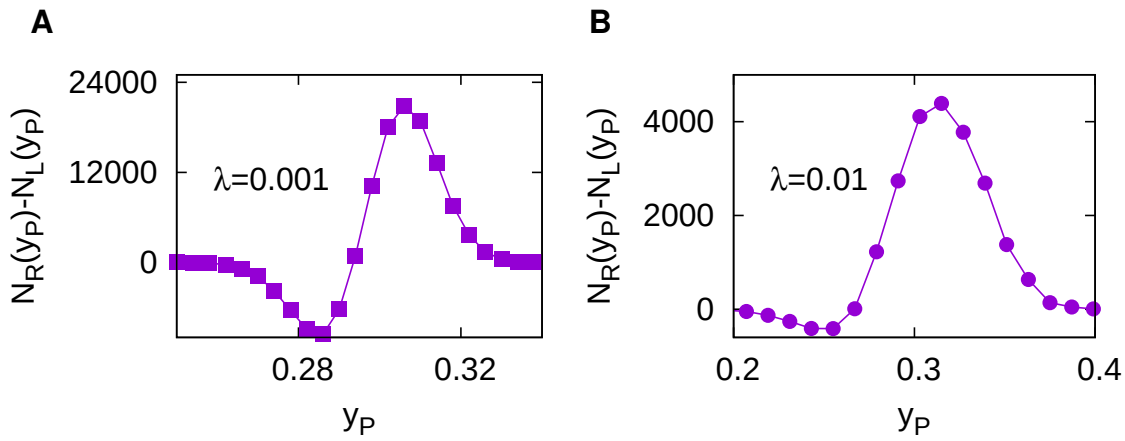

FIGURE 4.7: Variation of $N_R(y_P) - N_L(y_P)$ against y_P for different noise strengths. **(A):** As y_P increases, $N_R(y_P) - N_L(y_P)$ starts from zero, reaches a negative peak, followed by a positive peak, and again becomes zero for very large y_P values. The negative values observed at small y_P show that in this range, the cell motion is biased towards decreasing nutrient concentration. **(B):** Similar behavior is observed at large λ, but the point of zero-crossing shifts towards smaller y_P values. All simulation parameters are same as in Fig. 4.6

decreasing for large y_P. Thus $\Delta(y_P)$ approaches zero for large y_P, and must show a peak at intermediate y_P value. We have also verified that the difference in $N_R(y_P)$ and $N_L(y_P)$ vanishes even when y_P becomes very small in Fig. 4.7, since both $N_R(y_P)$ and $N_L(y_P)$ become zero here. When we average $\Delta(y_P)$ over the distribution $P_{tum}(y_P)$ to calculate Δ, small y_P values give negative contribution and reduces Δ. Note however, that negative $\Delta(y_P)$ values are near the left tail of $P_{tum}(y_P)$ and hence occur with low probability. Thus overall drift velocity still remains positive.

As noise increases, the distribution $P_{tum}(y_P)$ becomes wider and Fig. 3.2 (inset) also shows that the left tail becomes much longer than the right tail. Moreover, our argument above and data in Fig. 4.5B show that for very small y_P both rightward and leftward runs raise the y_P level, but leftward runs do so by a larger magnitude. As a result, a leftward run that precedes a rightward run and that terminates at a small y_P must have to start from an even smaller y_P, which has a low probability associated with it. Therefore, even when λ is relatively large, we still find $N_R(y_P) < N_L(y_P)$, but this happens at a much smaller y_P value, than what we have seen for low λ in Fig. 4.7. This means the zero-crossing of $\Delta(y_P)$ and its positive peak are both shifted towards smaller y_P. In other words, starting from a large value, as y_P is decreased, $\Delta(y_P)$ keeps increasing and this trend continues till a much smaller y_P value, after which it finally starts declining again. Averaging over such a curve yields

a higher value of Δ than what was observed for small noise. This explains why Δ increases as noise increases. However, when noise becomes too large, the cell cannot distinguish between rightward and leftward runs. The change in activity or y_P in a run is completely controlled by methylation level fluctuations now, and ligand concentration plays an insignificant role. Our data in Fig. 4.5C also shows that the two curves showing change in CheY-P level in a rightward and leftward run come closer as λ increases. This again reduces the value of Δ.

Above explanation and the accompanying data are presented for one dimensional motion of the cell with instantaneous tumbles. However, these arguments can be generalized for two dimensional case as well to explain our observation of optimal noise in that case.

4.4 Search time for favorable region

In this section, we discuss how quickly a cell manages to find for the first time, the region with higher nutrient concentration. First passage time is the suitable measure in this case [9]. Clearly, this is a response function measured away from the steady state. We measure the first passage time for different strengths of signaling noise in one and two dimensions.

In one dimension, we measure $T(x_i, x_f)$, defined as the time taken for a cell to reach a position x_f for the first time, starting from an initial position x_i, where $c(x_f) > c(x_i)$. A small value of first passage time indicates an efficient search strategy. In Fig. 4.8A we plot the mean first passage time, which is averaged over different trajectories of the cell. We consider two different types of nutrient concentration profile: a linearly varying $c(x) = c_0(1+x/x_0)$ and a Gaussian $c(x) = c_0\left(1 + \frac{1}{\sqrt{2\pi\sigma^2}}\exp\left[-\frac{(x-\bar{x})^2}{2\sigma^2}\right]\right)$. For comparison, we also show the data for a homogeneous concentration profile $c(x) = c_0$ in the same plot. Our data in Fig. 4.8A show that in all cases the mean first passage time decreases as the noise strength increases. Also, for large noise values, the curves for the three different concentration profiles merge. In Fig. 4.8B we present data for two dimensions for homogeneous and linear $c(x)$. In this case, since $c(x)$ is independent of y-coordinate, the initial position of the cell has been taken anywhere on the line parallel to y-axis, with x-coordinate $x_i = 300\mu m$. Similarly, the target position is another parallel line with $x_f = 490\mu m$. We find similar behavior as in the

one dimensional case here, although the values of the first passage time are larger in two dimensions.

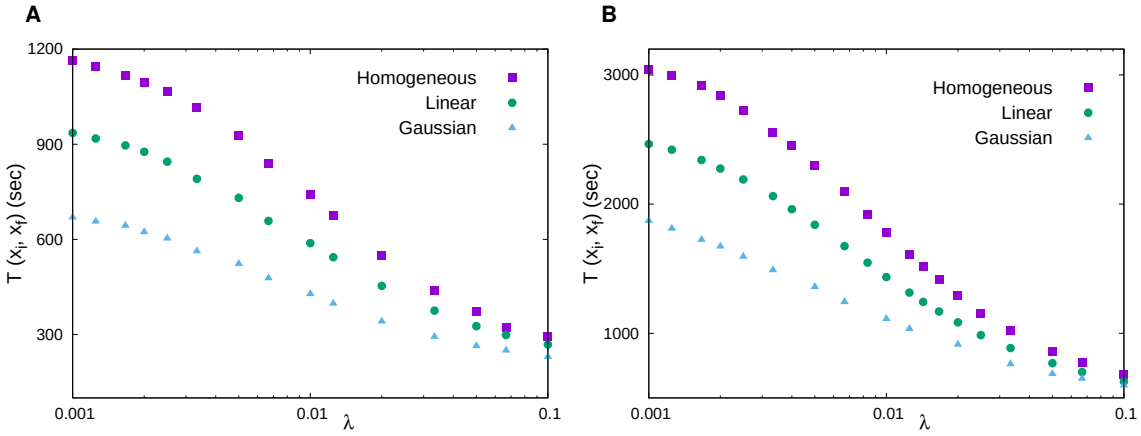

FIGURE 4.8: **Mean first passage time decreases as a function of noise strength. (A)** shows the data in one dimension and **(B)** shows the data in two dimensions. Square symbols correspond to a homogeneous concentration profile of the nutrient, $c(x) = c_0$, circles correspond to a linear concentration form $c(x) = c_0(1 + x/x_0)$ in both panels. The triangles in left panel correspond to a Gaussian $c(x) = c_0(1 + \frac{1}{\sqrt{2\pi\sigma^2}} \exp[-\frac{(x-\bar{x})^2}{2\sigma^2}])$. We have used $c_0 = 200\mu M$, $x_0 = 10^4\mu m$, $\sigma = 100\mu m$, $\bar{x} = 500\mu m$. The mean first passage time $T(x_i, x_f)$ has been measured from an initial position $x_i = 300\mu m$ to a final target position at $x_f = 490\mu m$.

As follows from our data in Fig. 3.1, for large noise, the long runs become more probable, which clearly help the cell to explore the medium quickly. As a result, it becomes possible for the cell to cover the distance to the target in a relatively small number of long runs. On the other hand, when the noise is small, run length distribution falls off exponentially and probability to observe long runs is negligible. In this case, the cell tumbles rather often and before it hits the target a large number of tumbles and hence directional changes have been executed. In this limit, the mean first passage time is longer and can actually be calculated analytically in one dimension [9].

From our data in Fig. 4.8 we therefore conclude that as noise increases, the search process becomes quicker. However, a very large noise brings about wild fluctuations of the protein levels and that is bound to affect the chemotactic performance in an adverse way. Long runs may be good for the cell to explore the whole environment quickly, but a good chemotactic performance in the long time limit actually demands that the cell is able to distinguish between runs up and down the concentration gradient. A strong fluctuation in the methylation level causes that distinction to become blurred since the change in activity in Eq. 3.1 is now dominantly controlled by the

methylation level changes, rather than local change in the ligand concentration. Indeed our data in Sec. 4.2 and 4.3 show that the steady state chemotactic performance becomes poor when the noise is very large.

4.5 Conclusion

In this chapter, we have studied the effect of methylation noise on the chemotactic performance of a single E. coli cell. We find that in the case of a nutrient environment that has spatial variation but no explicit time dependence, i.e., a static concentration nutrient profile, the chemotactic performance of the cell, measured in terms of localization and chemotactic drift velocity, shows a non-monotonic variation with the noise strength. There is an optimum noise strength where the best performance is observed. We explain this result from CheY-P level fluctuations for cell motion up and down the concentration gradient of the nutrient. We argue that for low values of CheY-P concentration, the cell is more likely to move down the nutrient gradient which is detrimental to its chemotactic performance. The threshold value of CheY-P level below which this happens moves up as the methylation noise strength is decreased. When we average over the CheY-P level statistics, for very low noise strength, the chemotactic performance is thus weaker. On the other hand, when the signaling noise is very large, the cell is unable to distinguish between runs up and down the gradient and its motion is totally controlled by stochastic methylation fluctuation. In this limit, the chemotactic performance is of course bad. Thus an intermediate noise level works best for the cell.

In [10] it was shown that for a shallow ligand gradient, the chemotactic drift velocity shows a peak at a specific noise strength, while the localization remains constant at low noise level and decreases to zero as noise increases. The optimal noise level observed for drift was explained by using a simplified model where (a) the internal state of the signaling pathway is described just in terms of activity and both methylation level and CheY-P level are expressed as a function of activity, (b) tumblings are assumed to be instantaneous, (c) the sigmoidal nature of dependence of tumbling rate on activity was approximated by making the tumbling rate zero as the activity value falls below a threshold. Within this simplified model, it was shown that the drift motion results from the difference in the amount of time a right-mover and a left-mover spends in the small activity state. With increasing noise these small activity states are reached more often and hence drift velocity also increases. For large noise, the

difference between right- and left-mover again decreases, causing the drift velocity to go down. In comparison, our data in Fig. 4.6 clearly show that for a given noise, high CheY-P level (which corresponds to high activity value) makes negligible contribution to drift velocity, and the contribution increases as CheY-P level (or the activity) becomes lower. Importantly, the same data also show that when CheY-P level falls below a certain (noise-dependent) threshold, the contribution starts decreasing again and even becomes negative. This threshold CheY-P level, which occurs at the left-tail of CheY-P distribution, goes down as noise strength becomes higher and this is a crucial factor in explaining the noise induced enhancement of chemotactic drift velocity, which was not captured in [10].

It should be possible to experimentally verify the existence of threshold CheY-P level that we predict from our model here. Monitoring the switching events from CCW to CW bias of flagellar motors, and keeping track of the cell position, one can obtain information about all the runs up and down the gradient. The CheY-P level at the tumbling event can be measured from the CW bias of the motors when the switching occurs. Using these data, it should be possible to determine $\Delta(y_P)$ experimentally and directly verify whether it becomes negative for low CW bias. Moreover, the methylation noise strength depends on the biochemical rate parameters and the total concentration levels of CheA, CheY and CheZ proteins [11]. Thus even within an isogenic cell population, with identical pathway topology where biochemical rates are same, the protein concentrations can vary due to noisy gene expression. It will be interesting to experimentally measure localization or chemotactic drift velocity for different methylation noise strengths and verify the existence of an optimum noise level.

Bibliography

[1] M. Binz, A. P. Lee, C. Edwards and D. V. Nicolau, Motility of bacteria in microfluidic structures, Microelectron. Eng. 87, 810 (2010).

[2] Z. Li, Q. Cai, X. Zhang, G. Si, Q. Ouyang, C. Luo, and Y. Tu, Barrier Crossing in Escherichia coli Chemotaxis, Phys. Rev. Lett. 118, 098101 (2017).

[3] H. C. Berg and D. A. Brown, Chemotaxis in Eschericia coli analysed by three-dimensional tracking, Nature 239, 500 (1972).

[4] Y.S. Dufour, X. Fu, L. Hernandez-Nunez and T. Emonet, Limits of Feedback Control in Bacterial Chemotaxis, PLoS Comp. Biol. 10, e1003694 (2014).

[5] R. Karmakar, R. V. S. Uday Bhaskar, R. E. Jesudasan, M. S. Tirumkudulu and K. V. Venkatesh, Enhancement of Swimming Speed Leads to a More-Efficient Chemotactic Response to Repellent, Appl. Environ. Microbiol. 82, 1205 (2016).

[6] P. G. de Gennes, Chemotaxis and the role of internal delays, Eur. Biophys. J. 33, 691 (2004).

[7] S. Chatterjee, R. A. da Silveira and Y. Kafri, Chemotaxis When Bacteria Remember: Drift versus Diffusion, PLoS Comp. Biol. 7, e1002283 (2011).

[8] Y. Kafri and R. A. da Silveira, Steady-state chemotactic response in E. coli, Phys. Rev. Lett. 100, 238101 (2008).

[9] S. Dev and S. Chatterjee, Optimal search time in E. coli chemotaxis, Phys. Rev. E 91, 042714 (2015).

[10] M. Flores, T. S. Shimizu, P. R. ten Wolde and F. Tostevin, Signaling noise enhances chemotactic drift of E. coli, Phys. Rev. Lett. 109, 148101 (2012).

[11] N. W. Frankel, W. Pontius, Y. S. Dufour, J. Long, L. Hernandez-Nunez and T. Emonet, Adaptability of non-genetic diversity in bacterial chemotaxis, eLife 3, e03526(2014).

Chapter 5

Effects of intracellular environment on the chemotactic performance of E. coli in a time varying nutrient profile

In many situations the chemoattractant concentration has an explicit time- dependence, *e.g.* the chemoattractant molecules can have a finite lifetime, beyond which it degrades, or the molecules can perform diffusive motion in the medium. In such situations, the long term chemotactic performance, based on the steady state location of the cells, may not be a suitable criteria to consider. Rather an efficient chemotaxis in this case will involve climbing up the concentration gradient while it lasts, and spotting the nutrient-rich regions as quickly as possible. The study of first passage properties of the system proves useful in this regard. We measure the time needed for the cell to reach the nutrient-rich regions for the first time, and averaged over several cell trajectories, this gives the mean first passage time. A low value of first passage time indicates an efficient search process and this proves to be particularly advantageous when the environment is depleting rapidly of the nutrient chemical. In an adverse environment where nutrient is sparse, or degrading rapidly, the amount of nutrient encountered by the cell along its trajectory, is an useful measure of chemotactic performance. This quantity is defined as uptake [1] and a high uptake means the cell moves in such a way that it intercepts a large quantity of nutrient along its trajectory, which is clearly the best it can do in an adverse situation.

We find that the first passage time of the cell decays monotonically with noise. Since long runs are more probable at large noise, the cell explores the system faster and the first passage time goes down. For time-dependent environment, when the nutrient is degrading, or diffusing in the medium, our measurement of uptake again shows a peak at a particular noise strength. However, in this case, there are more parameters in the system, *e.g.* lifetime or diffusivity of the nutrient, and one has to tune these parameters also to find the best chemotactic performance.

In this chapter, we consider a situation where a certain amount of chemo-attractant or nutrient is injected in the medium at a spatial location $\bar{x}$, following which the chemo-attractant undergoes diffusion and degradation in the medium. Then the concentration profile of the chemo-attractant has the shape of a Gaussian whose width keeps increasing with time and whose background level keeps falling with time. After a while, when the width of the Gaussian reaches a value σ_0, a bacterial cell is introduced in the medium at a position x_0. The nutrient concentration experienced by the cell at a position x at time t after its introduction is then given by

$$c(x,t) = c_0 e^{-t/\tau_d} \left[1 + \frac{\exp\left(-\dfrac{(x-\overline{x})^2}{\sigma_0^2 + 4\mathcal{D}t} \right)}{\sqrt{2\pi(\sigma_0^2 + 4\mathcal{D}t)}} \right], \tag{5.1}$$

where $\mathcal{D}$ is the nutrient diffusivity, τ_d is the time-scale of nutrient degradation. The chemotactic performance in this case is measured by (a) the first passage time of the cell measured at a region close to the peak of the Gaussian where the nutrient concentration is highest, and (b) uptake, defined as the mean amount of nutrient encountered by the cell along its trajectory up to a large enough observation time [1] . This is measured by the quantity $\mathcal{U} = \int_0^{t_{obs}} dt \int_0^L dx c(x,t) \mathcal{P}_\lambda(x,t)$. Note that due to degradation of the nutrient, the integrand vanishes for $t \gg \tau_d$ and the uptake saturates to a finite value, even as t_{obs} is increased. We examine the dependence of first passage time and uptake on the signaling noise. We limit our studies to one dimension.

5.1 Decaying nutrient profile

First we consider the limit when $\mathcal{D}$ is very small. In this case, the cell experiences a Gaussian concentration profile with almost fixed width σ_0, and an exponential decay

of the overall concentration level. Starting from an initial position x_i we measure the time taken by the cell to reach the peak region around $\bar{x}$ for the first time. Clearly, this first passage time is a stochastic variable and for different trajectories of the cell it takes different values. The probability distribution of the first passage time generally has a long tail which makes the mean much larger than the most probable or typical value [2, 3]. In Fig. 5.1A we plot the mean first passage time as a function of methylation noise strength λ. We find that the mean first passage time decreases with λ. This qualitative behavior is similar to our observation in Fig. 4.8 when there was no degradation of the nutrient. However, a quantitative comparison between these figures show that when the nutrient degrades, the first passage time takes higher value for the same noise strength. This effect is visible even when the medium is homogeneous (data points shown by circles in Fig. 5.1A). A simple way to understand why degradation of nutrients makes the search process slower is that when nutrient degrades, even when the cell is moving in a homogeneous medium, it experiences a decreasing concentration along its trajectory, which makes it tumble more. This makes the average run durations shorter and hence the mean first passage time longer [4]. Note that for small λ, the actual value of the mean first passage time is much longer than the degradation time-scale τ_d. In this case, the typical first passage time, which is much smaller than the mean first passage time, is perhaps a more suitable measure of chemotactic performance. In Fig. 5.1B we plot the typical first passage time as a function of λ and find that just like the mean, the typical value also shows similar qualitative dependence on noise.

The uptake $\mathcal{U}$ measures the amount of nutrient intercepted by the cell along its trajectory up to a certain observation time t_{obs}. We find that the uptake may increase or decrease monotonically with noise, or may even show a peak, depending on the degradation time-scale τ_d. For small values of τ_d's we find that uptake increases with noise (Figs. 5.2A-C). In this case, when the nutrient degrades very fast, the maximum contribution from uptake comes from those trajectories with very long runs, which enable the cell to reach the peak of the Gaussian before the nutrient had degraded significantly. As λ increases, the probability of such long runs increases and hence uptake also increases. On the other hand, when τ_d is large, then the degradation happens slowly and within the large but finite observation time t_{obs}, not much degradation has taken place. In this limit we expect to recover the results for the time-independent nutrient environment. Indeed our data in Figs. 5.2D-I show that uptake develops peak at particular λ values and as τ_d increases the peak position approaches the optimal λ^* observed in Fig. 4.1B.

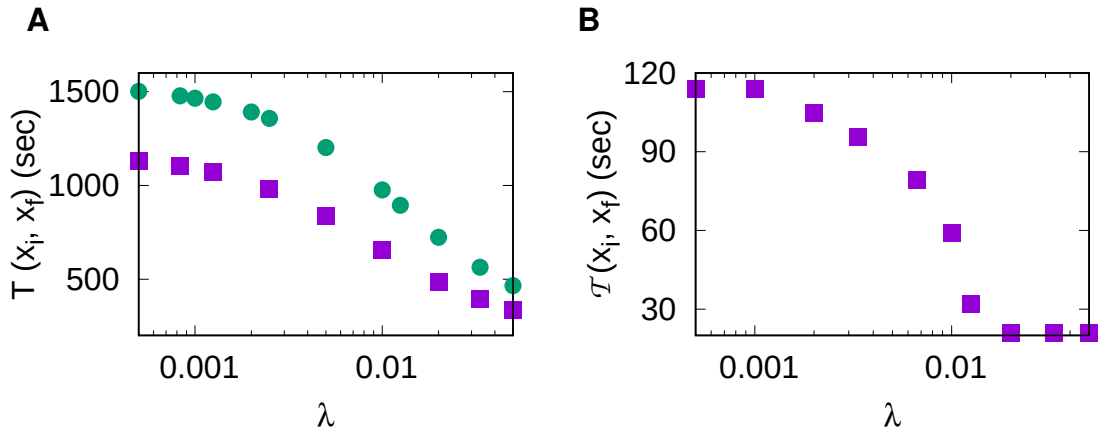

FIGURE 5.1: **First passage time vs noise strength for degrading nutrient profile.** **(A)**: Mean first passage time $T(x_0, x_f)$ decreases with λ. The mean first passage time has higher values than that in Fig. 4.8 where no degradation is considered. **(B)**: The typical first passage time $\mathcal{T}(x_i, x_f)$ has much smaller value than the mean, but also decreases with λ. The circles show the data for $c(x,t) = c_0 e^{-t/\tau_d}$ and squares are for $c(x,t)$ given by Eq. 5.1 with $\mathcal{D} = 0$. These data are for the one dimensional case and we have used $\tau_d = 500sec$, $\sigma_0 = 100\mu m$. Other parameters are as in Fig. 4.8A.

5.2 Nutrient profile with decay and diffusion

In the case when the nutrient diffusivity $\mathcal{D}$ is not so small, the nutrient diffusion cannot be neglected over the time-scale of cell movement, and the cell experiences the full time-dependent nutrient profile with decay and diffusion, given in Eq. 5.1. For a given value of $\mathcal{D}$ and τ_d, we find same qualitative behavior for the first passage time, as found in the previous subsection for negligible $\mathcal{D}$.

However, uptake shows interesting difference depending on the choice of $\mathcal{D}$. For a given value of τ_d, when $\mathcal{D}$ is very small, we recover the results of the previous subsection. In this regime, the behavior of uptake is controlled by τ_d. For our choice of $\tau_d = 100s$, we find that (see Figs. 5.3A-D) uptake increases with noise when $\mathcal{D}$ is small, in agreement with Fig. 5.2A-C. On the other hand, when $\mathcal{D}$ is very large, then the nutrient diffuses very fast and soon the concentration gradient in the medium disappears and the dependence of uptake on cell trajectory ceases to exist. The variation of uptake with λ is much weaker in this case. The short time dynamics of the cell in this case decides the uptake variation. The more time the cell is able to spend close to the peak of the Gaussian profile before the profile flattens or nutrient degrades, larger will be its uptake. When λ is large, the cell executes long runs and has shorter first passage time to the peak region, which reduces its residence time in

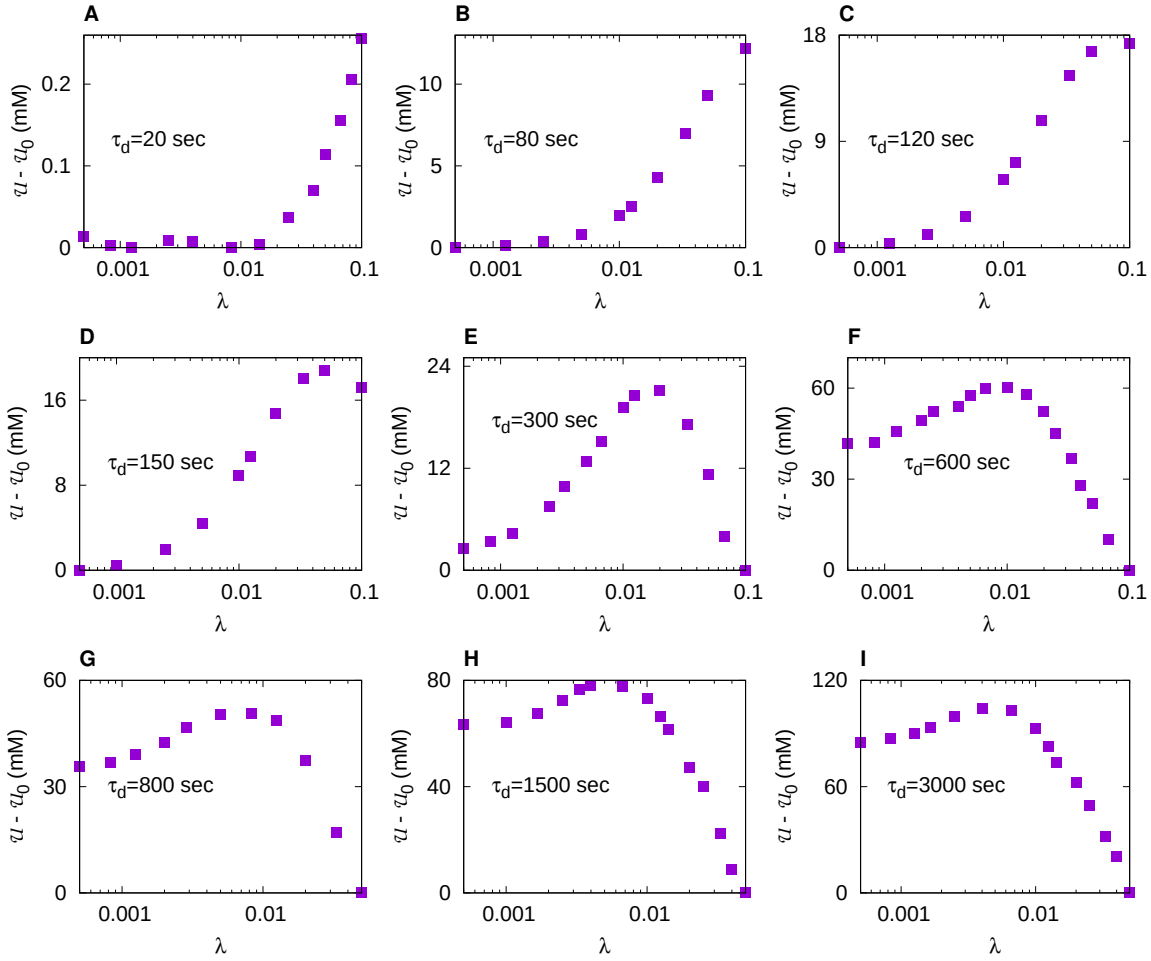

FIGURE 5.2: **Change in uptake as a function of noise strength for decaying Gaussian concentration profile**: **(A-C):** For fast degradation of the nutrient, uptake increases with λ, since maximum contribution to $\mathcal{U}$ in this case comes from those trajectories with small first passage times. **(D-G):** For a slower degradation of the nutrient, uptake starts decreasing for very large noise, and a peak is observed. Reaching the peak in the shortest possible time is not the single most important criterion any more. When the nutrient lasts for some time, those trajectories where the cell takes longer to reach the peak and then spends longer time in the peak region, contribute more towards uptake. **(H-I):** For a very slow degradation, the peak of uptake moves closer to the optimal noise λ^*, observed in Fig. 4.1B. The values of $\mathcal{U}_0$ used in panels **(A-I)** are 406, 1628, 2449, 3064, 5956, 10023, 11782, 15068, 17551 mM, respectively. These data are for one dimensional system and we have used $t_{obs} = 1000sec$. Other simulation parameters are as in Fig. 5.1.

the region that lies in between its initial position and the peak. So uptake is small for large λ. But when λ is small, the first passage time is larger and the cell spends most of its short time trajectory trying to climb up the concentration gradient, reaching the peak of the Gaussian profile. This increases the uptake. Thus for very large $\mathcal{D}$ uptake decreases with λ, as shown in Figs. 5.3G-I. Therefore, for intermediate $\mathcal{D}$'s uptake must show a peak with λ Fig. 5.3E-F.

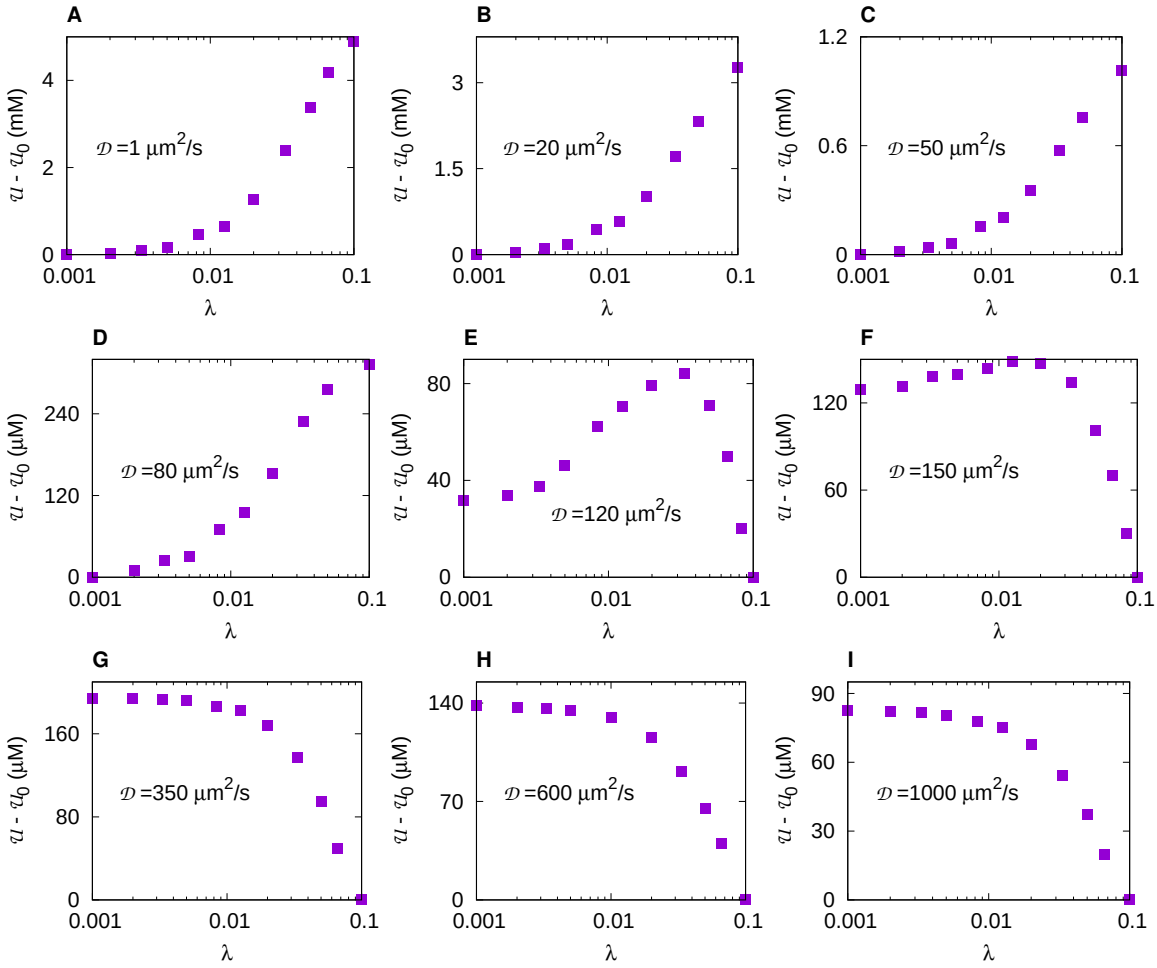

FIGURE 5.3: **Change in uptake as a function of noise strength for nutrient profile with diffusion and degradation. (A-D):** For slow diffusion of the nutrient, uptake increases with noise for our choice of τ_d. In this case, uptake is governed by those trajectories where cell executes long runs. **(E-F):** For a faster diffusion of nutrient, uptake shows a peak as a function of λ. But the variation is much weaker. **(G-I):** For very fast diffusion of nutrient, uptake decreases with noise. The values of $\mathcal{U}_0$ used are: 1730, 1736, 1738 mM in panels **A,B,I**, respectively, 1740mM in panels **C,H**, 1741mM in **G**, and 1742mM in **D,E,F**. We have used one dimensional system and the nutrient concentration in Eq. 5.1 with $\tau_d = 100sec$, $\sigma = 10\mu m$, $t_{obs} = 200sec$ here. Other simulation parameters are same as Fig. 5.2.

5.3 Conclusion

In this chapter, we have considered the case when the nutrient environment has spatio-temporal variation, caused by diffusion and degradation of the nutrient in the medium. For this case the chemotactic performance of the bacterium is best characterized by the first passage time and uptake. While first passage time shows a monotonic decrease with the methylaton noise strength, the uptake may show

a peak resulting from an interplay of time-scales associated with degradation and diffusion processes. In harsh environment also the bacterium can behave as a most efficient chemotactic performer depending on the various nutrient parameters and internal biochemical conditions. For any nutrient concentration profile which has both spatial and temporal variation, the best chemotactic performance depends both on the internal and external conditions.

Bibliography

[1] A. Celani and M. Vergassola, Bacterial strategies for chemotaxis response, Proc. Natl. Acad. Sci. U.S.A. 107, 1391 (2010).

[2] S. Redner, A Guide to First Passage Processes (Cambridge University Press, Cambridge, 2001).

[3] R. Metzler, G. Oshanin and S. Redner, First-passage phenomena and their applications (World Scientific, Singapore, 2014).

[4] S. Dev and S. Chatterjee, Optimal search time in E. coli chemotaxis, Phys. Rev. E 91, 042714 (2015).

Chapter 6

Effects of signaling noise and the motor adaptation on the behavior of E. coli in a spatially varying nutrient profile

In chapter 4 we have discussed the behavior of the cell in presence of a spatially varying nutrient profile and found the results for the effects of the signaling noise on the efficiency of chemotactic performance of the bacterium. It has been shown previously [1] that when cells were exposed to a step of attractant concentration, the CW bias of the motor changes and it eventually returns to the pre-stimulus CW bias within a few seconds. This adaption of CW bias to the changes of background concentration for repellent are also similar but inverted. In recent studies [2] it has been shown that this adaption in the CW bias happens not only due the methylation demethylation(i.e., CheR-CheB reactions) process of signaling pathway but also due to motor itself. For a mutant bacterium whose CheR-CheB reaction has been deleted, it has been shown that the CW bias partially returns to the prestimulus value when the background concentration of the bacterium is suddenly changed to a new level of concentration. This adaption occurs over time scale ($\approx 100sec$) longer than the typical bacterial adaptation time scale ($\approx 10sec$). So far we didn't consider this motor adaptation in the model of bacterial chemotaxis in our studies but it will be interesting to see that how the inclusion of the motor adaption in our model will affect the results that have been obtained in Chapter 4.

Model description

We used the same model for the time evolution of activity, CheY-P level and methylation level as in Chapter 4. But we explicitly include the adaptation of the motor's CW bias in our model. This also results in replacing instantaneous tumble by a finite tumble duration. Let us consider that the bacterium remains in two states run ($s = 1$) and tumble state($s = 0$). The CW bias of the motor depends on the CheY-P protein concentration level y_P [3] in the following relation,

$$CW = \frac{y_P^n}{y_P^n + K^n}, \tag{6.1}$$

where n is the Hill coefficient of the sigmoidal function obtained in [2] and K is the y_P level at which the CW bias becomes half. The time spent in tumble mode τ_{CW} would be the ratio between the CW bias and the switching frequency $\frac{dCW}{dy_P}$. In small time dt the probability that the cell in run mode will tumble is given by the [4]

$$P_{tum} = \frac{dt}{\tau_{CCW}} \tag{6.2}$$

where τ_{CCW} is the time spent in the CCW mode and is given by

$$\tau_{CCW} = \frac{1 - CW}{\frac{dCW}{dy_P}}. \tag{6.3}$$

We consider a one dimensional motion of the cell, with two reflecting boundary walls at the positions $x = 0$ and $x = L$. At each time step dt if the cell is in $s = 1$ state, the cell will tumble with probability $\frac{dt}{\tau_{CCW}}$ or it will move in the same direction with speed v. Similarly, if the cell is in tumble mode it will change its state from tumble to run with probability $\frac{dt}{\tau_{CW}}$ and choose the direction of motion randomly to the left or right with probability half each. We measure localization and the drift velocity of the cell as a function of the methylation noise in presence of a static nutrient concentration profile $c(x) = c_0(1 + x/x_0)$.

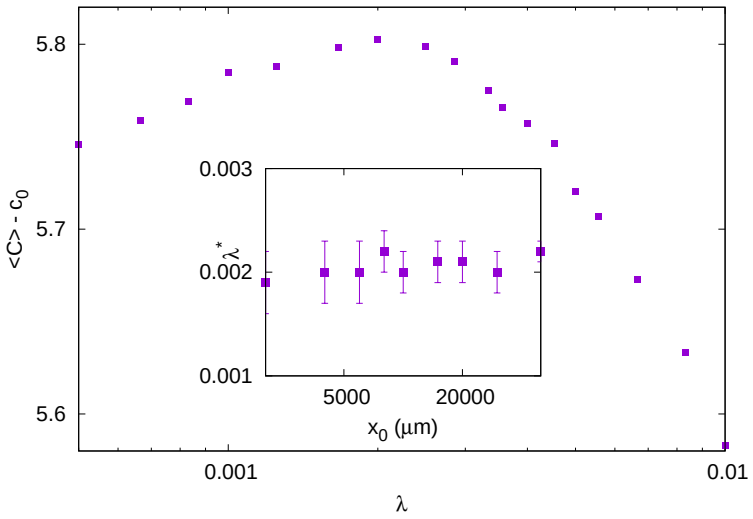

FIGURE 6.1: **Localization shows a peak as a function of noise strength.** $\langle C\rangle - c_0$ vs the noise strength λ with $c(x) = c_0(1+x/x_0)$ with $x_0 = 20000\mu m$. The optimum noise strength $\lambda^* \simeq 0.002$ in this case. Inset shows the plot for λ^* vs x_0. We find no strong dependence of λ^* on x_0. All others parameters are same as in Chapter 4

6.1 Peak of localization and drift velocity at optimum noise

As discussed in Chapter 4, the localization, $< C >= \int_0^L dx c(x) P_\lambda(x)$, is an useful performance criterion to judge how effectively the cell is able to exploit the nutrient-rich region in the long time limit. We find that localization is maximum for a certain $\lambda = \lambda^*$ (data in Fig. 6.1). As found in Fig. 4, even in this case, λ^* does not depend strongly on the concentration gradient of the nutrient. However, the quantitative value $\lambda^* = 0.002$ is lower than the λ^* observed in Fig. 4.1. Thus including motor adaptation in our description, does not change the qualitative conclusion that localization reaches a peak at an optimum noise, but the quantitative position of the peak shifts leftward. We find similar results even for our measurement of chemotactic drift velocity (see Fig. 6.2). In this case the position of peak is at $\lambda_o = 0.008$, somewhat higher than λ^*. This can also be explained in a similar way, as done in chapter 4, looking at the variation of average displacement in a run, and average run duration with noise.

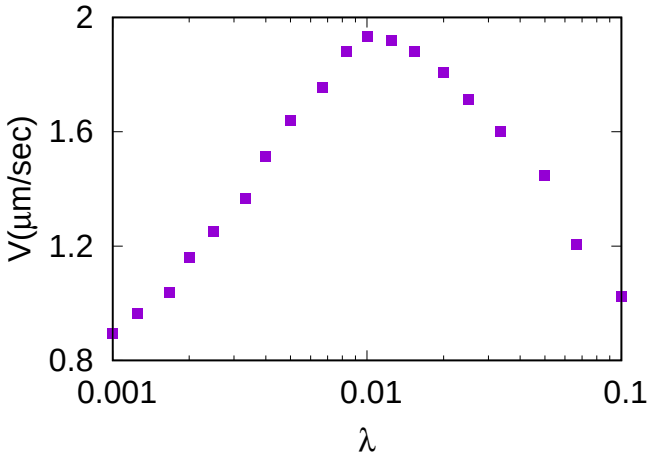

FIGURE 6.2: **Chemotactic drift velocity shows a peak as a function of the noise strength.** The optimal noise strength λ_o is found to be higher than that for localization data in Fig. 6.1. We have used $c(x) = c_0(1 + x/x_0)$ here and all simulation parameters are as in Fig. 4.1.

6.2 Conclusion

In this chapter we have included the motor adaptation part in the flagellar motor and have measured the chemotactic performance of the bacterium. In this chapter, we have studied the effect of signaling noise on chemotactic performance of an E.coli cell, whose intracellular pathway model now explicitly includes motor adaptation. We find that the main conclusion of Chapter 4 remains unchanged that there is an optimum noise where performance is the best. The value of the optimum noise is somewhat lower though. Thus presence of optimal noise is verified even when an entirely new module of motor adaptation has been added in our system.

Bibliography

[1] J, E. Segall, S. M. Block, and H. C. Berg Proc. Nati. Acad. Sci. USA Vol. 83, pp. 8987-8991, December 1986 Biophysics.

[2] J. Yuan, HC Berg (2013) Ultrasensitivity of an adaptive bacterial motor. Journal of molecular biology 425: 1760-1764

[3] P. Cluzel, M. Surette and S. Leibler, An ultrasensitive bacterial motor revealed by monitoring signaling proteins in single cells, Science 287, 1652 (2000).

[4] R. Karmakar, R. V. S. Uday Bhaskar, R. E. Jesudasan, M. S. Tirumkudulu and K. V. Venkatesh, Enhancement of Swimming Speed Leads to a More-Efficient Chemotactic Response to Repellent, Appl. Environ. Microbiol. 82, 1205 (2016).

Chapter 7

Run-and-tumble motion with step-like response to a stochastic input

7.1 Introduction

In the previous chapters 3-6 we have discussed the signaling pathway of the *E.coli* bacterium and the effects of the internal noise on the chemotactic behavior of the cell in presence of homogeneous, spatially varying and time dependent nutrient concentration profile. To see different aspect of the cellular behaviour we used the model present in the literature [1–3], where the cell perform a run-tumble motion and the motor of the cell fluctuates between CCW or CW state. The dependence of CW bias on CheY-P concentration[4] is very sensitive and is an almost sigmoidal dependence[5], where CW bias changes sharply from 0 to 1 as CheY-P concentration varies within a small range. Since CW bias is the direct measure of tumbling rate, this means the probability for a cell to tumble is vanishingly small when CheY-P level falls below a certain value, and when CheY-P level goes slightly higher, the tumbling probability becomes very close to 1 and the cell almost always tumbles.

These observations motivates us to ask a more general and interesting theoretical question: what is the effect of a sharp or sigmoidal switching response on a simple run-and-tumble motion? To address this general question, we consider a run-and-tumble random walker whose switching probabilities between run and tumble modes

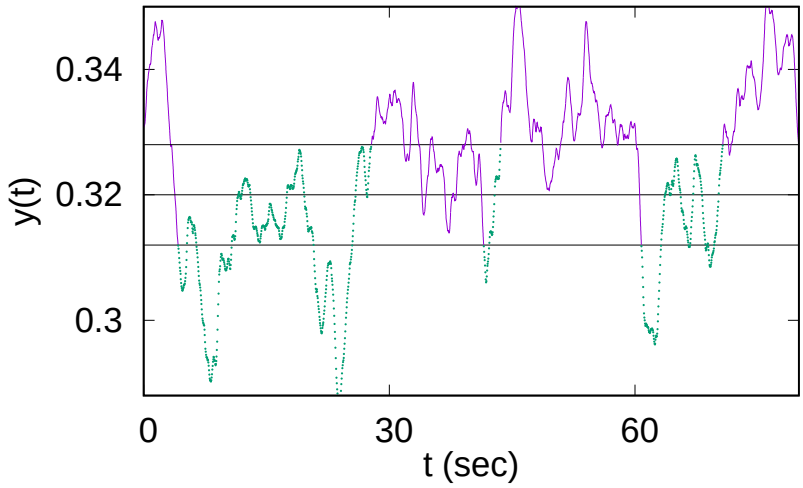

FIGURE 7.1: A typical time series of the signal $y(t)$. The purple (continuous) segments correspond to tumbles and the green (dashed) segments correspond to runs. The threshold value $y_0 = 0.32$ and the boundaries of the Δ range at $y_0 \pm \Delta/2$ are marked by horizontal line. Every time $y(t)$ exits the range through a boundary different from the one it had used to enter the range, a switch happens.

depend on a certain (stochastic) input signal. To study the system in the simplest possible setting, we consider only two values of the switching probabilities, 0 and 1. An infinitely sharp response curve would mean that as the input signal level crosses a certain threshold value, the switching probability jumps from 0 to 1. However, such a sharp response means that within a finite time-interval there can be an infinite number of switching events which is unphysical. So we introduce a small range of width Δ around the threshold value, such that the probability to switch from run to tumble mode is zero (one) as the input signal stays below (above) this range. In other words, run to tumble switch happens, as the input signal crosses the Δ range from below and goes above it. Once the random walker is in the tumble mode, the tumble to run switch happens with probability one when the input signal decreases and falls below the Δ range. Thus the two switches happen at two different values of the input signal level, which are separated by the range Δ. When the input signal has any other value, no switching event takes place and the random walker just continues in its current mode. In Fig. 7.1 we present a typical example.

We are interested to characterize the motion of the random walker in the long time limit, and to understand how the fluctuations present in the input signal affect the motion. We consider two types of cases here: one in which the dynamics of the input signal is an independent process, and another in which the time-evolution of the signal is also influenced by the position of the random walker. Since our study

is motivated from the run-and-tumble motion found in several organisms in nature, including E.coli, we choose the time-evolution of the signal from the well-studied physical system of chemotactic pathway of an E.coli cell. The CheY-P level inside the cell fluctuates with time and we consider this to be our input signal. In presence of a concentration gradient of the nutrient, the CheY-P dynamics depends on the local nutrient concentration, and hence on the cell position. However, when the cell moves in a homogeneous nutrient environment, CheY-P fluctuation does not involve the cell position. In the latter case, various quantities can be calculated exactly. We show that since switching events can have only probabilities 0 and 1, the switching can be described as a first passage process. From this, the probability to observe a certain run (or tumble) duration can be calculated exactly. We also calculate average run and tumble duration and show that both decrease as a function of the signaling noise strength. Our Monte Carlo simulations agree well with our analytical calculations. In the case when the signal dynamics also depends on the position of the random walker, we find the steady state distribution of the random walker position, for a given nutrient concentration profile in the medium, and show that it is more likely to find the random walker in a region where the nutrient concentration is higher. This shows that even within this very simple version of run-and-tumble, where switching probabilities between the two modes are either 0 or 1, the basic signature of chemotaxis, which is to find the walker in regions with more food with more likelihood, is recovered.

This chapter is organized as follows. In Sec. 7.2 we study run-and-tumble motion in a homogeneous environment, when the input signal dynamics is independent of the random walker motion. We present our exact calculation for the probability distribution of signal variable, run duration distribution of the random walker and variation of mean run duration and tumble duration as a function of signaling noise in this section. In Sec. 7.3 we consider a spatially varying nutrient environment and present our numerical results for the position distribution of the random walker. A summary and few conclusing remarks are presented in Sec. 7.4.

7.2 Run-and-tumble motion in a homogeneous environment

Consider a one dimensional random walker with two possible modes: run and tumble. During a run, the random walker moves with a fixed velocity along one particular direction, in this case, left or right. During a tumble, the random walker simply stays put at its current position. At the beginning of each new run, the random walker decides at random whether to run leftward or rightward. The switching between the two modes is controlled by a signal $y(t)$ whose stochastic time evolution can be written down (see below). If $y(t)$ crosses $y_0 + \Delta/2$ value from below, and the walker is in the run state, then it switches to tumble mode with probability 1. If it is already in the tumble state, then nothing happens. Similarly, a tumbler changes to a runner with probability 1 when $y(t)$ crosses $y_0 - \Delta/2$ from above. But at the time of crossing, if the walker is in the run mode, nothing happens. Clearly, for $y(t) < y_0 - \Delta/2$, the random walker can only have the run mode and for $y(t) > y_0 + \Delta/2$, only tumble mode can exist. In the range $y_0 - \Delta/2 < y(t) < y_0 + \Delta/2$, both modes can exist. Note however, that no switching event can take place in this range. When $y(t)$ enters the range through one end, and exits the range through a different end, switch happens at the time of exit. We have illustrated this process in Fig. 7.1.

It follows from the above description that our run-and-tumble dynamics is actually different from that of an E.coli cell. Since we consider only switching events with probability one, there is no additional source of stochasticity in our run-and-tumble motion, apart from that present in the stochastic time-evolution of $y(t)$. For a given time-series of $y(t)$, it is already fixed which modes are present at what times. We will show below that this makes it possible for us to calculate many things exactly in our system. For an E.coli cell, on the other hand, switching probabilities are sharply varying, but continuous function of the CheY-P concentration [5], and it is possible to have a switching event with small probability, which introduces another source of noise in the cell trajectory.

In our model, we use the same dynamics of $y(t)$ as that of CheY-P protein concentration inside an E.coli cell moving in a homogeneous nutrient background. Although the run-and-tumble motion studied by us, is not exactly same as that found in an E.coli cell, it is still interesting to see how our run-and-tumble system behaves when it receives input from the same type of a stochastic signal. In the case when the cell moves in a homogeneous nutrient background, $c(x) = c_0$, the activity $a(t)$ becomes a

function of $m(t)$ alone, and using Eqs. 3.1 and 3.3 in Chapter 3 one can write

$$\frac{da}{dt} = k_R N\alpha a(1-a)(1-2a)(1+\frac{N\alpha\lambda}{2}) + N\alpha a(1-a)\eta(t) \tag{7.1}$$

A quasi steady state approximation can be made at this stage, using the fact that the y-dynamics is sufficiently fast, and hence at the time-scale over which $a(t)$ is changing, an average y concentration is felt, which gives $y(t) = a(t)/(a(t) + k_Z/k_Y)$. Then Eq. 7.1 becomes

$$\frac{dy}{dt} = k_R N\alpha(1+\frac{N\alpha\lambda}{2})\frac{y(1-y-\frac{k_Z y}{k_Y})(1-y-\frac{2k_Z y}{k_Y})}{1-y} + N\alpha y(1-y-\frac{k_Z y}{k_Y})\eta(t). \tag{7.2}$$

Writing $q = k_R N\alpha$, $r = N\alpha$ and $w = k_Z/k_Y$, we get

$$\frac{dy}{dt} = q(1+\frac{r\lambda}{2})\frac{y(1-y-wy)(1-y-2wy)}{1-y} + ry(1-y-wy)\eta(t). \tag{7.3}$$

$\eta(t)$ is a Gaussian white noise with strength λ. To monitor the effect of input signal fluctuations on the run-and-tumble dynamics, we vary λ in our simulations. Note that the quasi steady state approximation used above, means that since $a(t)$ always stays within the range $[0, 1]$, the variable $y(t)$ should also stay in $[0, y_m]$, where $y_m = 1/(1 + k_Z/k_Y)$.

The value y_0, then naturally corresponds to that value of CheY-P concentration for which CW bias has the value 1/2. This value turns out to be about $3.1\mu M$ [5]. The total concentration of CheY protein in a cell is $\sim 9.7\mu M$ [6]. Since $y(t)$ in Eq. 7.3 stands for the ratio of CheY-P and CheY concentration (see Sec. 3.2), we have $y_0 = 0.32$. Moreover to ensure that the switching process is sufficiently smooth, and two switching events are separated from each other by a minimum time interval, we choose a small width Δ around y_0 that separates the two switching events from run to tumble, and from tumble to run. Here we present data for $\Delta = 0.016$ and we have also verified (data not shown) that our conclusions do not change for different choices of Δ.

In our simulations, we consider a one dimensional box of length L, at the two ends of which there are reflecting boundary walls. In a time-step dt, the random walker in the run mode moves a distance vdt where v is the run speed. In a tumble mode, there is no displacement. After each tumble the random walker will choose its direction randomly. Throughout the work we have used $L = 10000\mu m$, $v = 10\mu m/s$, $dt = 0.001s$. One point about the choice of λ range should be mentioned here. A very large

λ increases fluctuations in $y(t)$ so much that it crosses the Δ range too frequently, affecting smoothness of the underlying process. On the other hand, a very small λ makes the y-distribution too narrow and $y(t)$ hardly leaves the Δ range. For our choice of Δ, we find $0.001 \leq \lambda \leq 0.1$ to be suitable range. In the remaining part of this section, we present our exact calculations and numerical simulation results on various quantities.

7.2.1 Steady state probability distribution of y in run and tumble modes

Let $P(y,t)$ be the probability distribution of the stochastic variable $y(t)$. From Eq. 7.3 we can construct the Fokker-Planck equation for $P(y,t)$

$$\frac{\partial P(y,t)}{\partial t} = -\frac{\partial}{\partial y}[B_1(y)P(y,t)] + \frac{1}{2}\frac{\partial^2}{\partial y^2}[B_2(y)P(y,t)], \tag{7.4}$$

where, $B_1(y) = q(1+\frac{r\lambda}{2})\frac{y(1-y-wy)(1-y-2wy)}{1-y}$ and $B_2(y) = r^2 k_R \lambda y^2(1-y-wy)^2$. In steady state, left hand side of Eq. 7.4 vanishes. Also, by definition, y can not become negative. Therefore, we use reflecting boundary conditions at $y = 0$ and $y = y_m$ which gives the following solution in steady state

$$P(y) = \frac{w^\kappa (1-y)^{-2\kappa}[y(1-y-wy)]^{\kappa-1}}{\mathcal{B}(\kappa,\kappa)}, \tag{7.5}$$

where $\mathcal{B}(\kappa,\kappa) = \int_0^\infty (x(1-x))^{\kappa-1}dx = \frac{\Gamma[\kappa]^2}{\Gamma[2\kappa]}$ and $\kappa = 2/(r\lambda)$. In Fig. 7.2A we compare this result against numerical simulation and find good agreement for different values of the noise strength λ. In the right panel of the same figure we plot the individual probability of finding the random walker in run-state and in tumble-state for a given value of y, after steady state has been reached. We denote the run-state probability by $P_R(y)$ and the tumble-state probability by $P_T(y)$, and clearly, $P_R(y) + P_T(y) = P(y)$. Now, as follows from our dynamical rules, as y falls below the value $y_0 - \Delta/2$, tumble modes can not exist and the random walker is always in the run mode, *i.e.* $P_R(y) = P(y)$ for $y \leq y_0 - \Delta/2$. Similarly, for $y \geq y_0 + \Delta/2$, we have $P_T(y) = P(y)$ and $P_R(y) = 0$. Both $P_R(y)$ and $P_T(y)$ have non-zero values for $y_0 - \Delta/2 < y < y_0 + \Delta/2$. To solve for $P_R(y)$ in this range, we notice that it follows the same Fokker-Planck equation as Eq. 7.4 and in steady state this equation has

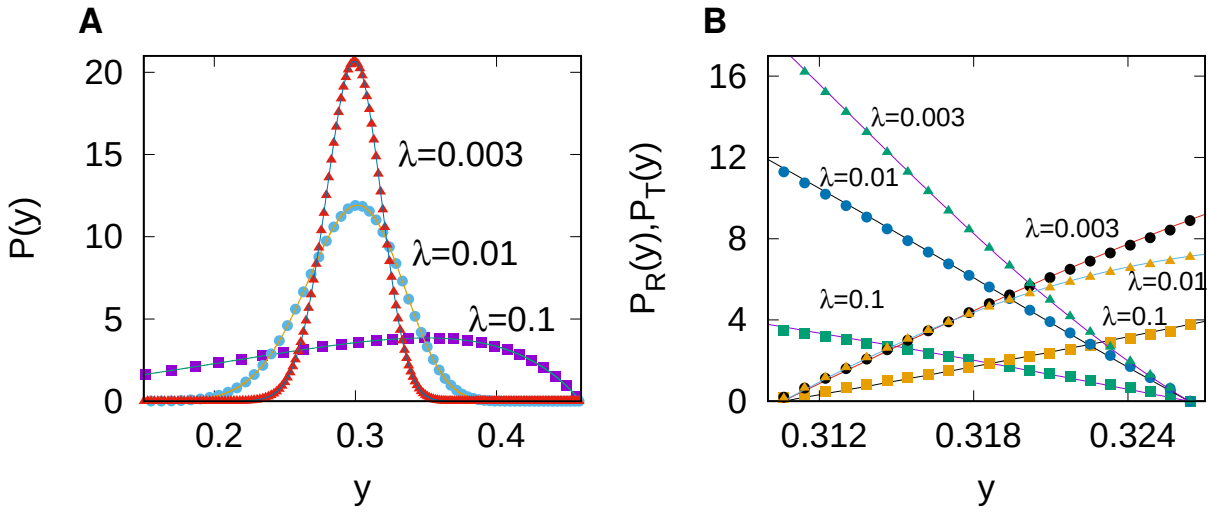

FIGURE 7.2: **Steady state probability distribution of the signal variable. A:** For different noise strength λ, probability to observe a particular value y of the signal variable is plotted against y. Discrete points are from simulation and continuous lines are from analytical calculation using Eq. 7.5. **B:** Probability $P_R(y)$ and $P_T(y)$ to observe a runner and a tumbler, respectively, with a given y value in the range $[y_0 - \Delta/2, y_0 + \Delta/2]$. The decreasing curves correspond to $P_R(y)$ and increasing curves are for $P_T(y)$. The discrete points from simulations show excellent agreement with continuous lines from analytics. All simulation parameters are as specied in Sec. 7.2 and Sec. 3.2.

the general solution

$$P_R(y) = \frac{w}{(1-y)^2}\left[\frac{1-(\frac{2wy}{1-y}-1)^2}{4}\right]^{\kappa/2-1}\left[C_1 P_\kappa^\kappa\left(\frac{2wy}{1-y}-1\right) + C_2 Q_\kappa^\kappa\left(\frac{2wy}{1-y}-1\right)\right], \tag{7.6}$$

where P_κ^κ and Q_κ^κ are associated Legendre polynomial of first and second kind, respectively. The constants C_1 and C_2 can be determined from the boundary conditions $P_R(y_0 - \Delta/2) = P(y_0 - \Delta/2)$ and $P_R(y_0 + \Delta/2) = 0$, discussed above. $P_T(y)$ can simply be obtained from $P_T(y) = P(y) - P_R(y)$. In Fig. 7.2 we verify our analytical calculation against numerical simulations for few different values of the noise strength λ and find good agreement.

7.2.2 Average run and tumble duration decreases with signaling noise

The simplest possible quantity to characterize the run-and-tumble motion is the average duration of a run mode and a tumble mode. In Fig. 7.3A we plot average

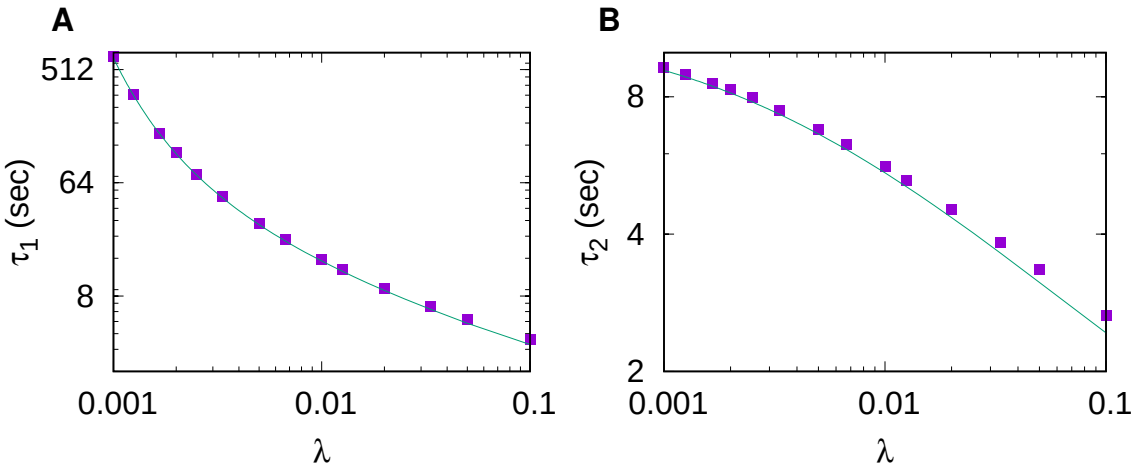

FIGURE 7.3: **Average run and tumble duration as a function of signaling noise strength λ. A.** The average run duration τ_1 decreases as a function of λ. The range of variation of τ_1 is quite significant. **B.** The average tumble duration τ_2 decreases with λ but the range of variation is much smaller than that for τ_1. Discrete points are from simulations and continuous lines are from analytics. The simulation parameters are same as in Fig. 7.2.

run duration as a function of the noise strength λ. We find that as signaling noise decreases, the average run duration increases. In fact for low λ values, average run duration becomes so large that in our simulations we have to consider large system size L to avoid finite size effects. Fig. 7.3B shows variation of average tumble duration with noise. Below we discuss how to calculate these averages exactly.

Note that at the beginning of a run, i.e. just at the instant when tumble to run switch happens, the input signal y always has the value $y_0 - \Delta/2$. Starting from this value, when y crosses $y_0 + \Delta/2$ for the first time, the run ends and a tumble begins. Therefore, a run can be viewed as a first passage event in the y-space. This makes it possible to calculate the average run duration and even the run-length distribution (see next subsection) exactly. If $T(y_i, y_f)$ denotes the mean first passage time for y to reach the value y_f for the first time, starting from an initial value y_i, then $T(y_0 - \Delta/2, y_0 + \Delta/2)$ represents the mean run duration and $T(y_0 + \Delta/2, y_0 - \Delta/2)$ stands for the mean tumble duration.

Let $p(y', t|y, 0)$ be the conditional probability that the input signal has the value y' at time t, given that it started with the value y at time $t = 0$. This conditional probability follows the backward Fokker-Planck equation [7]

$$\frac{\partial p(y', t|y, 0)}{\partial t} = B_1(y)\frac{\partial p(y', t|y, 0)}{\partial y} + \frac{1}{2}B_2(y)\frac{\partial^2 p(y', t|y, 0)}{\partial y^2} \tag{7.7}$$

where $B_1(y)$ and $B_2(y)$ are drift and diffusion terms appearing in Eq. 7.4. To calculate the mean first passage time at $y_0 + \Delta/2$, starting from $y_0 - \Delta/2$, we put an absorbing boundary condition at the target $y = y_0+\Delta/2$ and remember the reflecting boundary condition at $y = 0$. The survival probability $G(y, t; y_0 + \Delta/2)$ is defined as the probability that starting from $y < y_0+\Delta/2$, the signal variable has not reached the target value $y_0 + \Delta/2$ till time t. Clearly, $G(y, t; y_0 + \Delta/2) = \int_0^{y_0+\Delta/2} dy' p(y', t|y, 0)$. From Eq. 7.7 it follows that $G(y, t; y_0 + \Delta/2)$ satisfies the following equation

$$\frac{\partial G(y,t;y_0+\Delta/2)}{\partial t} = B_1(y)\frac{\partial G(y,t;y_0+\Delta/2)}{\partial y} + \frac{1}{2}B_2(y)\frac{\partial^2 G(y,t;y_0+\Delta/2)}{\partial y^2} \quad (7.8)$$

with the initial condition $G(y, 0; y_0 + \Delta/2) = 1$ and the reflecting and absorbing boundary conditions are implemented as $\partial_y G(y, t; y_0 + \Delta/2)|_{y=0} = 0$ and $G(y, 0; y_0 + \Delta/2)|_{y=y_0+\Delta/2} = 0$. The survival probability till time t can be alternatively stated as the probability that the first passage time is larger than t. Therefore, the first passage time distribution is simply $-\partial_t G(y, t; y_0+\Delta/2)$. The mean first passage time is then $T(y, y_0+\Delta/2) = -\int_0^\infty dt\ t\ \partial_t G(y, t; y_0+\Delta/2) = \int_0^\infty dt G(y, t; y_0+\Delta/2)$ which follows the equation

$$B_1(y)\frac{\partial T(y,y_0+\Delta/2)}{\partial y} + \frac{1}{2}B_2(y)\frac{\partial^2 T(y,y_0+\Delta/2)}{\partial y^2} = -1. \quad (7.9)$$

This equation can be solved to get the mean run duration as

$$T(y_0 - \Delta/2, y_0 + \Delta/2) = \tau_1 = 2\int_{y_0-\Delta/2}^{y_0+\Delta/2} \frac{dy}{\psi(y)} \int_0^y \frac{\psi(z)}{B_2(z)}, \quad (7.10)$$

where $\psi(x) = \exp\left[\int_0^x dx' 2B_1(x')/B_2(x')\right]$. Similarly, mean tumble duration can be written as

$$T(y_0 + \Delta/2, y_0 - \Delta/2) = \tau_2 = 2\int_{y_0-\Delta/2}^{y_0+\Delta/2} \frac{dy}{\psi(y)} \int_y^{y_m} \frac{\psi(z)}{B_2(z)}. \quad (7.11)$$

where reflecting boundary condition is used for $y = y_m$ and absorbing boundary condition for $y = y_0 - \Delta/2$. We find good agreement with the simulation data in Fig. 7.3.

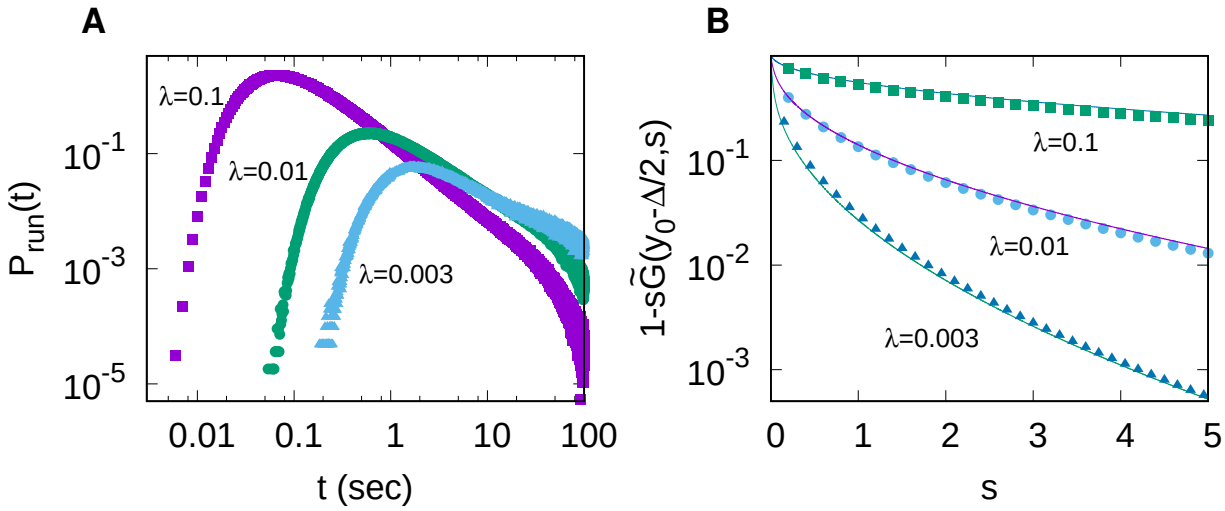

FIGURE 7.4: **Distribution of run duration for different value of noise strength. A:** Simulation results for the distribution of the run duration of the bacterium $P_{run}(t)$. The distribution has a peak whose position shifts leftward as noise increases. **B:** The Laplace transform of $P_{run}(t)$ analytically calculated and plotted in continuous lines. The discrete points show Laplace transform calculated from the data in panel A and we find good agreement. The simulation parameters are same as in Fig. 7.2

7.2.3 Distribution of the run duration of the random walker

Using the correspondence between the run and tumble durations of the random walker and the first passage events for the input signal, it is possible to calculate not only the average run and tumble durations, but also the full distribution function of these durations. We outline this calculation in this subsection. First we present our numerical data for the run duration distribution. In Fig. 7.4A we plot the probability $P_{run}(t)$ that the random walker has a residence time t in the run mode, for different values of the noise strength λ. We find that the probability vanishes for very small and large t, and shows a peak in between. The peak position depends on λ and as λ increases, the peak shifts towards smaller values of t. In other words, the most probable run duration becomes smaller and smaller as noise increases. This behavior is similar to that of the mean run duration shown in Fig. 7.3. As noise increases, the signal $y(t)$ takes less and less time to reach the value $y_0 + \Delta/2$, starting from $y_0 - \Delta/2$ since the diffusivity $B_2(y)$ becomes larger with noise.

To calculate the run duration distribution analytically, we focus on its Laplace transform. First we consider the Laplace transform of the survival probability $\tilde{G}(y,s) = \int_0^\infty dt\ e^{-st}\ G(y,t;y_0+\Delta/2)$, where for simplicity of notation we have dropped $y_0+\Delta/2$

from the argument of the $\tilde{G}$. From Eq. 7.8 it follows that

$$\frac{1}{2}B_2(y)\partial_y^2\tilde{G}(y,s) + B_1(y)\partial_y\tilde{G}(y,s) - s\tilde{G}(y,s) = -1, \tag{7.12}$$

Defining $\tilde{U}(y,s) = \tilde{G}(y,s) - \frac{1}{s}$ we get

$$\frac{1}{2}B_2(y)\partial_y^2\tilde{U}(y,s) + B_1(y)\partial_y\tilde{U}(y,s) - s\tilde{U}(y,s) = 0. \tag{7.13}$$

whose general solution is

$$\tilde{U}(y,s) = \left[\frac{wy(1-y-wy)}{(1-y)^2}\right]^{\kappa/2}\left[D_1 P_\kappa^{\sqrt{\kappa^2+4\mu(s)}}\left(\frac{2wy}{1-y}-1\right) + D_2 Q_\kappa^{\sqrt{\kappa^2+4\mu(s)}}\left(\frac{2wy}{1-y}-1\right)\right], \tag{7.14}$$

where $\mu(s) = \frac{2s}{\lambda q r}$. The constants D_1 and D_2 can be determined from the boundary conditions: $\tilde{G}(y_0+\Delta/2, s) = 0$ and $\partial_y\tilde{G}(y,s)|_{y=0} = 0$ for all s. The Laplace transform of first passage time distribution is given by $1 - s\tilde{G}(y,s)$ which can be evaluated at $y = y_0 - \Delta/2$ to obtain the Laplace transform of run-length distribution. We compare our calculation with simulation results in Fig. 7.4B and find good agreement.

7.3 Run and Tumble motion in an environment with spatial variation

In the previous section, we studied the situation, when the coupling between the stochastic signal $y(t)$ and the random walk motion is one way. While the random walk switches between the run and tumble modes depending on the value of the signal, the signal itself fluctuates independently according to Eq. 7.3. In this section, we consider a two-way coupling between the signal dynamics and the random walker motion. More specifically, we consider a time-evolution equation for $y(t)$ which involves the position x of the random walker as well. Thus, the random walker runs and tumbles following the $y(t)$ value as before, but the random walker position now influences the time-evolution of $y(t)$. In the case when the nutrient concentration is not uniform, but varies linearly in space, $c(x) = c_0(1 + x/x_0)$, activity $a(t)$ in Eq. 3.1 changes when the methylation level changes , or when the cell moves in the medium. In that

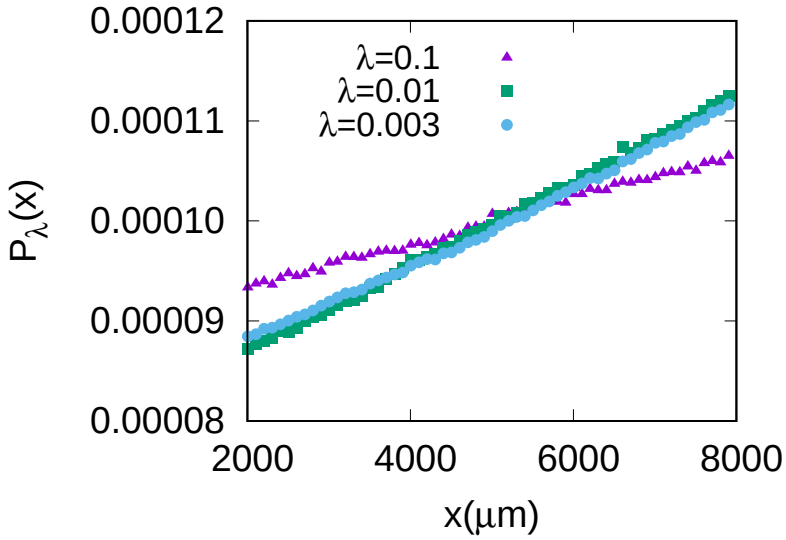

FIGURE 7.5: **The distribution $P_\lambda(x)$ of the random walker position x for different noise strengths.** We have used $c(x) = c_0(1 + x/x_0)$ here and for all λ values, $P_\lambda(x)$ shows a positive slope. For large λ, the slope is less. We have chosen $c_0 = 200\mu M$ and $x_0 = 200000\mu m$ here and all other parameters are as in Fig. 7.2.

case, Eq. 7.2 becomes

$$\frac{dy}{dt} = q(1+\frac{r\lambda}{2})\frac{y(1-y-wy)(1-y-2wy)}{1-y} - s\frac{y(1-y-wy)}{(K_A+c(x))(K_I+c(x))} + ry(1-y-wy)\eta(t). \tag{7.15}$$

The run-and-tumble motion of E.coli in such a nutrient environment gives rise to chemotaxis and in the long time limit there is larger probability to find the cell at regions with higher $c(x)$ [2, 8–10].

In Fig. 7.5 we show the data for the position distribution of the random walker in the long time limit. We find that $P_\lambda(x)$ increases with x, roughly linearly. This result shows that although the run-and-tumble dynamics is significantly different from and simpler than that of an E.coli cell, the walker still manages to locate itself in the region with higher nutrient concentration with larger probability. Our data show that $P_\lambda(x)$ varies as $c(x)$ for small and intermediate λ values. However, when λ becomes large, $P_\lambda(x)$ gradually becomes flat, as expected in the limit of large signaling noise, when the time-evolution of $y(t)$ is mainly governed by the stochastic fluctuations, and its x-dependence can be almost ignored.

7.4 Conclusion

In this chapter, we have investigated the effect of a sharp step-like response function on a run-and-tumble random walk. In nature run-and-tumble motion is ubiquitous in a wide variety of organisms. While an intra-cellular biochemical reaction network controls the motion in all these cases, some organisms, for example, E. coli bacteria, show a particularly sensitive dependence on these reactions. The transition rate of an E. coli cell from run mode to tumble mode depends strongly and sensitively on the fluctuating concentration of the motor protein CheY-P, which is an important component of its reaction network. This motivates a general theoretical question that we consider in this paper: what happens when a run-and-tumble motion is coupled to a stochastic input signal via a sensitive response. We are interested in two different cases: one in which the stochastic dynamics of the input signal is an independent process and another in which the signal variable dynamics also depends on the spatial location of the random walker. In the first case, we specifically choose the signal variable dynamics from that of CheY-P protein concentration for an E. coli cell in a homogeneous nutrient environment. The simple switching dynamics that we use for our run-and-tumble walker makes it possible to calculate many things exactly in this case. In the second case, we consider a signal variable whose time-evolution mimics CheY-P dynamics for an E. coli cell in a spatially varying nutrient environment. Interestingly, our numerical simulations show that even with its simple run-and-tumble strategy, the random walker manages to localize in a region where nutrient density is higher.

The run-and-tumble motion that we consider here, is significantly different from that executed by an E.coli cell. While for an E.coli cell, the tumbling bias varies sensitively, but continuously as a function of the CheY-P level, in our model the switching probability between the run and tumble modes show a sharp jump from 0 to 1. This allows us to address the theoretical question of the effect of sharp response in the simplest possible setting. Although our results in Fig. 7.5 show that the basic signature of chemotaxis is still retained in our model, we also find some important differences from well-known E.coli behavior. One such crucial difference is observed in run duration distribution. For low signaling noise, E.coli shows exponential distribution of run duration and as the signaling noise gets larger, longer runs become more probable and the distribution changes to a power law [11–15] . In contrast, in our model, runs can be described as first passage events, whose distribution (see Fig. 7.4A) has a peak and shows a power law tail for all values of λ. Moreover, we also find that

with increasing noise, longer runs become less probable in our case. As noise level becomes lower, the mean run duration in our model increases rather strongly. For E.coli motion also mean run duration becomes larger for lower signaling noise, but the variation is much weaker in that case [15].

As we mentioned in Sec. 7.2, the run-and-tumble trajectory of E.coli has an additional level of stochasticity coming from the fact that switching probability can be less than one, which means for a given time-series of the input signal, it is possible to generate different run-tumble trajectories. However, in our model, switching probability is either 0 or 1 and can be nothing in between. This deterministic nature means that only one run-and-tumble trajectory is possible for a given signal time-series. Although the direction of a new run is still chosen randomly at the time of every tumble to run switch in our model, but in a homogeneneous nutrient background it makes no difference whether the random walker is running towards left or right. The differences mentioned in the previous paragraph may be alternatively viewed as the result of this deterministic vs stochastic aspect. It also shows that although CW bias of E.coli increases really sharply as CheY-P level changes, when that response is actually replaced by a jump in the switching probability, system shows qualitatively different behavior in many aspects. It may be interesting to gradually vary the steepness of a sigmoidal response curve and see if there is a crossover between the two behaviors.

Bibliography

[1] Y. Tu, T. S. Shimizu and H. C. Berg, Modeling the chemotactic response of Escherichia coli to time-varying stimuli, Proc. Natl. Acad. Sci. U.S.A. 105, 14855 (2008).

[2] L. Jiang, Q. Ouyang and Y. Tu, Quantitative modelling of Escherichia coli chemotactic motion in environments varying in space and time, PLoS Comp. Biol. 6, e1000735 (2010).

[3] M. Flores, T. S. Shimizu, P. R. ten Wolde and F. Tostevin, Signaling noise enhances chemotactic drift of E. coli, Phys. Rev. Lett. 109, 148101 (2012).

[4] Bren A, Eisenbach M (2000) How signals are heard during bacterial chemotaxis: protein-protein interactions in sensory propagation. J Bacteriol 182: 6865-6873.

[5] Cluzel P, Surette M, Leibler S (2000) An ultrasensitive bacterial motor revealed by monitoring signaling proteins in single cells. Science (New York, NY) 287:1652-1655.

[6] Milo *et al.* (2010) Nucl. Acids Res. 38 (suppl 1): D750-D753

[7] Gardiner CW (2004) Handbook of stochastic methods for Physics, Chemistry and the Natural Sciences. Berlin: Springer-Verlag.

[8] de Gennes PG (2004) Chemotaxis and the role of internal delays. Eur Biophys J 33: 691-693.

[9] Chatterjee S, Silveira RA da, Kafri Y (2011) Chemotaxis When Bacteria Remember: Drift versus Diffusion. PLoS Comp. Biol, vol 7 issue 12 e1002283.

[10] Dev S, Chatterjee S (2015) Optimal search time in E. coli chemotaxis. Phys. Rev. E 91, 042714.

[11] Korobkova E, Emonet T, Vilar JM, Shimizu TS, Cluzel P (2004) From molecular noise to behavioural variability in a single bacterium. Nature 428:574-578.

[12] Tu Y, Grinstein G (2005) How White Noise Generates Power-Law Switching in Bacterial Flagellar Motors, Phys Rev Lett 94: 208101.

[13] Matthaus F, Jagodic M, Dobnikar J (2009) E. coli Superdiffusion and ChemotaxisSearch Strategy, Precision, and Motility, Biophysical Journal, Volume 97, 946-957.

[14] Matthaus F, Mommer MS, Curk T, Dobnikar J (2011) On the Origin and Characteristics of Noise-Induced Lévy Walks of E. Coli, PLoS One, Volume 6 Issue 4 e18623.

[15] Dev S, Chatterjee S (2018) Optimal methylation noise for best chemotactic performance of E. coli. Phys Rev E 97, 032420.

Appendix A

Drift velocity of a random walker in presence of a linear nutrient concentration field for response function $R(t) = \delta(t)$

Let us consider a random walker(RW) whose motion consist of two modes: run and tumble. In run mode it moves in a straight line with constant speed v where in tumble motion it does not move at all. After each tumble it chooses a new direction. In one dimension there is only two direction either right or left. Let us consider that the tumble is instantaneous so that the walker changes its current direction at each tumble instantaneously with probability q . If τ is the average run duration of the random walker then the probability then it will change its direction at tumble or the tumbling probability in time between t and $t + dt$ is $\frac{dt}{\tau}$. For a random walker which is moving in a concentration profile like *E. coli* bacterium in a nutrient concentration gradient, the tumbling probability depends on the concentration gradient and the response function of the cell as described in Chapter 2. Let us consider that the Random walker is placed in a linear concentration profile $c(x) = x/x_0$, where x_0 is the concentration gradient. We also consider the response function of the random walker $R(t) = \delta(t)$. If the walker starts a run from a fixed position x, where a tumble has occurred, with an initial velocity v_i and T is the average time duration for occurring n tumbles and at each tumble the walker changes its direction with probability unity ($q = 1$). Where T_1, T_2... are the average run-duration between two

successive tumble and x_1, x_2... are the average tumble positions, so that

$$\begin{aligned} T &= T_1 + T_2 + T_3 + ... + T_n \\ T_1 &= \frac{T_{1+} + T_{1-}}{2} \\ T_2 &= \frac{T_{2+} + T_{2-}}{2}.. \\ x_1 &= \frac{x_{1+} + x_{1-}}{2} \\ x_2 &= \frac{x_{2+} + x_{2-}}{2}... \end{aligned} \tag{A.1}$$

Where T_{1+}, T_{2+}... are the average time duration between two tumbles for the trajectories with initial velocity $v_i = v$ and T_{1-}, T_{2-}... are the average time duration between two successive tumble for the trajectories with initial velocity $v_i = -v$. x_{1+}, x_{2+}... are average tumble positions for trajectory with initial velocity $v_i = v$ and x_{1-}, x_{2-}... are average tumble positions for trajectory with initial velocity $v_i = -v$. Let us now consider the first case when $v_i = v$. For this case the persistence probability $P_+(\xi)$ is given by,

$$\begin{aligned} P_+(\xi) &= \exp[-\int_t^{t+\xi} \frac{dt'}{\tau(t')}] \\ &\approx \exp^{-\frac{\xi}{\tau}}[1 + \frac{\alpha}{\tau}\int_t^{t+\xi} c(t')dt'] \\ &\approx \exp^{-\frac{\xi}{\tau}}[1 + \frac{\alpha}{\tau}\int_t^{t+\xi} dt'(c(x) + \frac{vx(t'-t)}{x_0})] \\ &= \exp^{-\frac{\xi}{\tau}}[1 + \frac{\alpha x\xi}{\tau x_0} + \frac{\alpha v\xi^2}{2x_0\tau}] \end{aligned}$$

where we have used the condition $\alpha << 1$. Now the probability of stopping during the interval ξ and $\xi + d\xi$ is given by,

$$-\frac{dP_+(\xi)}{d\xi} = \exp^{-\frac{\xi}{\tau}}[\frac{1}{\tau} - \frac{\alpha x}{\tau x_0} + \frac{\alpha x\xi}{\tau^2 x_0} - \frac{\alpha v\xi}{\tau x_0} + \frac{\alpha v\xi^2}{2\tau^2 x_0}] \tag{A.2}$$

So from the above probability distribution we can now calculate the average runtime upto the first tumble and which is given by

$$\begin{aligned} T_{1+} &= \int_0^\infty \xi(-\frac{dP_+(\xi)}{d\xi})d\xi \\ &= \tau(1 + \frac{\alpha x}{x_0} + \frac{\alpha v\tau}{x_0}). \end{aligned} \tag{A.3}$$

So the first tumble after x will be at $x_{1+} = x + vT_{1+} = x + v\tau(1 + \alpha c(x) + \alpha v\tau/x_0)$. Now if the bacterium would start the run with initial velocity $v_i = -v$, one can similarly write down the expression for persistence probability $P_-(\xi)$ and which is given by

$$P_-(\xi) = \exp^{-\frac{\xi}{\tau}}[1 + \frac{\alpha x\xi}{\tau x_0} - \frac{\alpha v\xi^2}{2\tau x_0}] \tag{A.4}$$

From which one can calculate the average runtime T_{1-} and is given by

$$T_{1-} = \tau(1 + \frac{\alpha x}{x_0} + \frac{\alpha v\tau}{x_0}). \tag{A.5}$$

So that the average tumbling position after x if the bacterium would have started with $v_i = -v$ is given by $x_{1-} = x - vT_{1-} = x - v\tau(1 + \frac{\alpha x}{x_0} - \frac{\alpha v\tau}{x_0})$. Now the average tumbling position x_1 is given by

$$x_1 = \frac{x_{1+}}{2} + \frac{x_{1-}}{2} = x + \frac{\alpha v^2\tau^2}{x_0}. \tag{A.6}$$

The average displacement is given by,

$$\Delta x_1 = x_1 - x = \frac{\alpha v^2\tau^2}{x_0}. \tag{A.7}$$

For $n = 2$ case, similarly the T_{2+}, T_{2-}, x_{2+} and x_{2-} can be calculated and are given by

$$\begin{aligned}
T_{2+} &= \tau[1 + \alpha c(x_{1+}) - \frac{\alpha v\tau}{x_0}] = \tau(1 + \frac{\alpha x}{x_0}) \\
T_{2-} &= \tau[1 + \alpha c(x_{1-}) + \frac{\alpha v\tau}{x_0}] = \tau(1 + \frac{\alpha x}{x_0}) \\
x_{2+} &= x_{1+} - vT_{2+} = x + \frac{\alpha v^2\tau^2}{x_0} \\
x_{2-} &= x_{1+} - vT_{2+} = x + \frac{\alpha v^2\tau^2}{x_0} \\
x_2 &= \frac{x_{2+}}{2} + \frac{x_{2-}}{2} = x + \frac{\alpha v^2\tau^2}{x_0}.
\end{aligned} \tag{A.8}$$

The average displacement after two tumble can be given by

$$\Delta x_2 = x_2 - x = \frac{\alpha v^2\tau^2}{x_0}. \tag{A.9}$$

One can similarly calculate the average displacement for many number of tumbles. For n number of tumbles the average displacement will be

$$\Delta x_n = \frac{n}{2}\frac{\alpha v^2\tau^2}{x_0}, \text{ if } n = \text{even} \tag{A.10}$$

$$\Delta x_n = \frac{n+1}{2}\frac{\alpha v^2\tau^2}{x_0}, \text{ if } n = \text{odd}. \tag{A.11}$$

The total time T for n number of tumbles is given by,

$$T = \Sigma_{i=1}^{i=n}\frac{T_{i+} + T_{i-}}{2} = n\tau + O(\alpha). \tag{A.12}$$

So the drift velocity can be given by

$$V(x) = \frac{\Delta x_n}{T} = \frac{\alpha v^2\tau}{2x_0} \tag{A.13}$$

Now for any q not equals to unity, the Eq. A.13 would be

$$V(x) = \frac{\alpha v^2\tau}{2qx_0}. \tag{A.14}$$

In chapter 2 for first passage time analysis the $c(x)$ has been chosen as Gaussian form. Since now the gradient of the nutrient profile depends upon the position x, the drift velocity of the cell will no longer be independent of the position x. For this Gaussian nutrient profile we used the form

$$V(x) = \frac{\alpha v^2\tau}{2q}c'(x), \tag{A.15}$$

where $c'(x)$ is the spatial derivative of the Gaussian concentration profile and using this particular form of the drift velocity our analytics shows a good agreement with the simulation results.